ADHESION ENHANCEMENT OF DIAMOND AND DIAMOND-LIKE CARBON THIN FILMS ON TITANIUM ALLOY

A Thesis Submitted to the College of

Graduate Studies and Research

In Partial Fulfillment of the Requirements

For the Degree of Doctor of Philosophy

In the Department of Mechanical Engineering

University of Saskatchewan

Saskatoon

By

CHUNZI ZHANG

PERMISSION TO USE

In presenting this thesis in partial fulfilment of the requirements for a Postgraduate degree from the University of Saskatchewan, I agree that the Libraries of this University may make it freely available for inspection. I further agree that permission for copying of this thesis in any manner, in whole or in part, for scholarly purposes may be granted by professor Qiaoqin Yang who supervised my thesis work or, in her absence, by the Head of the Department or the Dean of the College in which my thesis work was done. It is understood that any copying or publication or use of this thesis or parts thereof for financial gain shall not be allowed without my written permission. It is also understood that due recognition shall be given to me and to the University of Saskatchewan in any scholarly use which may be made of any material in my thesis.

Requests for permission to copy or to make other use of material in this thesis in whole or part should be addressed to:

Head of the Department of Mechanical Engineering

University of Saskatchewan

57 Campus Drive

Saskatoon, Saskatchewan (S7N 5A9)

ABSTRACT

Titanium (Ti) and its alloys have been widely used in aerospace, biomedical, chemical processing, marine facilities, and sports equipment because of their low density, very high tensile strength and toughness, and high corrosion resistance. However, the poor tribological properties has been a major problem and limited their widespread applications. Deposition of wear/corrosion resistant diamond-like carbon (DLC) coatings on Ti alloys is promising to significantly enhance the durability and service performances of these materials. However, the adhesion between DLC coatings and Ti alloy substrates is too weak to meet the application requirements. Up to now, approaches including optimization of deposition conditions, surface treatment of the substrate, deposition of an interlayer, and incorporation of metallic or nonmetallic elements have been used for adhesion enhancement of DLC on Ti alloys. In this research, a new method, nanodiamond particles incorporation, was developed for adhesion enhancement of DLC coatings on Ti alloys. In order to achieve high diamond nucleation without damaging the Ti alloy, nucleation enhancement of diamond on Ti alloys by nanodiamond seeding, tungsten (W) interlayers, and high methane concentration were studied. Diamond, DLC and W deposition were carried out by microwave assisted chemical vapor deposition, direct ion beam deposition and hot filament assisted chemical vapor deposition, respectively. Scanning electron microscopy, Atomic force microscopy, X-ray diffraction, Raman spectroscopy and synchrotron-based near edge extended X-ray absorption fine structure spectroscopy were used to characterize the microstructure and chemical bonding of the as-deposited particles and films, and indentation testing was used to evaluate the adhesion of the as-deposited coatings.

By nanodiamond seeding or applying a W interlayer, significantly enhanced diamond nucleation has been obtained on Ti alloys, and consequently high quality nanocrystalline diamond thin films have been obtained on Ti alloys at decreased deposition temperature and

reduced deposition time, which mitigates the deterioration of Ti alloy substrates due to hydrogen diffusion during diamond deposition and also enhances the adhesion of diamond on Ti alloys. Based on these results, nanodiamond particles (NDP) with high nucleation density and high adhesion were deposited on Ti alloys initially to enhance the adhesion of DLC films on Ti alloys. Results show that the pre-deposited NDP can significantly increase the adhesion of DLC on Ti6Al4V, probably due to the increased interfacial bonding, mechanical interlocking, and stress relief by the incorporation of NDP into DLC to form NDP/DLC composite films.

ACKNOWLEDGMENTS

I would like to express my deepest thanks and appreciation to my supervisor, Prof. Qiaoqin Yang, for her invaluable encouragement, guidance and support through my study program. Her personality, expertise, and enthusiasm not only inspired me in my research, but also in my personal development. I will be always grateful.

I also would like to extend my appreciation to my advisory committee members: Prof. Assem Hedayat, Prof. Jerzy A. Szpunar, and James D. Johnston, for their invaluable support, constructive criticism and useful advices.

Especially I would like to thank Dr. Akira Hirose, for his generous permission to use the MPCVD and HFCVD reactors in the Plasma Physics Laboratory of the University of Saskatchewan.

My special thanks also go to Dr. Yongji Tang, Yuanshi Li, and Yongfeng Hu, for their insightful discussions and fruitful collaboration in experiments. Many thanks should also be given to the members of our research group for their help and support during my research.

Finally, I wish to express my gratitude to Mr. Robert Peace for his technical assistance in materials synthesis and characterization facilities in the Department of Mechanical Engineering, Mr. David McColl for the help of CVD equipment in the Plasma Physics Laboratory, Mr. Hans-Jürgen Steinmetz, Jason Maley, Jigang Zhou, and Xiaoqi Chen for their helps in samples characterization.

Financial assistance provided by the China Scholarship Council, Canada Research Chair Program, the Natural Sciences and Engineering Research Council of Canada is gratefully acknowledged.

Dedication

To my parents, my husband Jingyang, and my daughter Athena.

TABLE OF CONTENTS

page

LIST OF TABLES

LIST OF FIGURES

LIST OF ABBREVIATIONS

CHAPTER 1
INTRODUCTION

Diamond and diamond-like carbon (DLC) are renowned for their excellent tribological properties: low friction coefficient and high wear resistance, and thus are very promising to be used as protective coatings for tribological applications. However, the limited adhesion between the coating and the metallic substrate restricts their applications. In this research, diamond and DLC coatings with enhanced adhesion are synthesized on Titanium (Ti) alloy for improving its tribological properties. This chapter focuses first on the motivation and objectives of this research and then shows the organization of the thesis.

1.1 Motivation

Ti and its alloys have been widely used in aerospace, chemical, and power industries, biomedical devices, transportation, armament, and sports. Their increasing industrial importance is because of their excellent properties such as low density, high strength, superior corrosion resistance, and good biocompatibility. However, Ti alloys have significant drawbacks of poor abrasive wear resistance and high friction coefficient, which limit its tribological applications. Deposition of wear/corrosion resistant DLC coatings on Ti alloys is a promising way to address these limitations owning to the unique properties of DLC including high hardness, low friction coefficient, chemical inertness, high wear resistance, and excellent biocompatibility. However, DLC coatings often suffer from poor adhesion on Ti alloy substrate, which shortens the service lifetime of DLC coated Ti alloy parts and devices and restricts their applications. This thesis work aims to enhance the adhesion between DLC coatings and Ti alloy substrates to improve the tribological properties of Ti alloy for their wider applications.

1.2 Research objectives

The overall goal of this research is to enhance the adhesion of DLC coatings on Ti alloys. In order to achieve the goal, the research includes following specific research themes.

1.2.1 Adhesion investigation of DLC coatings on Ti alloy sheets for identifying the key factors affecting adhesion

Ion energy is the key factor that controls the quality of DLC coatings. In this work, adhesion of DLC coatings grown on Ti alloy substrates will be investigated using direct ion beam deposition under different ion energies. Tungsten (W), titanium nitride (TiN), and nanodiamond particles (NDP) will be applied as interlayers to explore the mechanism of adhesion enhancement of DLC coatings on Ti alloy. The samples prepared will be characterized by Raman spectroscopy, scanning electron microscopy (SEM), X-ray diffraction (XRD), and nanoindentation testing. Indentation testing by micro-hardness tester will be used for adhesion evaluation.

1.2.2 Diamond nucleation enhancement on Ti alloy for reducing deterioration of Ti alloy

NDP is going to be used as adhesion promoter of DLC coatings grown on Ti alloy. However, the diamond deposition by chemical vapor deposition (CVD) techniques is usually undertaken at high temperature (700- 850°C) in a hydrogen-rich environment, the diffusion of hydrogen can lead to deterioration of the mechanical properties of the Ti alloy substrate, in particular, fatigue life and impact strength [1-4]. Normally, this diffusion of hydrogen can be reduced by using low deposition temperature and short deposition time, which can be achieved by very high nucleation density of diamond. In this work, innovative seeding and deposition processes will be studied to deposit

nanocrystalline diamond (NCD) coatings on Ti alloy in shorter time and thus reduce the property deterioration of Ti alloy. SEM and Raman will be used for characterization.

1.2.3 Interfacial investigation of diamond coatings on Ti alloy for understanding the mechanism of adhesion

Interfacial behaviors are extremely important for revealing the mechanism of adhesion between diamond coatings and Ti alloy substrate. In this work, low deposition temperature and extremely high methane concentration is going to be used to enhance the adhesion strength of diamond coating and reduce substrate damage. In addition, the nucleation, growth, adhesion behaviors of the diamond coating and the interfacial structures will be investigated using Raman, XRD, SEM, Transmission electron microscopy (TEM), synchrotron radiation and indentation testing.

1.2.4 Adhesion enhancement of DLC coatings on Ti alloy by incorporation of nanodiamond particles

NDP incorporated in DLC may greatly relieve the stress due to the ion bombardment in DLC deposition process. In addition, good interfacial adhesion may be achieved because of the much higher adhesion of NDP than DLC on Ti alloy by chemical bonding, the physical and chemical affinity of NDP and DLC, and the mechanical interlocking effect of NDP with DLC. So it is expected to get a highly adherent DLC on Ti alloy by NDP incorporation. First, NDP will be deposited on Ti alloy by microwave assisted chemical vapor deposition (MPCVD), then, DLC coating will be synthesized by low energy ion beam deposition. In addition, the effect of nanodiamond density on adhesion of DLC will be studied. SEM, Atomic force microscopy (AFM), XRD and Raman spectroscopy will be used to characterize the microstructure and chemical bonding of the

deposited particles and films, and Rockwell indentation testing will be used to evaluate the adhesion of the deposited coatings.

1.2.5 Evaluation of nucleation and adhesion of diamond coatings on Ti alloy with tungsten interlayer

In this work, diamond nucleation and growth on Ti alloy substrates with W interlayers will be investigated using hot filament chemical vapor deposition (HFCVD). W interlayers will be firstly deposited on Ti alloy substrates under different conditions by sputtering and diamond will be then deposited on W coated Ti alloy using the same HFCVD reactor. The effect of thickness and surface morphology of W interlayer on the nucleation, growth, and adhesion of diamond on the Ti alloy will be studied using XRD, SEM, Energy disperse spectroscopy (EDS), AFM, Raman spectroscopy, synchrotron near-edge X-ray absorption fine structure spectroscopy (NEXAFS) and Rockwell C indentation testing.

1.3 Organization of the Thesis

This thesis consists of 9 chapters. The organization of this thesis is listed as follows:

Chapter 1 gives a brief introduction of the research project including motivation, objectives, and thesis organization.

A comprehensive literature review is shown in Chapter 2. It firstly gives an overview of carbon materials. Then introductions of diamond and DLC including structure, properties, synthesis methods, diamond nucleation, and diamond and DLC adhesion enhancement on Ti alloy are presented. In the end, the microstructure and properties of Ti6Al4V alloy is introduced.

Chapter 3 introduces experimental methodologies adopted in this research. The ion beam system for DLC deposition, MPCVD and HFCVD reactors for diamond and W

deposition will be described in details. In addition, techniques used for microstructure, chemical bonding, and mechanical properties characterization will be explained.

Chapter 4 presents an adhesion investigation of DLC coatings grown on Ti6Al4V using direct ion beam deposition under different ion energies. Results show that the sp^3 concentration in the films increases with the increase of ion energy used for DLC deposition while adhesion decreases when ion energy is higher than 70 eV. In order to achieve both high sp^3 concentration and high adhesion on Ti6Al4V, interlayers of W, TiN, and NDP are applied for adhesion enhancement. Results show that the adhesion of DLC coatings on Ti6Al4V can be greatly enhanced by pre-deposited W, TiN, and NDP interlayers, in which, NDP works best. This is possibly because of the enhanced interfacial bonding and reduced stress by chemical and mechanical affinity of diamond and DLC.

NDP is proved to be great adhesion promoter of DLC on Ti6Al4V. However, the deterioration of the mechanical properties of Ti6Al4V caused by diamond deposition is significant. In Chapter 5, diamond nucleation and growth on Ti6Al4V using MPCVD under different seeding and deposition conditions are investigated. Results show that the nucleation density of diamond can be enhanced up to $10^{11}/cm^2$ by nanodiamond seeding and two-step deposition. By optimizing the seeding and deposition parameters, nanocrystalline diamond thin films were synthesized at relatively low microwave power (600 W) within a short time deposition; consequently, the microstructure change of Ti6Al4V as a result of hydrogen diffusion was significantly reduced due to the low deposition temperature and short deposition time.

Chapter 6 presents the effect of NDP density on adhesion of NDP/DLC composite coatings grown on Ti6Al4V. The results show that the adhesion of DLC composite coatings on Ti6Al4V increases with the increase of NDP density. The enhanced adhesion between DLC coating and the Ti6Al4V substrate by incorporation of NDP is probably caused by enhanced interfacial bonding, mechanical interlocking, and stress relief.

As more NDP incorporation results in higher adhesion of DLC on Ti6Al4V, a NCD interlayer with high adhesion is promising for DLC adhesion enhancement. In Chapter 7, interfacial investigation of NCD diamond thin films on Ti6Al4V grown by MPCVD under a high CH_4 concentration and moderate deposition temperature is presented. This work is cooperated with Dr. Yuanshi Li. Results show that the low deposition temperature and extremely high methane concentration demonstrate beneficial to enhance coating adhesion strength and reduce substrate damage.

In Chapter 8, W interlayers with different thickness and surface morphology are applied for diamond deposition by HFCVD in order to further enhance the nucleation and adhesion of diamond on Ti6Al4V. The results show that the pre-deposited W interlayers act as a diffusion barrier for carbon, and thus significantly enhance the nucleation of diamond. In addition, the W interlayer reacts with carbon to form WC and W_2C during the diamond deposition, and thus enhances the adhesion of diamond on Ti6Al4V, which would be beneficial for later DLC deposition.

Finally, the main results, conclusions, and suggestions for future work are summarized in Chapter 9.

CHAPTER 2
LITERATURE REVIEW

Due to the high hardness of diamond, diamond-related coatings and thin films have attracted increasing research attention in the past decades. One of the focuses is to deposit adherent diamond or DLC coatings on Ti alloys for improving their wear/corrosion resistance [1-8]. However, deposition of wear/corrosion resistant diamond-related coatings onto Ti alloys is not easy and the coatings usually suffer from poor adhesion [9, 10]. This chapter will give a comprehensive review on Ti6Al4V, diamond-related carbon materials, and diamond based coatings on Ti6Al4V.

2.1 Overview of Ti6Al4V alloy

Ti and its alloys find applications in aerospace, chemical engineering, biomedical engineering, power, transportation, armament, and sports due to its excellent combination of low density, high strength, high corrosion resistance, and relatively high strength at moderately high temperatures [11].

In most applications, a kind of Ti alloy referred to as Ti6Al4V, which contains 6% of aluminum and 4% of vanadium by weight, is used. This alloy is generally employed in annealed or solution treated and aged metallurgical conditions. Table 2-1 shows the magnitudes of selected properties of this alloy [12].

Table 2-1. Properties of Ti6Al4V alloy in its two main metallurgical conditions [12].

Material	TS [MPa]	YS [MPa]	*E* [GPa]	Hardness [HV]	*K* [W/mK]	β-Transus [°C]
Ti-6Al-4V (annealed bar)	895	825	110	340	7.3	995
Ti-6Al-4V (solution + age bar)	1035	965	-	360	7.5	995

TS – Tensile Strength; YS – Yield Strength; *E* – Elastic modulus; *C* – Thermal conductivity.

Hydrogen embrittlement of Ti6Al4V alloy becomes an important issue limiting the engineering applications of this alloy. This is because hydrogen diffuses easily in Ti6Al4V and reacts with Ti to form hydride [12, 13]. In applications of Ti6Al4V alloy involving hydrogen-rich environments, hydrogen diffusion results in high amounts of hydrides and solid solution at the grain or phase boundaries, which decrease the interfacial bonding at the grain and phase boundaries and lead to the decrease of tensile strength of Ti6Al4V [14]. In addition, the alloy is susceptible to wear, fretting fatigue, and erosion. All these issues limit the applications of Ti6Al4V.

2.2 Carbon materials

Carbon is one of the most abundant elements on the earth. Almost all the organisms are carbon based, and different carbon materials play an increasingly significant role in many technical areas and in our daily life.

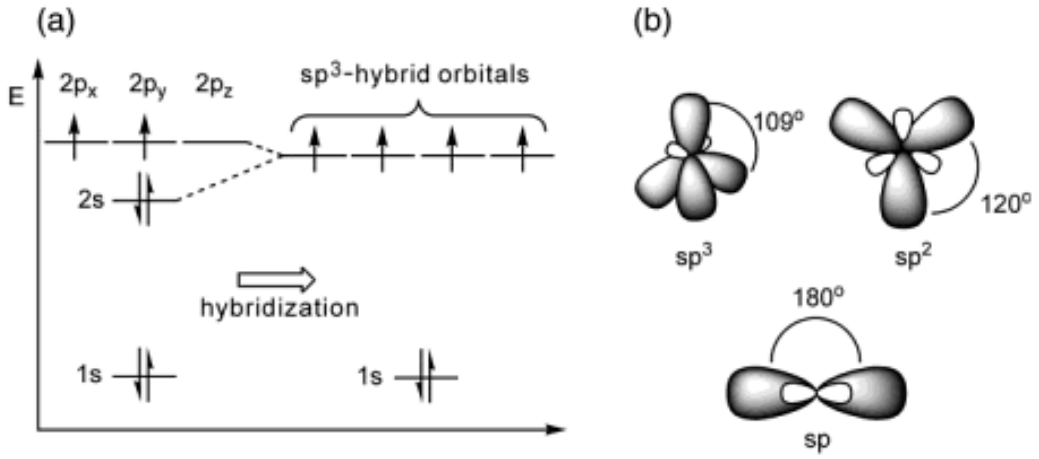

Figure 2-1. (a) Diagram of atomic orbitals and sp^3 hybridization, (b) hybrid orbitals of carbon [15].

One carbon atom has six electrons in which two are inner and four are valence electrons. The four valance electrons, $2s^2$ and $2p^2$, can form three different hybridizations, sp^3, sp^2, and sp^1, as shown in Figure 2-1, and several different chemical bonds [15, 16]. This variety in chemical bonds gives carbon material many crystalline and disordered structures, including diamond, graphite, fullerenes, carbynes, amorphous carbon (a-C), C_{60}, and newly discovered carbon nanotubes, and graphene [17-19]. In this thesis work, diamond and diamond-like amorphous carbon materials are investigated.

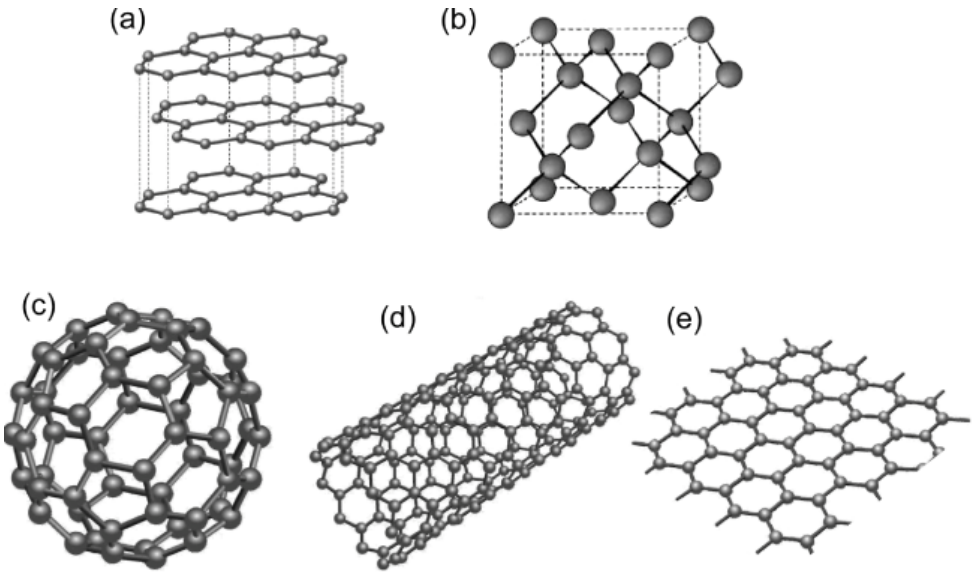

Figure 2-2. Structures of some carbon allotropes: (a) graphite, (b) diamond, (c) C_{60}, (d) carbon nanotube, (e) graphene [19].

2.3 Diamond

Diamond, the hardest natural material, is considered an ideal material for many applications due to its unique and extreme properties [20].

2.3.1 Structure and properties of diamond

The crystalline structure of diamond is shown in Figure 2-3. In which, each carbon atom is connected tetrahedrally by strong σ bonds with a short bond length of 1.54 Å. This crystalline structure is categorized as face-centered cubic (FCC) lattice, and the lattice constant a=3.567 Å (1 Å=0.1 nm). There are 8 atoms in each crystallographic unit cell, and the atomic density is $1.77\times10^{23}/cm^3$ [21].

Due to the strong symmetric σ bonds, diamond has many unique and extreme physical properties, including the highest hardness, bulk modulus, atom density, thermal conductivity, and the lowest coefficient of thermal expansion [22]. It is also chemically inert with very low friction coefficient, excellent wear resistance and biocompatibility [23, 24].

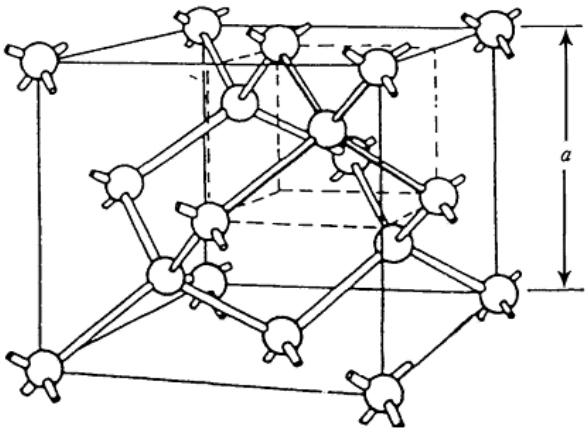

Figure 2-3. Diamond structure. The lattice constant of diamond is a=3.567 Å [21].

2.3.2 CVD growth of diamond

Diamond was firstly synthesized by using high pressure and high temperature (HPHT) techniques on a commercial scale in the mid-1950s [25]. However, it is difficult and

expensive to synthesis large diamond crystals by HPHT. In the 1980's, a CVD method was developed for diamond thin film deposition using hydrogen (H_2) and methane (CH_4) gas mixture [26, 27]. The required conditions for diamond CVD include: (i) high substrate temperature T_s, typically in the range of 700 to 1200 °C, (ii) low gas pressure P, typically in the range of 20 to 150 Torr, and (iii) the concentration ratio of CH_4 to H_2 usually being 1 % to 5 %. In the diamond CVD process, CH_4 and H_2 molecules are firstly decomposed into various hydrocarbon ions and radicals, molecular and atomic hydrogen, and hydrogen ions. The hydrocarbon ions and radicals then diffuse onto the substrate surface, forming sp^2 and sp^3 carbon clusters. Comparing to sp^2 carbon clusters, it is more difficult for sp^3 carbon clusters to be etched by atomic hydrogen. Consequently, only sp^3 carbon clusters are left on the substrate to grow, forming diamond film. The diamond CVD techniques developed quickly. Such techniques can be categorized according to the methods employed for plasma generation, including microwave plasma CVD, hot filament CVD, DC plasma CVD, radio-frequency (RF) plasma CVD, plasma jet CVD, and combustion CVD [21]. The MPCVD and HFCVD are adopted in this thesis work, and they will be described in Chapter 3.

2.3.3 Diamond nucleation

The main problem of diamond growth by CVD is that the nucleation density is low when the deposition is on materials other than diamond. For instance, the nucleation density of diamond on polished single crystal silicon wafer is in the order of $10^4/cm^2$ [28]. In order to enhance the diamond nucleation on non-diamond substrates, polishing the substrate surface with diamond powders, ultrasonically treating the substrate with

diamond powders and alcohol suspension, and applying negative bias voltage on the substrate are usually used [21].

During the development of CVD diamond deposition, diamond single crystals were firstly used as substrates [29], and then diamond seeds were used [30, 31]. Diamond growth on non-diamond substrates without using diamond seeds succeeded in 1982. In 1987, scratching of the substrate surface with diamond powders was developed for diamond nucleation enhancement [32]. Besides diamond, SiC [33], c-BN [34], Cu or stainless steel [35], ZrB_2 [36], and Al_2O_3 [37] powders were also used. Among all the abrasive powders used, diamond was found to be the most effective one. The mechanism can be attributed to diamond seeding and creation of defects during diamond powder scratching [38, 39]. Later, coating the substrate surface with carbon materials, for instance, graphite, amorphous carbon, and DLC was found to be beneficial for diamond nucleation enhancement [40].

In 1991, a breakthrough was made by Yugo et al., that a high nucleation density of diamond on mirror-polished substrate without scratching was achieved by using bias-enhanced nucleation (BEN) method [41]. The BEN method involves applying a negative voltage bias to the substrate during diamond nucleation, by which the nucleation density could be enhanced to as high as 10^9-$10^{10}/cm^2$ on Si. Subsequent developments of BEN by Jiang et al. [42, 43] and Stoner et al. [44] led to the heteroepitaxial growth of diamond on silicon and silicon carbide substrates, respectively.

To explain the mechanism of diamond nucleation, Yugo et al. suggested a shallow ion implantation model. This model proposed that low energy ion implantation formed sp^3 bonded carbon clusters, which function as nucleation precursors [45]. Stoner et al.,

though, suggested that the change in plasma chemistry was the main factor affecting critical processes, with substrate biasing increasing the concentration of atomic hydrogen resulting in formation of a carbide surface layer [46]. Jiang found that a surface kinetic model could effectively represent the relationship between the evolution of the nucleation density and the immobile active nucleation sites, germs, and nuclei [47]. Based on these proposals, the diamond nucleation sequence can be summarized as follows: first, nucleation sites with high local surface energy are generated; second, carbon clusters are formed because of the enhanced surface diffusion; and finally, diamond nuclei grow.

2.3.4 Growth of NCD thin film on Ti6Al4V

Ti6Al4V is a widely used engineering material owning to its superb physical and mechanical properties like high strength, good corrosion resistance, low density, and good biocompatibility. Occasionally, surface modification is needed for long-term use due to its low resistance against wear, fretting fatigue, and erosion. Deposition of wear/corrosion resistant DLC and NCD thin films could be useful to prevent these damages owning to their high hardness and low friction coefficient. In this part, the emphasis will be on the growth of NCD thin films on Ti6Al4V (DLC growth on Ti6Al4V will be discussed in Section 2.4.4).

The earlier attempts to deposit diamond films onto Ti base substrates resulted in weak adhesion due to the high stress caused by the high mismatch of thermal expansion of substrate and diamond coating [48]. In addition, it is hard to deposit diamond on Ti alloys because of the rapid carbon diffusion in Ti. The rapid carbon diffusion in Ti reduces the surface carbon concentration and consequently decreases the diamond nucleation and growth rates [49]. Furthermore, the aggressive conditions during deposition (hydrogen

atmosphere and substrate temperatures of 800 ˚C or above) can lead to a deterioration of the mechanical properties of the base material, in particular, fatigue life and impact strength [50].

After more than a decade of efforts by researchers, deposition conditions in terms of substrate pretreatments, diamond growth, and post treatments have been studied to solve the problems. Deposition at moderate temperature, i.e. equal or less than 600 ˚C, and with the temperature slowly dropping has been investigated to decrease the deterioration of mechanical properties of Ti alloys substrates [23, 50-51]. Vandenbulcke et al. used a lower deposition temperature to decrease the thermal stresses and obtained high film nucleation density [52]. Substrate pretreatments including polishing, seeding, ion implantation, and BEN were used to enhance nucleation [53]. NCD was successfully deposited on curved Ti6Al4V surface by MPCVD [3, 54]. Many researchers have reported improvements in adhesion using various methods ranging from Ar, N_2, O_2, or CO incorporation in CH_4/H_2 plasma [55, 56], increasing CH_4 concentration during the film growth process [1], application of TiN and DLC interlayers [57-58], to post treatment like annealing [50].

2.4 Diamond-like carbon

DLC films with properties falling between those of diamond (sp^3 local bonding) and graphite (sp^2 local boding) have been investigated in the past 40 years.

2.4.1 Structure and properties of Diamond-like carbon

DLC is described as an amorphous carbon material with a significant fraction of sp^3 bonded carbon atoms [18]. The significant fraction of sp^3 bonds makes it have some extreme properties similar to diamond including high hardness, high Young's modulus, and good chemical inertness. Besides that, DLC has some more advantages: relatively

smooth due to its disordered structure without grain boundaries and lower production cost than diamond.

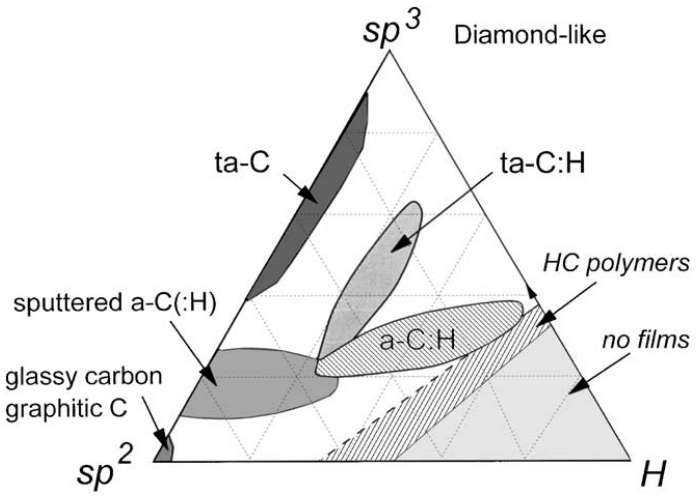

Figure 2-4. Ternary phase diagram of bonding in amorphous carbon-hydrogen alloys [18].

There are two types of DLC: amorphous carbon (a-C) and hydrogenated amorphous carbon (a-C: H). Jacob and Moller used a ternary phase diagram to display the compositions of various forms of amorphous C-H alloys, as shown in Figure 2-4 [59]. The graphitic carbon and glassy carbon with a significant amount of sp^2 bonds lie in the lower left corner. The central area is occupied by the a-C: H with both sp^2 and sp^3 bonded carbon. The hydrocarbon polymers remain at the limits of the triangle in the right corner, beyond which no films can form, and only molecules form [18]. The major properties of DLC are listed in Table 2-2.

Table 2-2. Comparison of major properties of amorphous carbons with those of reference materials: diamond, graphite, C_{60} and polyethylene [18].

	sp^3 (%)	H (%)	Density (g cm^{-3})	Gap (eV)	Hardness (GPa)
Diamond	100	0	3.515	55	100
Graphite	0	0	2.267	0	
C_{60}	0	0		1.6	
Glassy C	0	0	1.3–1.55	0.01	3
Evaporated C	0	0	1.9	0.4–0.7	3
Sputtered C	5	0	2.2	0.5	
ta-C	80–88	0	3.1	2.5	80
a-C:H hard	40	30–40	1.6–2.2	1.1–1.7	10–20
a-C:H soft	60	40–50	1.2–1.6	1.7–4	<10
ta-C:H	70	30	2.4	2.0–2.5	50
Polyethylene	100	67	0.92	6	0.01

2.4.2 Synthesis methods of Diamond-like carbon

The first synthesis of DLC thin films was reported by Aisenberg and Chabot in 1971 [60]. The method employed was ion beam deposition. After that, various CVD and physical vapor deposition (PVD) methods have been developed for DLC deposition. Now DLC thin films can be synthesized by a wide range of techniques, such as plasma enhanced chemical vapor deposition (PECVD), ion beam deposition, sputtering, cathodic arc, pulsed laser deposition, and arc discharge [61-63]. The schematics of different deposition systems are given in Figure 2-5.

Among all the DLC synthesis methods, PECVD is the most common used laboratory deposition method [64]. Sputtering is preferred for industrial processes due to its versatility and ease of scaling up. But the films deposited by this technique usually have low sp^3 content due to the low ratio of energetic ions to neutral species [18, 65]. The cathodic arc method can generate plasma with ion density as high as 10^{13} cm^3. But the unstable cathode spot and insufficient filtering limit its applications [66]. The pulse laser deposition is a laboratory scale method with limited industrial applications [67]. Because

of the ability to independently control the ion energy and the ion current density, the ion beam deposition method has been widely used and adopted to produce DLC thin films in this work, the description of ion beam deposition method will be given in Chapter 3.

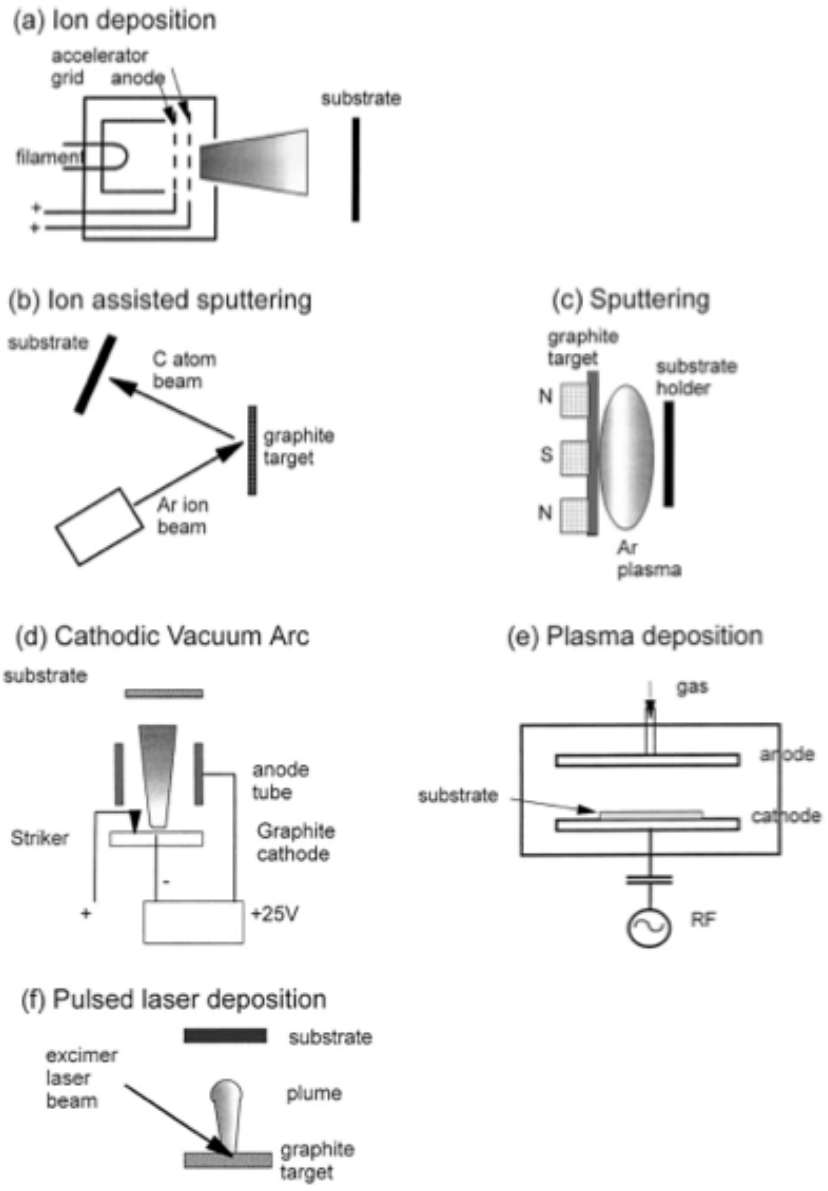

Figure 2-5. Schematics of various deposition systems for DLC [18].

2.4.3 Characterization of Diamond-like carbon

A host of analysis methods are applied for the study of DLC films. Most of them start with a precise determination of the structure of DLC films (sp^3 fraction, uniformity, purity). The most frequently used techniques include Auger electron spectroscopy (AES), X-ray photoelectron spectroscopy (XPS), low/high electron energy loss spectroscopy (EELS), and Raman spectroscopy [68, 69]. Among them, AES measurements can probe the carbon chemical states of DLC for investigation of the deposition mechanism [70]. High energy (~100keV) EELS is the most reliable technique currently available for evaluation of the sp^3 fraction of DLC films [71]. Raman is probably the most common technique for distinguishing different C-C bonds in DLC films [59].

Surface morphology is usually investigated by the use of AFM and SEM. AFM was a powerful technique to accurately measure the surface morphology of DLC films from which the film growth processes can be elucidated [72].

As a protective or tribological coating, DLC is always characterized by a variety of mechanical and tribological tests [59]. The Young's modulus can be determined using an ultrasonic surface wave technique [73]. Hardness is usually measured through indentation techniques and it could also be estimated from the Young's modulus (H=0.1E). Different abrasive tests are performed to evaluate the wear resistance of the films. Pin/ball on disc tests are usually performed for friction coefficient determination and ambient conditions should be taken into account in analysis of the results. Stress measurements are also very often conducted using the beam bending technique. Attention has been paid to the compressive stress build up in DLC films since it limits the maximal thickness of the films [63].

2.4.4 Growth of Diamond-like carbon thin film on Ti6Al4V

DLC film has emerged as a promising surface protective technique for Ti6Al4V. However, one of the greatest challenges of coating Ti6Al4V with DLC is the poor adhesion between DLC thin film and the Ti6Al4V substrate because of the high internal stress in DLC [74].

Various approaches have been used to relieve the internal stress of DLC films in order to enhance adhesion on Ti6Al4V. The adhesion has been enhanced by optimized deposition conditions [75]. Surface hardening treatments, including ion implantation [76], plasma immersion ion implantation [77], nitriding [78] and oxidising [76, 79], and high ion energy induced ion beam mixing [18, 80] were also successful in enhancing adhesion. A carbide-forming adhesion layer such as Si, Cr or W can absorb the effect of compressive stress and improve adhesion [81]. The deposition of hard films including TiN, TiC, TiCN and CrN by physical vapor deposition prior to DLC coating has been attempted [82, 83]. Enhanced adhesion and higher wear resistance were achieved by this kind of 'bilayered' DLC films compared to 'single-layered' DLC films. Similarly, formation of an adhesion layer with gradually varied mechanical characteristics from the substrate to DLC coating has also been investigated introduced, such as, Ti/CN, Ti/TiC, Ti/TiN/TiC, and Ti/TiN/TiCN/TiC [84]. The soft-hard multilayer system has been also employed to enhance adhesion due to stress relaxation and deflection of cross-sectional cracks, such as Ti-DLC and TiC-DLC multilayer [85]. In addition, metal incorporated diamond like carbon (M-DLC) has been developed to enhance the adhesion, in which the homogeneously dispersed metal clusters (Al, Cu, Ti, W, etc.) can significantly reduce the stress in DLC thin films [86]. Using those approaches, enhanced adhesion of DLC on

Ti6Al4V has been achieved. However, the enhancement is not so significant and sometimes at the expense of hardness [18].

CHAPTER 3
EXPERIMENTAL EQUIPMENTS AND CHARACTERIZATION TECHNIQUES

In this thesis work, a HFCVD and a MPCVD reactor in the Plasma Physics Laboratory of University of Saskatchewan were used for deposition of diamond, TiN, and W interlayer and an ion beam system was employed for DLC deposition. This chapter will provide detailed description of these three systems. SEM, AFM, Raman spectroscopy, XRD, synchrotron based NEXAFS, and nanoindentation testing were used to characterize the microstructure, chemical bonding, and mechanical properties of the as-deposited materials and indentation testing using Rockwell indentation tester and Vickers hardness tester were used to evaluate the adhesion of deposited films. Principles and descriptions of these analyzing techniques will also be given in this chapter.

3.1 Experimental equipment

3.1.1 CVD reactors

CVD is the deposition of solid materials onto a heated surface from a chemical reaction in the vapor phase. A schematic illustration of CVD is shown in Figure 3-1, in which, a reducing agent (usually H_2) is used for reducing a gaseous compound.

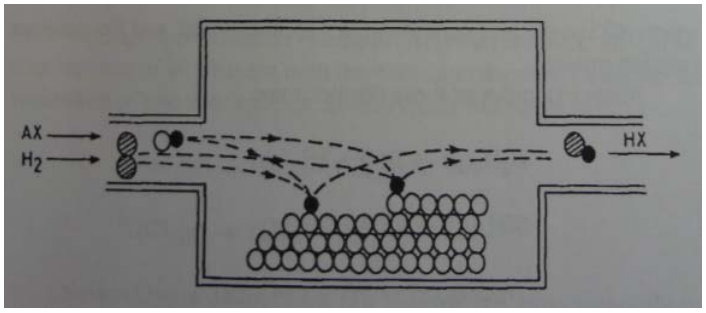

$2AX(g)+H_2(g)$ ---$2A(s)+2HX(g)$

Figure 3-1. Schematic of the CVD process [87].

MPCVD. MPCVD is one of the plasma enhanced CVD methods. The first MPCVD reactor designed at NIRIM consists of a waveguide, which is perpendicularly penetrated by a quartz tube of 40-55 mm in diameter [88]. A schematic of MPCVD reactor is presented in Figure 3-2, where microwave (usually 2.45 GHz, a typical industrial frequency) is directed along a waveguide and is coupled into the chamber via an antenna. The microwave passes through a quartz window and into the reactor. The substrate holder is usually made of Mo or stainless steel, and placed at the location where the quartz tube and the waveguide meet.

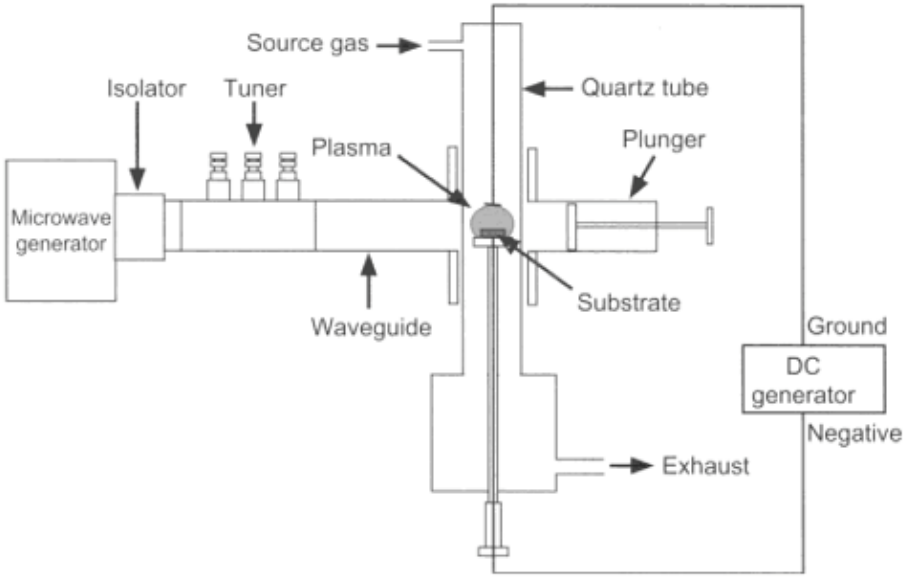

Figure 3-2. Schematic of the NIRIM-type MPCVD reactor [21].

There are some advantages of MPCVD over other CVD methods. First, it is clean since it is electrode-free, without high potentials to cause sputtering. Second, the plasma density can be very high. Third, the reproducibility of diamond film deposition is the best among all the CVD methods. A MPCVD manufactured by Plasmionique Inc. (model number: MWPECVD 1250UOS) (as shown in Figure 3-3) was used to synthesize NCD thin films and particles on

Ti6Al4V in this thesis work. CH_4 and H_2 mixture was used as precursor. For diamond deposition, typical conditions were as follows: gas pressure P=30 Torr, microwave power P_m=500~1200 W, gas mixture: 0.5 vol.% CH_4 +H_2, and gas flow rate: 100 sccm in total.

Figure 3-3. MPCVD reactor (MWPECVD 1250UOS, 2.45 GHz).

HFCVD. In the HFCVD technique, the required atomic hydrogen is produced with electrically heated glowing filaments made from refractory metals (W, Ta, or Re) [89]. The filaments are held above the substrate and the distance between them ranges from 5 to 10 mm. A schematic structure of the reactor is shown in Figure 3-4. The pressure of the gas is usually kept at 20~30 Torr. A bias voltage could be applied either to the filaments or the substrate for bias enhanced deposition. During diamond deposition by HFCVD, C-H radicals and atomic hydrogen

are produced by thermally decomposing CH_4 and H_2 molecules and these C-H radicals and atomic hydrogen diffuse onto the substrate, forming diamonds [21].

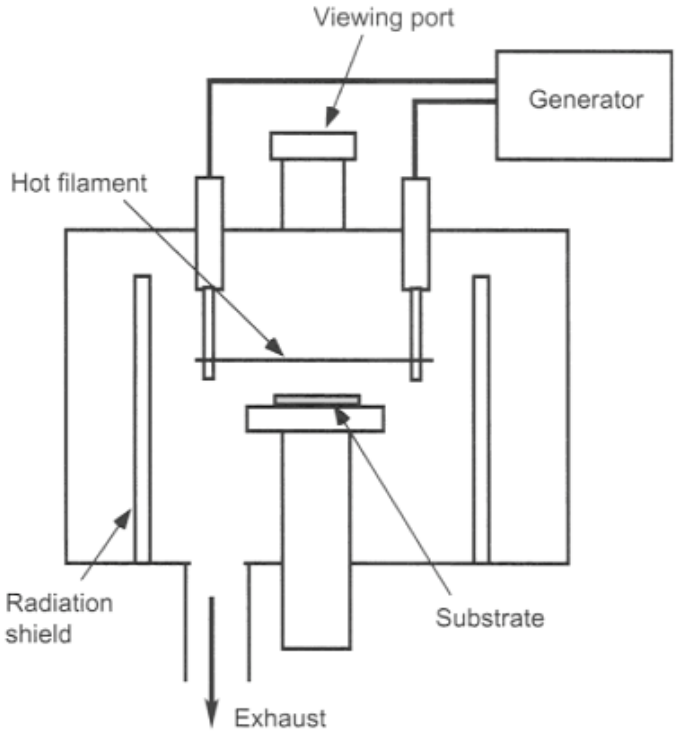

Figure 3-4. Schematic diagram of a HFCVD reactor [21].

The main advantage of HFCVD reactor is the simplicity of the system. However, the reproducibility of diamond film deposition by HFCVD is inferior compared to that of MPCVD.

The custom-made HFCVD reactor used in this thesis work is shown in Figure 3-5. There are four major components in this HFCVD reactor: a gas flow system, a pumping system, a vacuum chamber, and an electric power supply. The vacuum chamber is made from a cross-shaped glass vessel with four round openings of 150 mm in diameter. The pumping system includes a mechanical pump and a diffusion pump. The flow rate of the precursor gas is measured by a two-channel gas flow meter and adjusted manually. Electric current is applied to the W filament and

the heat thus generated activates the precursor gas mixture into fragmented hydrocarbons and atomic hydrogen to form diamonds. A thermocouple is installed beneath the substrate holder for substrate temperature measurement.

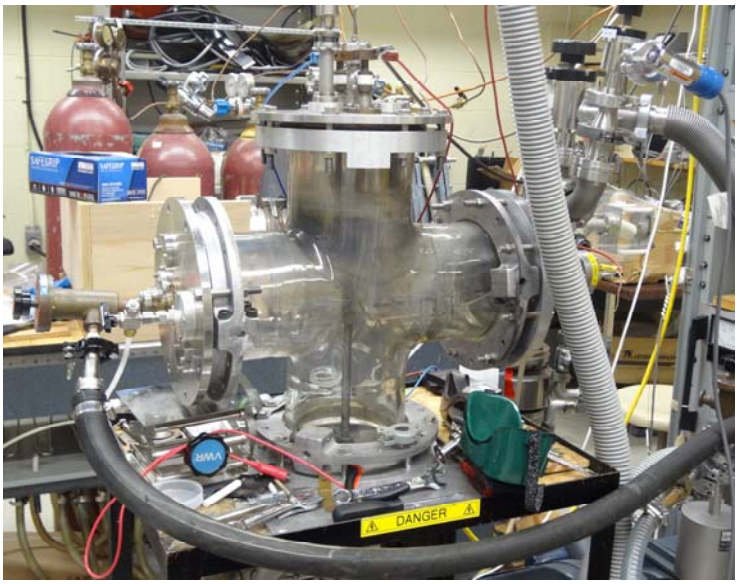

Figure 3-5. HFCVD reactor used in this work.

3.1.2 Ion beam deposition system

The End hall ion beam system manufactured by 4Wave is used in this thesis work for DLC films deposition. Its schematic structure is shown in Figure 3-6. The main components include a high vacuum chamber, a high vacuum pumping system, two ion sources (one for direct ion beam deposition and the other for sputtering), a substrate holder that can be rotated from 0 to 90 degree, and a target assembly with 4 targets.

(a)

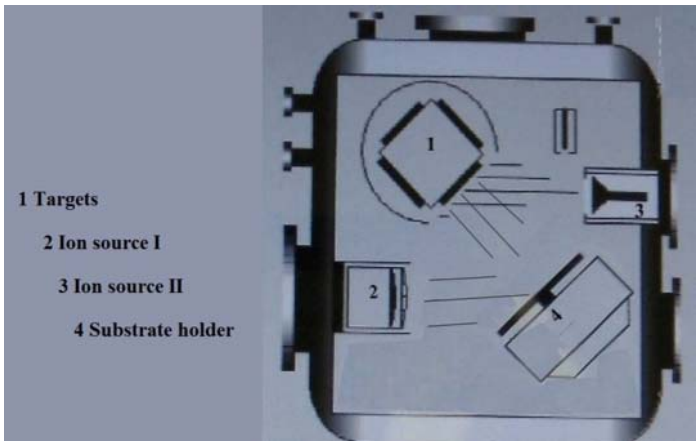

(b)

Figure 3-6. (a) End hall ion beam deposition system and (b) its schematic structure.

The deposition system can be used for the deposition of DLC thin films either by direct ion beam deposition or by ion beam assisted sputtering deposition. Direct ion beam deposition was

adopted in this work. In DLC deposition process, hydrocarbon and Ar radicals and ions are produced by decomposing and ionizing CH_4 and Ar precursor gases in the ion source. Such radicals are then directed to bombard the surface of the substrate, thus forming DLC thin films.

3.2 Main characterization techniques

Characterization of structure and property is very important in materials research and development. In this work, a very wide variety of techniques were used for characterize surface morphology, microstructure, composition, mechanical properties and adhesion of the deposited materials.

3.2.1 Morphological characterization

The characterization of surface morphology of coating materials is of significant importance as it is related to some surface related properties including tribological properties and wettability. Widely used morphological characterization techniques include SEM and AFM.

SEM. SEM is one of the most versatile techniques to characterize the surface morphology and chemical composition of materials. The first SEM used for surface characterization was developed at the RCA laboratory in the United States [90]. The principal structure of SEM is shown schematically in Figure 3-7 [91]. In the electron source, the electrons are emitted thermionically from a tungsten filament cathode or produced by field emission, and then accelerated and focused to form a beam by electrical and magnetic field optics. The focused beam of high-energy electrons (typically 30 keV) is then hit the specimen, causing three kinds of effects in the backward direction, which include high energy electrons being scattered backward, secondary electrons (typical energy lower than 50 eV) being knocked out from the specimen surface and escaping backward, and X-rays emitting from the specimen in all directions. Those signals are amplified by various electronic amplifiers and then displayed and recorded in a computer terminal. The resulting SEM images are actually distribution maps of the signal

intensities, providing details of the scanned area of the specimen. In order to prevent electrostatic charge accumulation on the surface, the specimen is required to be electrically conductive or with electrically conductive coating and to be grounded.

SEM can generate images with resolution down to a few nanometers, compared to several hundred nanometers for optical microscopes. In addition, the large depth of view in SEM allows it to image rough surfaces.

In this research, a JSM-6010LA SEM manufactured by JEOL with a maximum resolution of 5 nm (located in the Department of Mechanical Engineering, University of Saskatchewan) was used to characterize the surface morphology of the deposited materials, as shown in Figure 3-8. The operating voltage used was 15 kV.

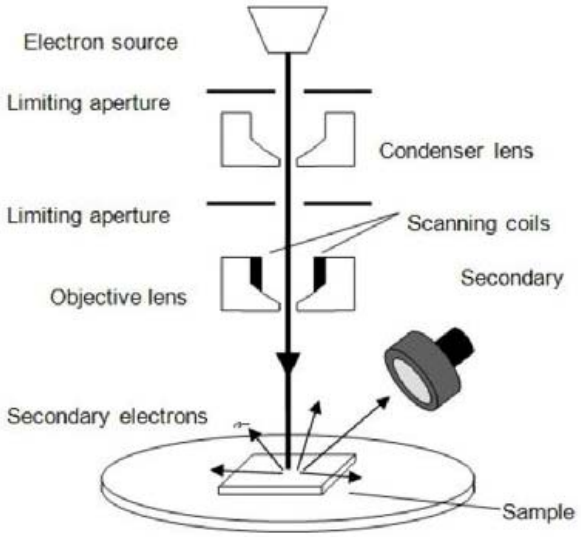

Figure 3-7. Schematic diagram of a SEM [91].

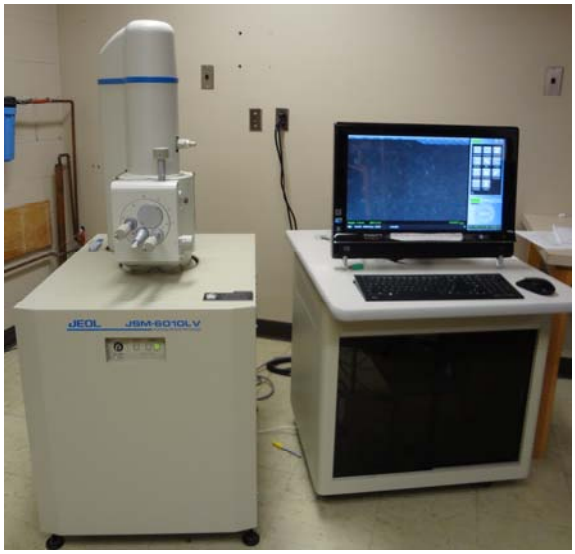

Figure 3-8. JSM-6010LA SEM manufactured by JEOL.

AFM. Compared to SEM, AFM is usually used for generating three-dimensional images of surface with higher resolution. It can be used to study conductors, semiconductors and insulator materials. The AFM technique was developed by Binning, et al. in 1986 to measure ultra small forces on the order of 1 nN or less presented between the AFM tip surface and a sample surface [92]. The tip is fixed at the end of a flexible cantilever, which is usually made of silicon. During operation, the tip scans across the sample surface. The schematic of a typical AFM is shown in Figure 3-9.

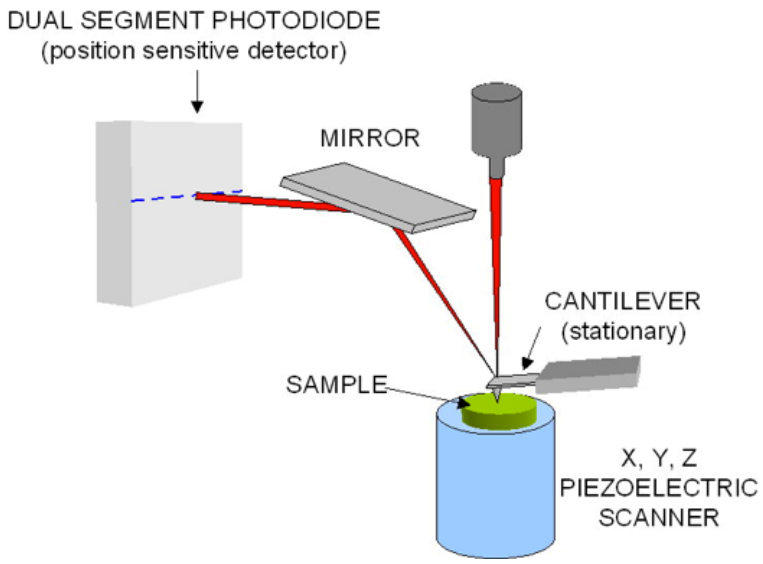

Figure 3-9. Schematic diagram of AFM [93].

The most commonly used operation modes of AFM are contact and tapping modes. In contact mode, as its name suggests, the tip is always kept close physical contact with the sample surface during scanning. The interaction force between the tip and sample surface is repulsive, and it is kept constant during scanning, causing the cantilever to bend with the changes in topography. Simultaneously, the cantilever deflection is monitored and compared with a desired value. The feed back circuit applies a voltage to the piezoelectric scanner to raise or lower the sample surface for maintaining a constant cantilever deflection. The image is generated from the lateral positioning of the scanner. In contact mode, sample surface damage may occur if high contact force is used. In tapping mode, the cantilever is driven to oscillate up and down making the tip to tap the sample surface, which can avoid damage caused by dragging the tip across the surface . The interaction force between tip and sample surface in tapping mode is the Van der Waals force. Tapping mode is suitable for the imaging of soft materials and surfaces that are easily damaged.

The main advantages of the AFM methods include: its flexibility by using different types of cantilevers and its operation in ambient air or liquid environment. The disadvantages are: the influence of surface topography on the torsion signal; the accuracy of the spring stiffness of the cantilever being used; and the adhesion effects between the cantilever and the sample surface. The maximum height of features can be imaged by AFM is on the order of micrometers. And an image captured by AFM can only cover an area up to around 150 by 150 micrometers.

In this thesis work, a PicoSPM instrument (Molecular Imaging, Tempe, AZ) was used for contact mode AFM measurements. It is located at the Saskatchewan Structural Science Center (SSSC), University of Saskatchewan.

3.2.2 Chemical and structural characterization

Raman spectroscopy. Raman spectroscopy, which is based on Raman effect (inelastic scattering of monochromatic light from a laser source), has been widely used to analyze the bonding structure of different carbon materials. Raman spectroscopy mainly consists of three components: a light source, an optical system (for collecting the scattered light from the sample), and a detection system, as shown in Figure 3-10. In Raman operation, the monochromatic light emitted from the laser source interacts with molecular vibrations on the sample surface, resulting in a shift of energy of the laser photons. The scattered light is then collected and detected with shifted wavelength, which gives information about the vibrational modes of the molecular system of the material under testing.

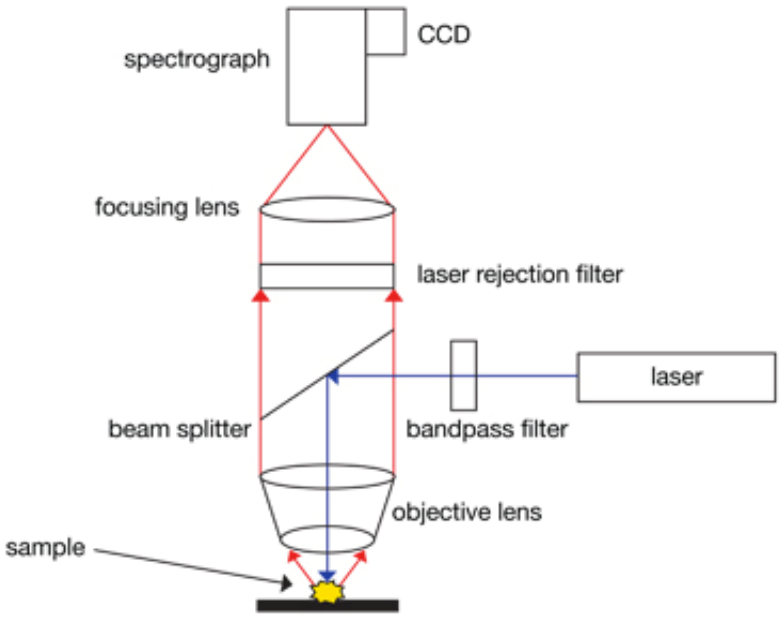

Figure 3-10. Schematic of Raman spectroscopy [94].

The interpretation of Raman spectra involves comparing the measured spectra with reference spectra. The typical Raman spectra of diamond, graphite and some disordered carbons are presented in Figure 3-11. Diamond has a single sharp peak at 1332 cm^{-1}. Single crystal graphite peaks at 1580 cm^{-1}, labeled 'G' for 'graphite'. Besides the 'G' band at 1580 cm^{-1}, DLC shows a disordered 'D' band at around 1350 cm^{-1}, corresponding to breathing vibrations of rings at the K zone boundary [95].

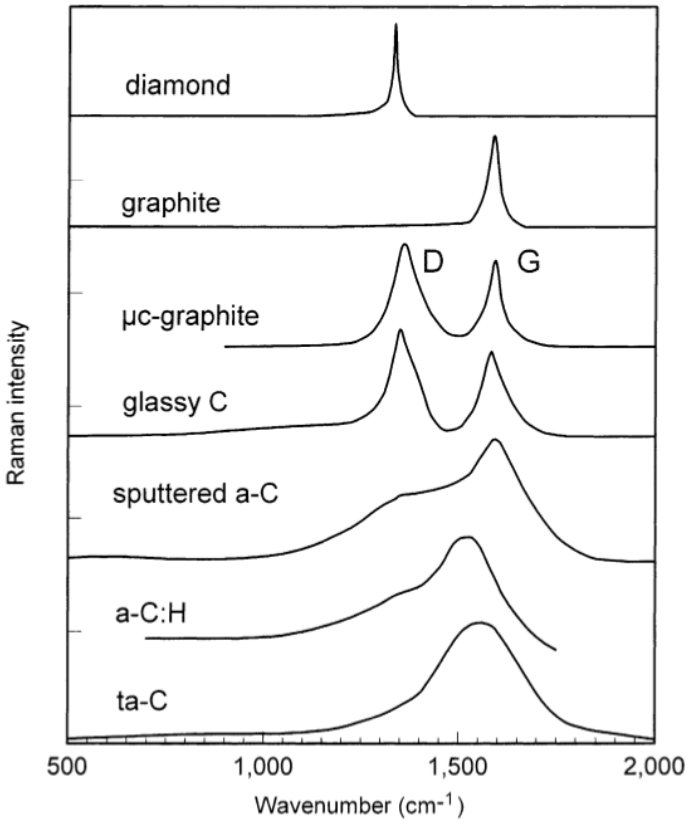

Figure 3-11. Comparison of typical Raman spectra of carbons [18].

In this research, the Raman spectra of diamond and DLC were obtained using a Renishaw micro-Raman system 2000 spectrometers located at the Saskatchewan Structural Science Center (SSSC), University of Saskatchewan. The operating laser wavelength was 514.5 nm.

XRD. Since each material has its own specific X-ray diffraction pattern, the x-ray diffraction is used for investigating the crystal structure of materials. One can take crystalline materials as multilayered structures. When X-rays strike the sample surface, those incident X-rays with wavelength satisfying Bragg's Law ($n\lambda=2d\sin\theta$) can be diffracted, as shown in Figure 3-12, where d is the distance between two crystal planes, θ is the X-ray incident angle, λ is the X-ray wavelength, and n is an integer multiplier. As such, the lattice spacing can be calculated based on the wavelength of the incident X-ray and the diffraction angle. Typically, the interpretation of the

XRD results involves comparing the measured lattice spacings (d) with standard reference patterns [96].

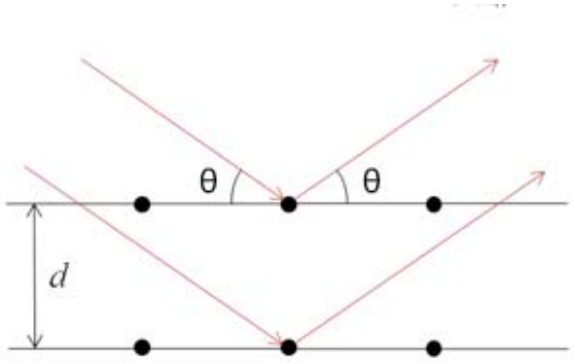

Figure 3-12. A schematic diagram of Bragg's Law [97].

A typical X-ray diffractometer consists of four basic components: an X-ray source, a sample stage, an X-ray detector, and a rotary stage for changing the angle θ, as shown in Figure 3-13. Among them, the X-ray source and the X-ray detector lie on the circumference of a "focusing circle" [98]. In XRD operation, X-ray is generated in a cathode ray tube by bombarding the target (Cu, Co) with accelerated electrons, which are in turn produced by heating a filament. After that, the X-ray is focused and strikes the sample surface at an angle θ (θ is increased over time). Meanwhile, the diffracted X-ray is received by the detector at 2θ with respect to the source path. The intensities of the diffracted X-rays and the angles 2θ are recorded to create a XRD pattern.

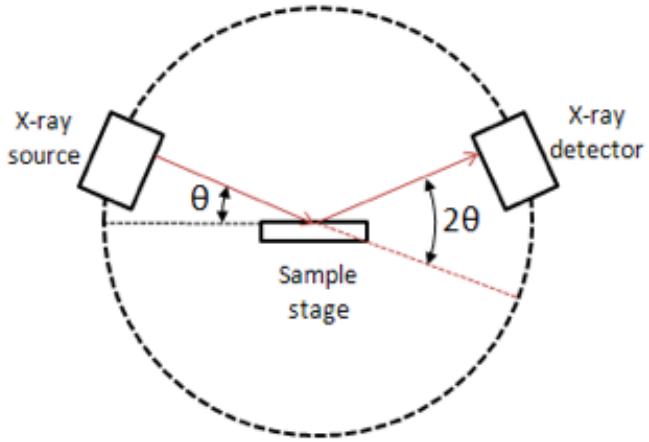

Figure 3-13. Schematic of a powder X-ray diffractometer [97].

XRD patterns in this thesis work were measured by a Rigaku diffractometer in Plasma Physics Laboratory, University of Saskatchewan, which uses X-rays of the Co Kα line (λ=0.178 nm), produced by impinging an electron beam on a Co target.

Synchrotron based NEXAFS. NEXAFS is suitable for characterizing the chemistry and structure of surface layers. Furthermore, investigation of the molecular structure of ultra-thin surface films can be achieved by NEXAFS using highly polarized synchrotron light sources [99, 100]. The working principle of NEXAFS involves the excitation of electrons from a core level to unoccupied electronic states when the incident X-rays has sufficient energy. This decay of core electrons occurs via the emission of Auger electrons, which are detected by a detector, resulting in a NEXAFS electron yield spectrum (Figure 3-14). In the excitation process, the emission of fluorescent photons may also occur, which originate from a deeper surface level (around 200 nm, while Auger electrons are emitted from surface within 10 nm), as shown in Figure 3-14. Thus, this technique is both surface and bulk sensitive and it is capable to probe the molecular orientation and bonding structure from bulk to the specimen surface [101].

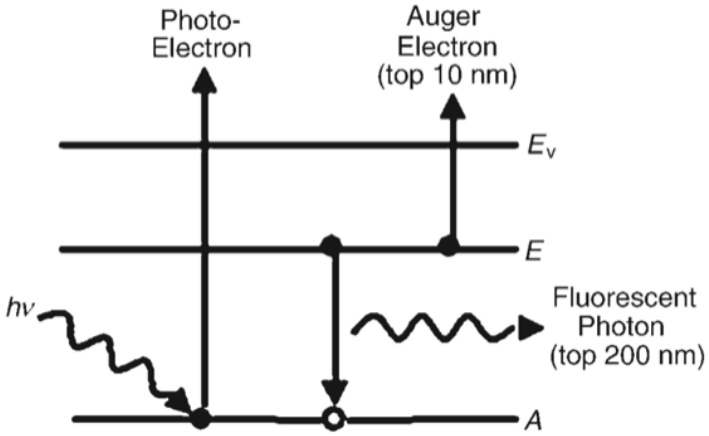

Figure 3-14. Schematic representation of the basic theory of NEXAFS [101].

Figure 3-15 shows the C K-edge NEXAFS spectra of three typical carbon materials recorded in total electron yield (TEY). For CVD diamond film, a sharp spike at 289 eV as well as a large dip at 302 eV can be found. While for graphite, the characteristic peak is at 285 eV, attributed to the sp^2 bonded carbon of π^* states. DLC shows both π bonding and σ bonding features. In this thesis work, The NEXAFS experiments were performed using the high-resolution spherical grating monochromator (SGM) beamline at the Canadian Light Source Inc. (CLS), University of Saskatchewan. NEXAFS was recorded in TEY mode by monitoring the sample current.

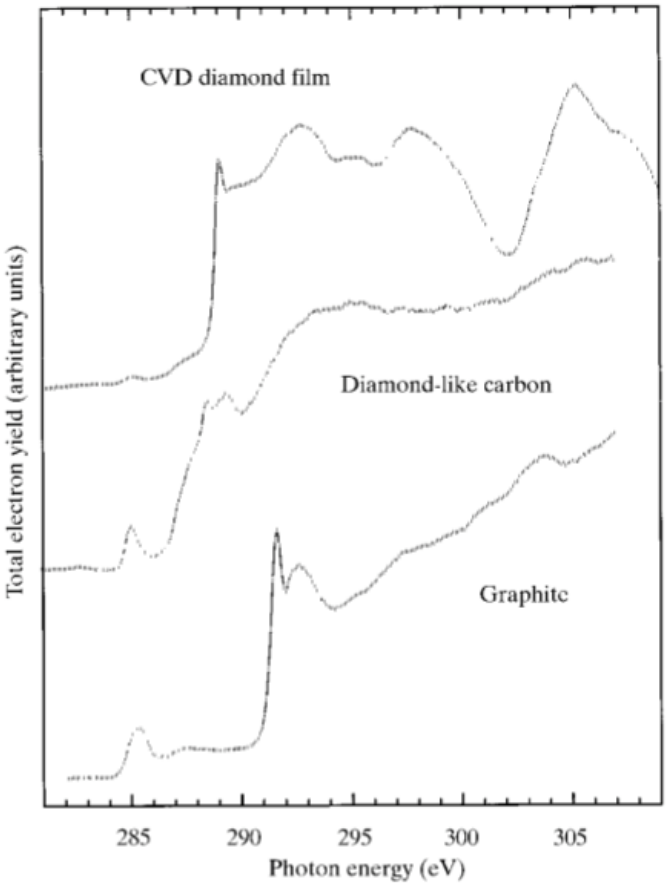

Figure 3-15. C K-edge photoabsorption spectra of diamond, diamond-like carbon and graphite [102].

3.2.3 Mechanical characterization

Nanoindentation testing. Nanoindentation is recently widely adopted for the investigation of mechanical properties of materials at the nanoscale [103]. The first use of nanoindentation was for obtaining the hardness of small volumes of materials and developed in the mid-1970s. A typical nanoindentation tester consists of three main components: a motorized stage, an indenter, and a displacement sensor for measuring the indenter displacement (Figure 3-16). The indenter tip is usually made of diamond and formed in pyramid shape. During nanoindentation experiments, the applied force and the resulting displacement are recorded when the indenter tip

is pressed into the sample surface, resulting in a load-displacement curve (often called the *P-h* curve) [104]. Meanwhile, specifically designed computer software is used for the identification of hardness and Young's modulus through analyzing the measured *P-h* curves.

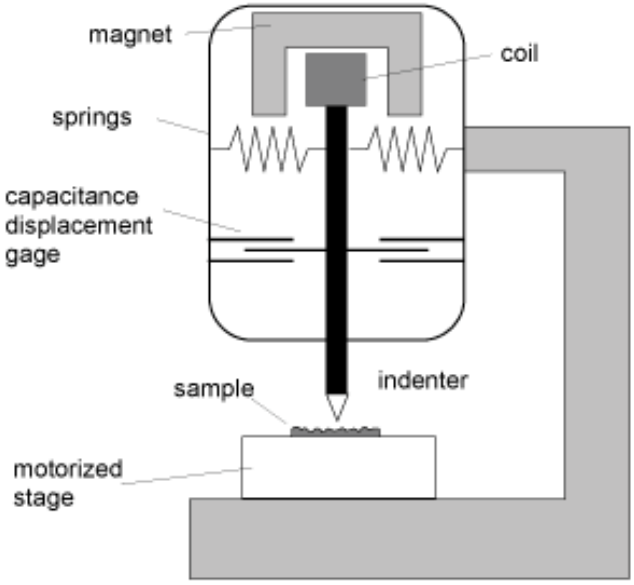

Figure 3-16. Schematic of a nanoindentation tester [105].

In this thesis work, mechanical properties (hardness and Young's modulus) of thin film samples were measured by the Berkovich nanoindenter in the department of Mechanical Engineering, University of Saskatchewan, which was manufactured by Centre for Tribology Inc.

Adhesion evaluation by indentation testing. From a common point of view, adhesion evaluation is the measurement of the force required to separate two different materials that attached to each other. Mittal [106] suggested that adhesion could be categorized as basic adhesion and practical adhesion. Basic adhesion attributes to the intermolecular or interatomic interactions, in electrostatic, chemical, or van der Waals type. On the other hand, practical adhesion reflects the forces of separating two adhering substances, which depends on factors

including measurement technique, specimen size and geometry, temperature, etc. It is noted that adhesion measurement techniques measure practical adhesion.

Among all the adhesion test methods, indentation and scratch tests are the two mechanical methods that have been used extensively. Both methods are simple, reliable, and utilized by commercially available equipment. Semiquantitative results can be obtained by the scratch test. In this thesis work, indentation test was adopted for adhesion evaluation due to the availability.

The early use of indentation test for adhesion measurement was reported by Engel and Pedroza [107]. Figure 3-17 shows a schematic of the indentation test. In adhesion evaluation of a coating system, an indenter is gradually pressed into the coating. At the edge of the indenter, cracking and delamination of the coating may occur and extend outwards [108]. The resistance to propagation of the crack along the interface is then used as a measure of adhesion of the coating system. The most widely used indentation tests include the Rockwell, Vickers, Brinell, and Knoop tests [109].

The indentation test has a number of clear advantages, including being applicable to a wide range of coating/substrate system, easy operation and sample preparation, and the availability of commercial equipment. The main disadvantages are that it is destructive and the loading and resulted delamination mechanism is complicated, making it difficult for quantitative analysis.

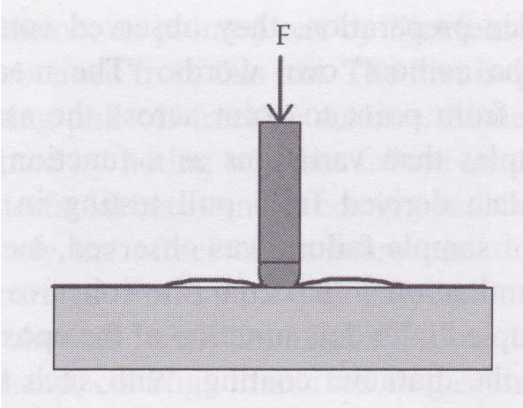

Figure 3-17. Idealized representation of indentation test [108].

In this thesis work, Rockwell and Vickers indenting tests were used for adhesion evaluation of deposited films.

CHAPTER 4
INVESTIGATION OF ADHESION OF DIAMOND-LIKE CARBON ON TI6AL4V

Adhesion of DLC thin films on Ti6Al4V substrates was investigated using direct ion beam deposition with ion energy varying from 65 eV to 100 eV. The samples prepared were characterized by Raman spectroscopy, synchrotron near-edge X-ray absorption fine structure spectroscopy, scanning electron microscopy, X-ray diffraction, and nanoindentation testing. Indentation testing by Vickers hardness tester was used for adhesion evaluation. Results show that the adhesion of DLC thin films on Ti6Al4V substrates mainly depends on ion energy used in the deposition process. Higher ion energy resulted in higher sp^3 concentration of DLC thin films but lower adhesion of DLC on Ti6Al4V substrates, in which ion energy of 70 eV shows the best adhesion. Interlayers of NDP, W, and TiN were applied for adhesion enhancement of DLC thin films on Ti6Al4V. Results show that better adhesion was achieved by incorporated NDP compared with W and TiN interlayers due to greatly enhanced interfacial bonding.

4.1 Introduction

DLC thin films are usually sought for in many applications due to their extreme hardness, stiffness, corrosion resistance, good biocompatibility and tribological properties [18]. In particular, deposition of DLC thin film on Ti alloy is considered an important goal in biomedical engineering because of the profound commercial importance of enhancing the wear resistance of Ti alloys used for orthopedic implants [110].

However, DLC thin films often suffer from poor adhesion on Ti alloy [111, 112]. Various approaches have been used to enhance adhesion of DLC thin films on Ti alloys: (1) optimization of deposition conditions; (2) surface treatment of the substrate, including ion implantation, plasma immersion ion implantation, nitriding and oxidizing, (3) deposition of an interlayer, including a single (Si, Cr, W, TiN, TiC, TiCN and CrN), or a graded layer (Ti/CN, Ti/TiC,

Ti/TiN/TiC, and Ti/TiN/TiCN/TiC), (4) incorporation of a metal or metal compound layer to form alternative multilayered films such as Ti/DLC and TiC/DLC, and (5) incorporation of non-metallic or metallic elements such as Si, Al, Cu, Ti, and W into DLC films [113]. However, the enhancement of adhesion is limited.

In this work, the effect of ion energy on adhesion of resulted DLC thin films on Ti6Al4V is studied. Widely used adhesion enhancing interlayers of W and TiN are also applied between DLC thin films and Ti6Al4V substrates for comparison with our newly developed NDP incorporation method [113] for adhesion enhancement of DLC on Ti6Al4V, to demonstrate the good performance of the NDP incorporation method and reveal the adhesion enhancement mechanism.

4.2 Experimental details

Ti6Al4V sheets with dimensions of 10 mm × 10 mm × 1 mm were ground and polished using silicon carbide paper (350 grit), 9 μm diamond slurry, and 3 μm diamond slurry sequentially and then cleaned in ethanol for 15 min. The prepared sheets were used as substrates for nanodiamond and DLC thin film deposition.

Nanodiamond deposition on Ti6Al4V was conducted in a 2.45 GHz MPCVD reactor, with a gas mixture of methane CH_4 and hydrogen H_2. Before deposition, the sheets used for nanodiamond deposition were ultrasonically seeded for 1hr in a suspension of ethanol and nanodiamond powder (average crystal size of 4–5 nm) to enhance diamond nucleation, followed by ultrasonic cleaning, rinsing in ethanol and drying in air. The deposition parameters are listed in Table 4-1.

Table 4-1. Deposition condition of NDP on Ti6Al4V by MPCVD.

Parameters	First step (nucleation enhancement)	Second step (diamond growth)
H_2 flow rate (sccm)	40	199
CH_4 flow rate (sccm)	10	1
Total flow rate (sccm)	50	200
Gas pressure (kPa)	4	4
Microwave power (W)	600	600
Temperature (°C)	350	350
Deposition time (min)	10	60

W interlayer was deposited on Ti6Al4V by sputtering using a HFCVD reactor, described in a previous work [114], in an argon environment. The deposition parameters are listed in Table 4-2.

Table 4-2. Deposition condition of W interlayer sputtered on Ti6Al4V by HFCVD.

Bias (V)	Current (A)	Ar flow rate (sccm)	Temperature (°C)	Gas pressure (kPa)	Deposition time (min)
500	8	20	470	1.33	40

TiN interlayer was deposited on Ti6Al4V using the same HFCVD reactor in argon and nitrogen environment. The deposition parameters are listed in Table 4-3.

Table 4-3. Deposition condition of TiN interlayer deposited on Ti6Al4V by HFCVD.

Bias (V)	Current (A)	Ar flow rate (sccm)	N_2 flow rate (sccm)	Temperature (°C)	Gas pressure (kPa)	Deposition time (h)
500	8	50	20	490	1.33	4

DLC thin films deposition was conducted using an End-Hall (EH) ion source (KRI EH-1000, manufactured by Kaufman & Robinson, Inc. USA) in an ion beam deposition system [115]. The sample stage was tilted 45° with respect to the ion beam, the ion source was supplied with 5

sccm of methane and the mean ion energy of the beam used ranging from 60 eV to 100 eV as listed in Table 4-4. The deposition was performed without any additional substrate heating and with duration of three hours. The chamber base pressure was 2.67×10^{-5} Pa and the working pressure was 1.2×10^{-1} Pa. The thickness of the as-deposited DLC thin film was approximately 150 nm.

Table 4-4. Deposition conditions of DLC thin films on Ti6Al4V.

Ion energy (eV)	CH_4 flow rate (sccm)	Temperature (°C)	Deposition time (h)
60, 70, 75, 80, 90	5	30	3

The morphology, microstructure, and chemical bonding of the as prepared particle and film samples were characterized by SEM, Raman spectroscopy, NEXAFS, and XRD. The Raman spectrometer was operated at a laser wavelength of 514 nm generated by an argon laser. The adhesion of DLC thin films on Ti6Al4V was examined by Vickers hardness indentation tests at a load of 1000N.

4.3 Results and discussion

Figure 4-1 shows the Gaussian-fitted Raman spectra of DLC thin films directly deposited on Ti6Al4V by different ion energy ranging from 60 eV to 80 eV. All the spectra show two broad peaks centered at around 1350 cm^{-1} (D band) and 1580 cm^{-1} (G band), a typical DLC feature [113]. The intensity ratio of D and G band, I_d/I_g, obtained from Gaussian line simulations for all the samples are listed in Table 4-5. It can be seen that the I_d/I_g value depends on ion energy, as shown in Figure 4-2. The I_d/I_g value decreases with the increase of the ion energy used in DLC deposition process. According to Ferrari *et al.*, the sp^3 bond content in DLC thin films increases

with the decrease of I_d/I_g value [116]. So it can be concluded that the content of sp^3 bonded carbon increases with the increase of the ion energy used in DLC deposition process.

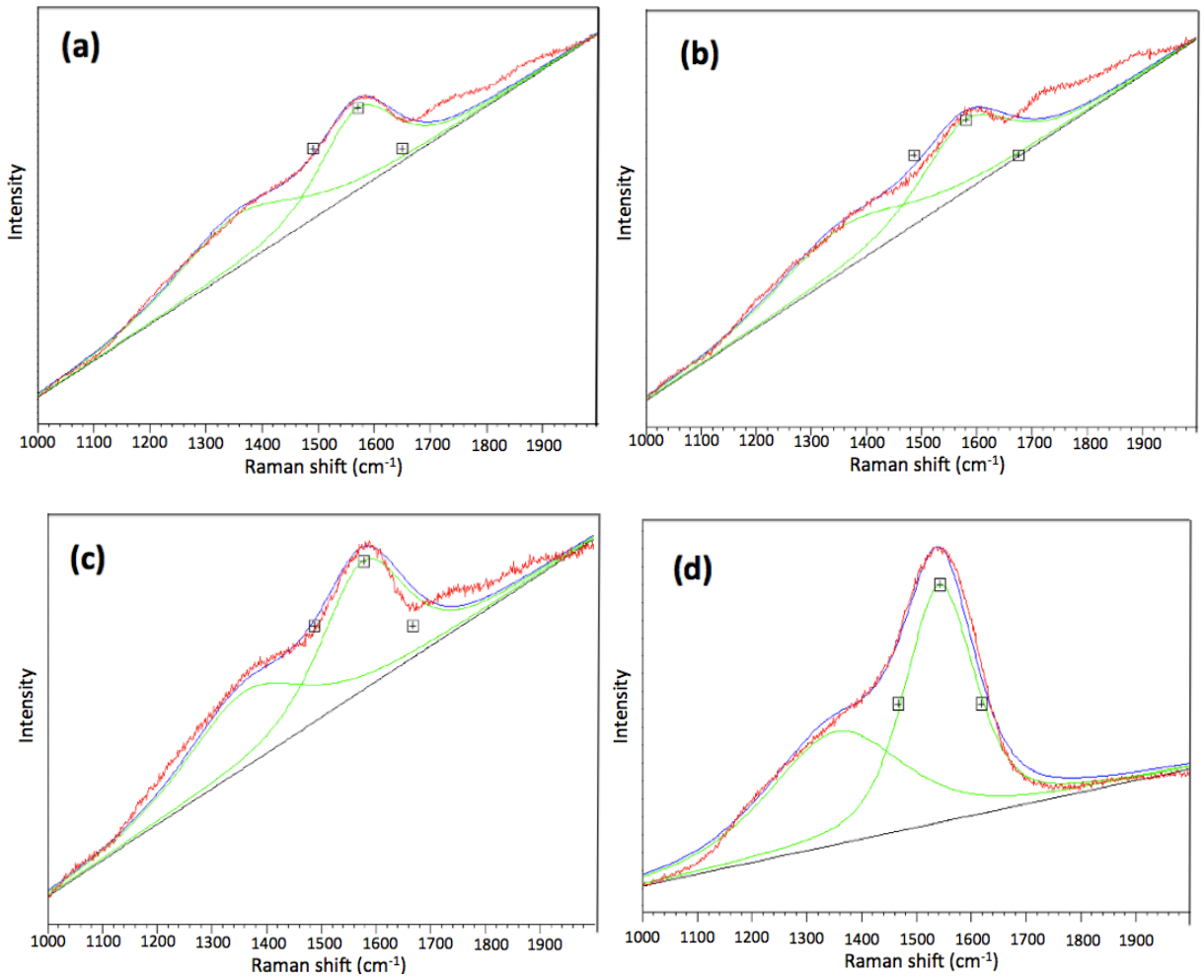

Figure 4-1. Gaussian-fitted Raman spectra of DLC coatings grown on Ti6Al4V by different ion energy: (a) 60 eV, (b) 70 eV, (c) 75 eV, (d) 80 eV.

Table 4-5. I_d and I_g ratio of DLC thin films on Ti6Al4V deposited with varying ion energy.

Ion energy (eV)	60	70	75	80
I_d/I_g	1.0289	0.9109	0.8256	0.7184

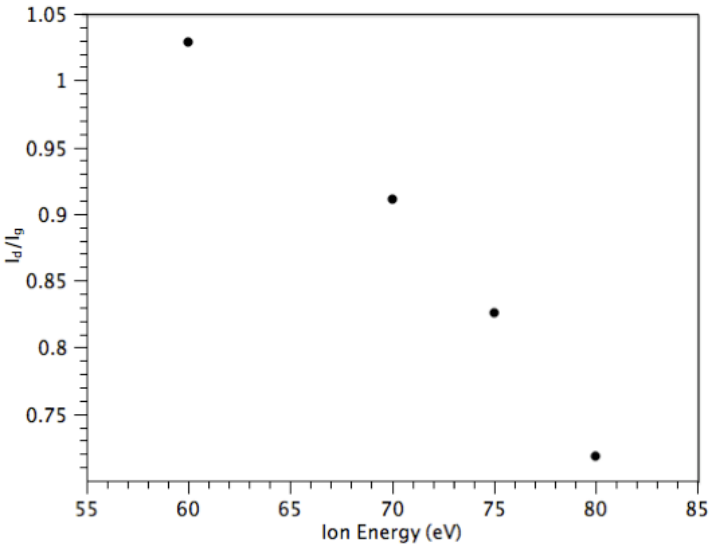

Figure 4-2. Variation of the I_d/I_g with ion energy of DLC coatings grown on Ti6Al4V.

Indentation testing was conducted at a load of 1000 N to evaluate the adhesion of DLC thin films directly deposited on Ti6Al4V with varying ion energy. Figure 4-3 shows the typical SEM images of DLC thin films after indentation testing (Figure 4-3 a-c) and without indentation testing (Figure 4-3 d). The light area corresponds to the exposed substrate, and the dark area corresponds to the film remaining adhered to the substrate. For the samples #a to #c with ion energies ranging from 60 eV to 75 eV, partial spallation or cracking of the films is observed in the areas around the imprint. For sample #a with an ion energy of 60 eV, the spallation area accounts for about half of the imprint area, and small pieces of delaminated film can be found at the edge of the imprint, as shown in Figure 4-3 (a). With the ion energy increased to 70 eV, much less spallation of the film is observed on sample #b, and cracking instead of spallation can be found at most of the area in the imprint, as shown in Figure 4-3 (b), suggesting good adhesion of DLC on Ti6Al4V. With the ion energy further increased to 75 eV, more spallation area can be

observed indicating poor adhesion, as shown in Figure 4-3 (c). With the ion energy increased to 80 eV, the DLC thin film cracks and delaminates from Ti6Al4V substrate even without indentation. The spallation area accounts for almost half of the total film area. And with the ion energy increased up to 90 eV, no DLC deposition is achieved on Ti6Al4V by direct ion beam deposition in this work. So the best adhesion happens at the ion energy of 70 eV. As Robertson reported, the best deposition process that induces the highest sp^3 bonded carbon of DLC involves "a carbon ion flux at about 100 eV per carbon atom" [18]. However, it is impossible for DLC grown on Ti6Al4V substrate at this high ion energy by direct ion beam deposition in this work. The adhesion failure of DLC on Ti6Al4V deposited with ion energy ranging from 80 eV to 100 eV is due to the significant compressive intrinsic stress in DLC thin film induced by the film deposition process-energetic particles bombardment of the film surface. The magnitude of the intrinsic stress depends on the film-substrate structure and the impact energy per atom [117]. For DLC grown on Ti6Al4V substrate, best interfacial adhesion happens at ion energy of 70 eV, and the adhesion of film decreases with increases of the ion energy when the ion energy used is higher than 70 eV, indicating that DLC deposition on Ti6Al4V at ion energy of 70 eV ensures the lowest intrinsic stress. When ion energy increases, the excessive stress level may induce delamination of film [117].

When adhesion failure for a given film-substrate structure cannot be avoided, application of interlayer is promising for producing mechanical stable film-substrate structures. In this work, NDP was chosen due to its chemical, mechanical, and structural similarity to DLC to minimize the free energy of the formed interface [118]. Widely used adhesion enhancement interlayers of W and TiN were applied for comparison.

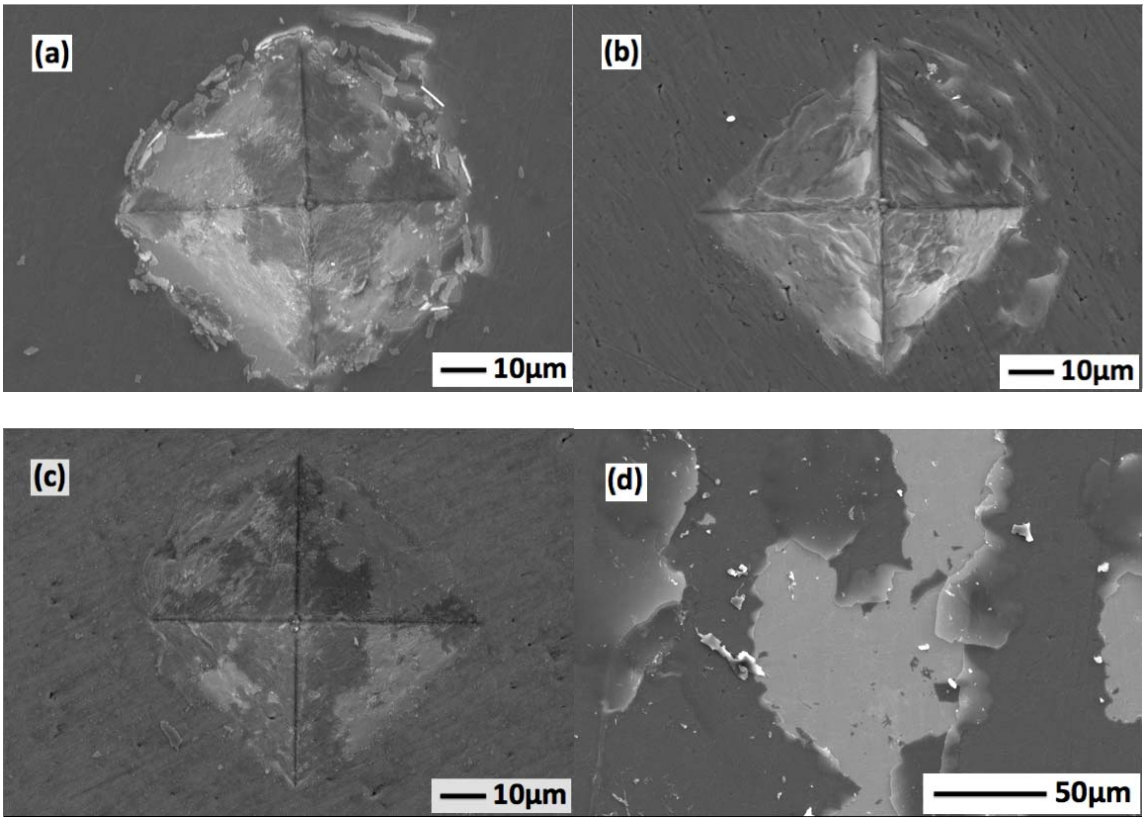

Figure 4-3. Typical SEM images of DLC coatings on Ti6Al4V after indentation testing deposited by different ion energy: (a) 60 eV, (b) 70 eV, (c) 75 eV, (d) 80 eV (without indentation).

Typical SEM images of these as-deposited interlayers formed on Ti6Al4V substrates are shown in Figure 4-4. It can be seen that the NDP (light dots) covered most of the Ti6Al4V surface as shown in Figure 4-4 (a), this high density would result in good adhesion as reported in our previous work [113]. Continuous films of W and TiN with similar surface topography are synthesized on Ti6Al4V substrates for comparison, as shown in Figure 4-4 (b) and (c). The particle sizes of the as-deposited diamond, W, and TiN are all less than 100 nm.

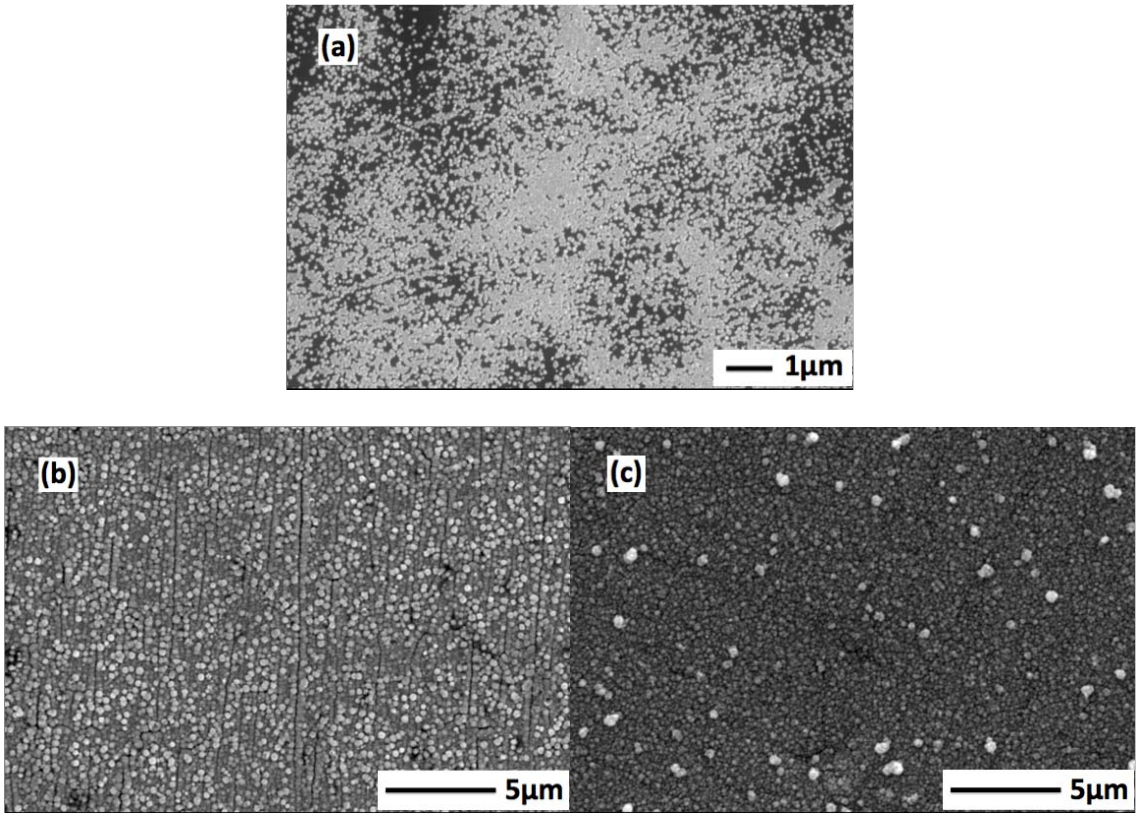

Figure 4-4 Typical SEM images of (a) diamond, (b) W, and (c) TiN interlayers grown on Ti6Al4V.

Figure 4-5 shows the typical XRD patterns of NDP, W, and TiN interlayers on Ti6Al4V, where the diamond peaks are denoted as D. In Figure 4-5 (a), it can be seen that there are diamond peaks at 2θ = 51°, and 91°, Ti peaks at 44°, 62°, 75°, 84°, and 99° (from the substrate), and TiC peaks at 41° and 92°, indicating the formation of a TiC intermediate layer on the substrate surface. The formation of a TiC interfacial layer is beneficial to the enhancement of adhesion of top films and the reduction of substrate damage caused by hydrogenation, as revealed by our recent investigations [113, 119]. The W peaks can be found at 2θ=47°, 68°, 87°, respectively, indicating that polycrystalline W thin films have been deposited onto the Ti6Al4V substrate, as shown in Figure 4-5 (b). Figure 4-5 (c) demonstrates TiN peaks at 2θ=41°, 92°, and

94°, with Ti peaks at 44°, 47°, 62°, 75°, and 84° (from the substrate), confirming the crystalline nature of the TiN interlayer.

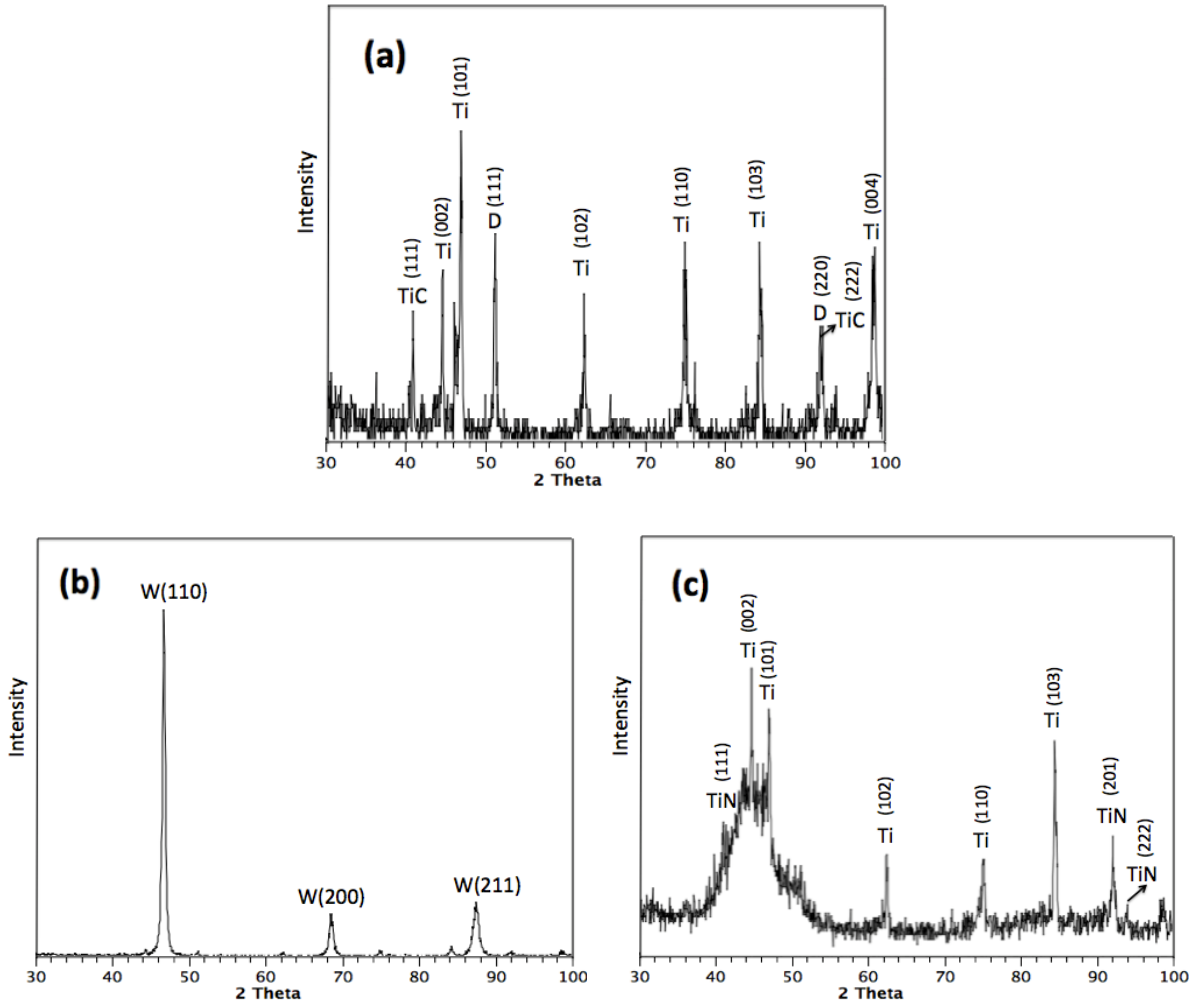

Figure 4-5. XRD patterns of (a) diamond, (b) W, and (c) TiN interlayers on Ti6Al4V.

Indentation testing by Vickers hardness tester was conducted at a load of 1000 N to evaluate the adhesion of the NDP/DLC, W/DLC, and TiN/DLC composite thin films. Figure 4-6 shows the SEM images of the as-deposited DLC thin films with different interlayers after indentation testing. It can be found that all the DLC composite thin films show better adhesion on Ti6Al4V

substrate comparing with the DLC thin films directly deposited on Ti6Al4V without interlayer. For DLC grown on Ti6Al4V with W and TiN interlayers as shown in Figure 4-6 (c) and (d), much less cracking in the imprint and much less spallation around the edge of the imprint is observed comparing with DLC samples without interlayer. It can also be seen that the adhesion of DLC with W interlayer is slightly better than that with TiN interlayer. And the size of the imprint of NDP/DLC and W/DLC is slightly smaller than that of TiN/DLC. This is possibly because of the higher Young's modulus of the as-deposited diamond and W interlayers than TiN. It should be noted that among all the DLC composite thin films, NDP/DLC sample shows almost no spallation both within and around the imprint area, as shown in Figure 4-6 (a). In addition, only fine cracking lines can be observed inside the imprint as shown in the Figure 4-6 (b) (an image of the imprint with higher magnification). All the results indicate that application of adherent interlayer with high hardness and Young's modulus values between DLC and Ti6Al4V substrate is promising to enhance the adhesion of DLC on Ti6Al4V. In addition, the NDP has been demonstrated to be a more effective adhesion promoter comparing with W and TiN interlayers for DLC grown on Ti6Al4V substrate. This is due do the reduced stress and increased interfacial strength and toughness [113].

To reveal the quality of as-deposited NDP/DLC composite thin film, synchrotron NEXAFS spectroscopy was used for characterization. Figure 4-7 shows the C K-edge NEXAFS spectra of NDP/DLC thin films grown on Ti6Al4V substrate recorded in TEY. The peak located around 286.3 eV corresponds to the transition C 1s$\rightarrow\pi^*$ for the sp^2 C=C bond, and the peak located around 289.8 eV is the most interesting one as it is associated with the excitations from C 1s to σ^* in sp^3-rich material, characteristic feature of DLC [120].

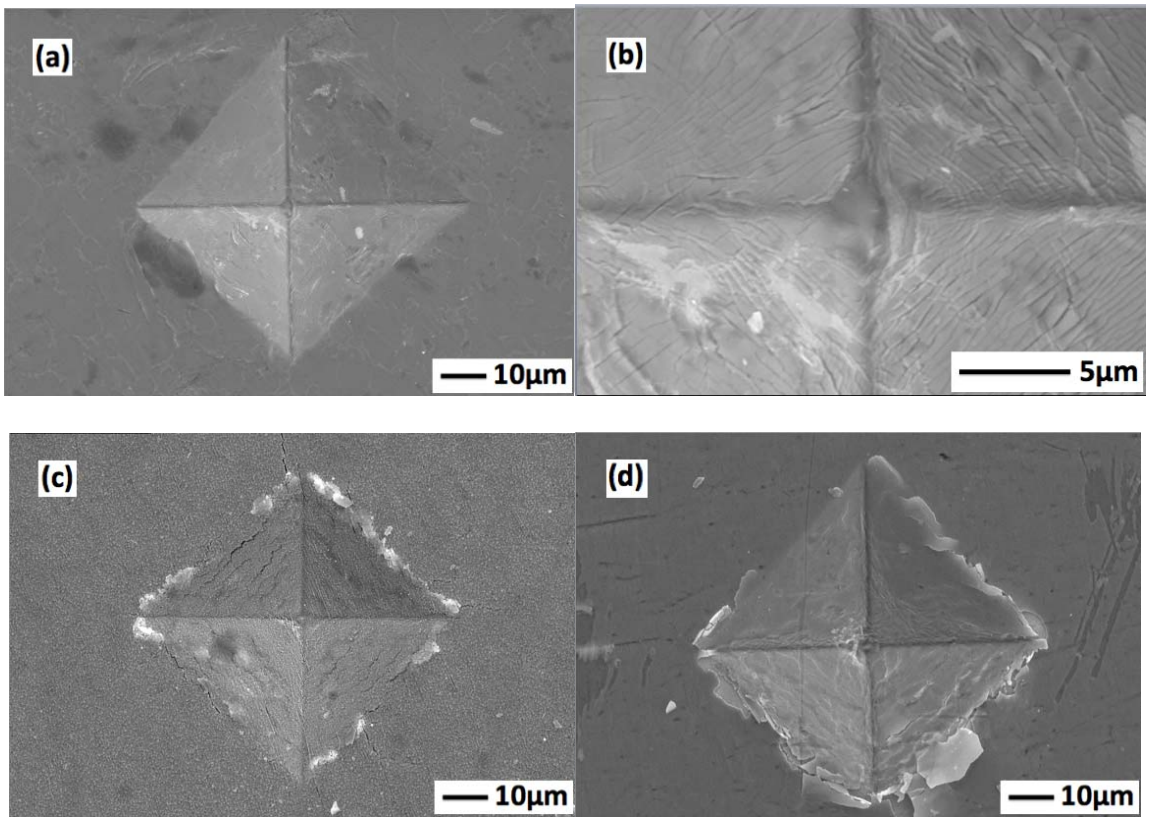

Figure 4-6 Typical SEM images of DLC coated Ti6Al4V after indentation testing with different interlayers: (a) (b) diamond, (c) W, and (d) TiN.

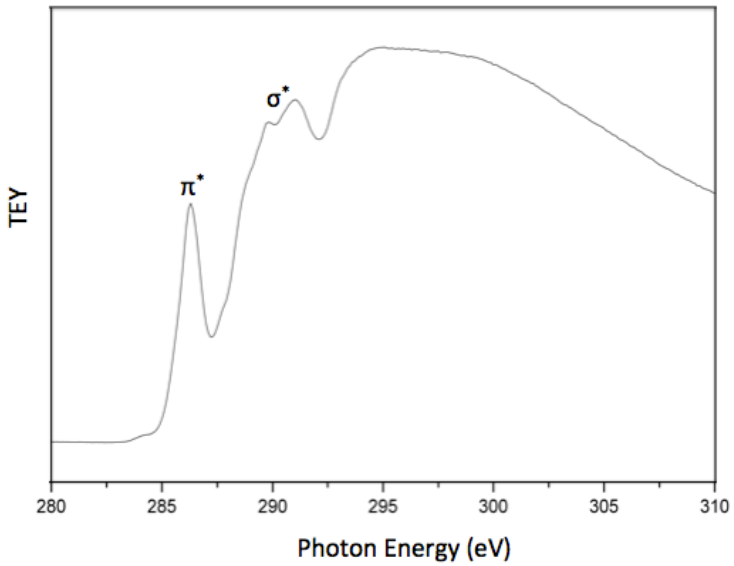

Figure 4-7. C K-edge NEXAFS spectrum of NDP/DLC composite thin film grown on Ti6Al4V.

4.4 Conclusions

The research demonstrates that the adhesion of DLC thin films directly deposited on Ti6Al4V substrates by direct ion beam deposition mainly depends on the ion energy used in the deposition process. Higher ion energy resulted higher sp^3 concentration of DLC thin films, but lower adhesion of DLC on Ti6Al4V substrates when the ion energy used is higher than 70 eV. Application of adherent interlayer with high hardness and Young's modulus values between DLC and Ti6Al4V substrate is promising to enhance the adhesion of DLC on Ti6Al4V. In addition, our newly developed NDP incorporation method works best for DLC adhesion enhancement on Ti6Al4V comparing with W and TiN interlayers due to greatly enhanced interfacial bonding.

CHAPTER 5
CVD NANOCRYSTALLINE DIAMOND COATINGS ON TI ALLOY: A SYNCHROTRON-ASSISTED INTERFACIAL INVESTIGATION

Diamond coating on Ti6Al4V alloy was carried out using microwave plasma enhanced CVD with a super high CH_4 concentration, and at a moderate deposition temperature close to 500 ℃. The nucleation, growth, adhesion behaviors of the diamond coating and the interfacial structures were investigated using Raman, XRD, SEM/TEM, synchrotron radiation and indentation test. Nanocrystalline diamond coatings have been produced and the nucleation density, nucleation rate and adhesion strength of diamond coatings on Ti alloy substrate are significantly enhanced. An intermediate layer of TiC is formed between the diamond coating and the alloy substrate, while diamond coating debonding occurs both at the diamond-TiC interface and TiC-substrate interface. The simultaneous hydrogenation and carburization also cause complex micro-structural and microhardness changes on the alloy substrates. The low deposition temperature and extremely high methane concentration demonstrate beneficial to enhance coating adhesion strength and reduce substrate damage.

5.1 Introduction

Titanium and its alloys have been widely used in aerospace, biomedical, chemical processing industries, marine facilities, sports equipment because of their promising properties including low density, very high tensile strength and toughness, and high corrosion resistance [121,122]. Their extended applications are mainly restricted by the poor tribological properties. Chemical vapor deposition of wear/corrosion resistant diamond coatings on such materials can markedly enhance the durability and service performances of these materials [123, 124]. However, it is difficult to obtain adherent diamond coatings on such Ti alloys due to the large mismatch of the thermal expansion coefficients of the diamond and the substrate materials [125]. In addition,

severe chemical reaction between the gas reactants and the base materials strongly alters the microstructures of the substrate materials and deteriorate their mechanical properties [126-130]. For instance, although atomic hydrogen is usually considered crucial to synthesize high quality diamond during the chemical vapor deposition process, as it preferentially etches non-diamond carbon species, hydrogen also readily dissolves into Ti substrate and induces phase transformation and microstructure changes, leading to increased embrittlement [131, 132]. Furthermore, the formation of an intermediate titanium carbide layer at the early stage of CVD processing introduces a new hetero-interface and complicates the adhesion failure models of diamond coatings [133, 134].

Extensive investigations have been conducted so far to exploit new processing methods to produce continuous, smooth and well adherent diamond coatings on metallic Ti and its alloys of different shape and dimensions. However, barrier still exists in obtaining smooth, adherent diamond coatings without altering the microstructure and mechanical properties of the base materials. In this study, the diamond has been synthesized from pure methane to mitigate the impact of hydrogen on the substrate microstructure and to enhance the nucleation and growth of diamond. Furthermore, to decrease the thermal stress impact, a moderate deposition temperature is adopted simultaneously to improve the interfacial adhesion. The structure changes of the alloy material after plasma exposure are also characterized by synchrotron fluorescence spectroscopy and micro-diffraction.

5.2 Experimental materials and methods

Ti6Al4V alloy was used as substrate material for diamond deposition. The Ti alloy plate was cut into specimens of 10 mm ×10 mm × 1 mm and mechanically polished with 600# SiC sandpapers, ultrasonically cleaned in acetone and dried by flowing N_2. To enhance diamond nucleation density, some Ti alloy samples were further subjected to a supersonic pretreatment for

20 min in pure ethanol mixed with a suspension of ultra-nanocrystalline diamond powder (5 nm on average), followed by an ultrasonic rinse in distilled water for another 10 min. Diamond deposition was conducted in a 2.45 GHz microwave plasma enhanced CVD system (Plasmionique) at a working pressure of 30 Torr. Basically, a pure methane precursor was used for diamond synthesis, while single hydrogen plasma etching and a 99% H_2 – 1% CH_4 gas mixture were also applied for comparison. The microwave input power was kept at 600 W, producing a deposition temperature approximately 500 ℃, as measured by a thermal couple mounted underneath a stainless steel substrate holder.

The morphology, composition and structure of the diamond coating, coating-substrate interface and the underlying substrate near-surface were characterized by SEM, micro-Raman spectroscope, XRD, AFM, and micro-hardness measurement. Synchrotron-based NEXAFS, X-ray Laue micro-beam diffraction were performed at the 10ID-2, 06B1-1 and 07B2-1 beamlines of the Canadian Light Source, to address the bonding states of the diamond coatings and the structure changes (granular lattice orientation, coarsening, phase transformation) of the Ti alloy substrate. The adhesion ability of the diamond coatings were evaluated by Rockwell C indentation testing using a 150 kg load.

5.3 Results and discussion

Figure 5-1 shows the SEM images of diamond nucleation and growth on Ti alloy with two different pre-treatments and deposition parameters. For the Ti alloy without pre-scratching with diamond suspension, the nucleation density with a 1% CH_4 concentration is very low. After 2 h of deposition, the diamond crystals are only sparsely distributed on Ti alloy surface, as shown in Figure 5-1 (a). The diamond crystallites are not as well faceted as those grown on Si wafer under the same deposition conditions, probably due to a significant diffusion of carbon in the Ti

substrate, which causes a lack of carbon oversaturation on the substrate surface and delays diamond nucleation. The diamond nucleation density can be markedly increased by applying a diamond scratching pretreatment, normally ascribed to a pre-seeding effect. Our study shows that even without such a scratching pre-treatment, using a 100% CH_4 precursor can also markedly enhance the diamond nucleation density, as shown in Figure 5-1 (b). In addition, a nanocrystalline diamond coating has been produced from the pure methane on the alloy surface, as shown in Figure 5-1 (c). Figure 5-2 shows the AFM top surface images of the nanocrystalline diamond coating. The RRMS value is 235±31 nm (N = 5) for a 5 μm × 5 μm areas taken at different spots on the sample. The film shows that the nanodiamond is aggregated into larger cauliflower structures approximately 1 μm in diameter. Higher resolution imaging reveals that these large structures are composed of smaller nanodiamond clusters with approximate diameters of 50 nm. Some pinhole defects are apparent in the film. Figure 5-2 (d) shows the AFM surface image of diamond film synthesized with 1% CH_4 diluted in 99% H_2. The microcrystalline diamond grains have well faceted orientation and result in a much rougher surface.

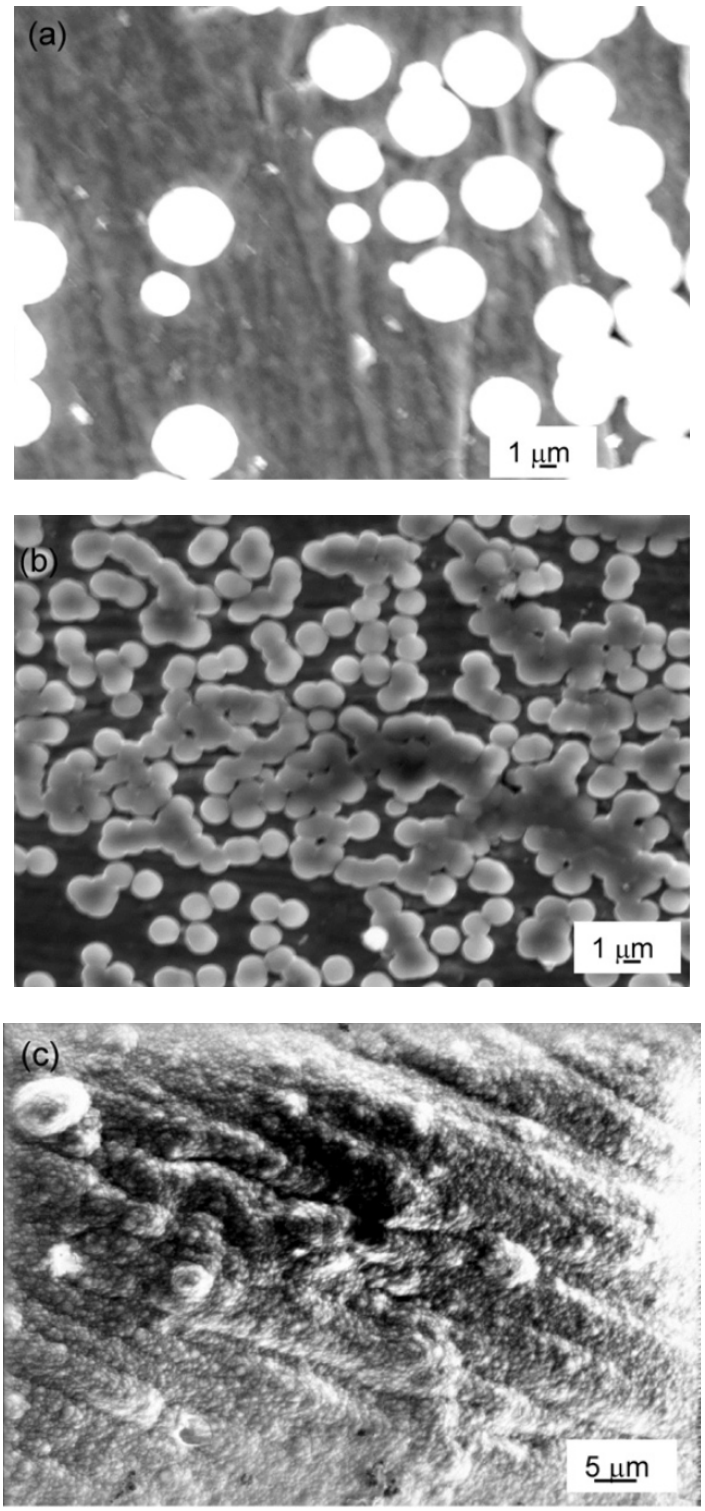

Figure 5-1. SEM images of diamond nucleation and growth on Ti alloy. (a) 1% CH_4, 2 h, (b) 100% CH_4, 0.5 h and (c) 100% CH_4, 5 h.

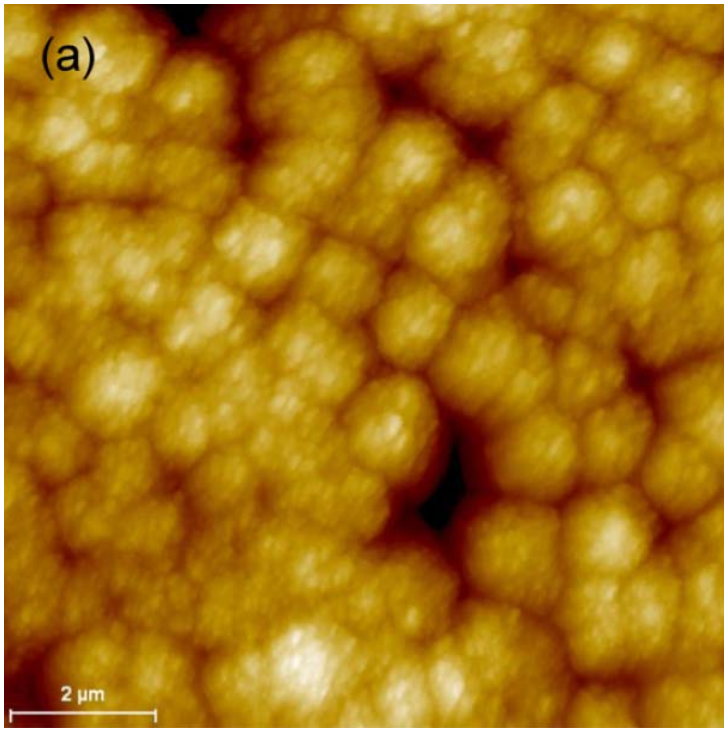
(a)
2 µm

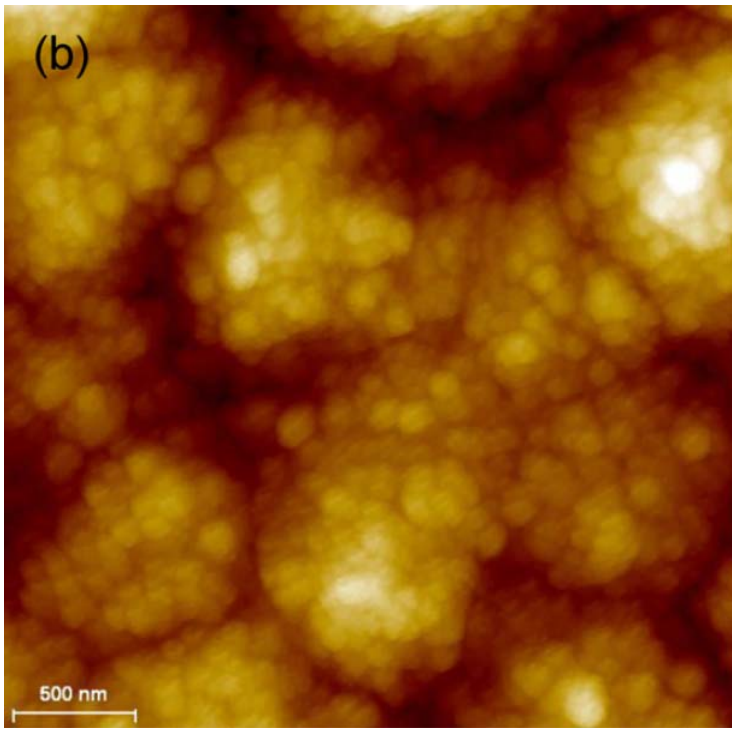
(b)
500 nm

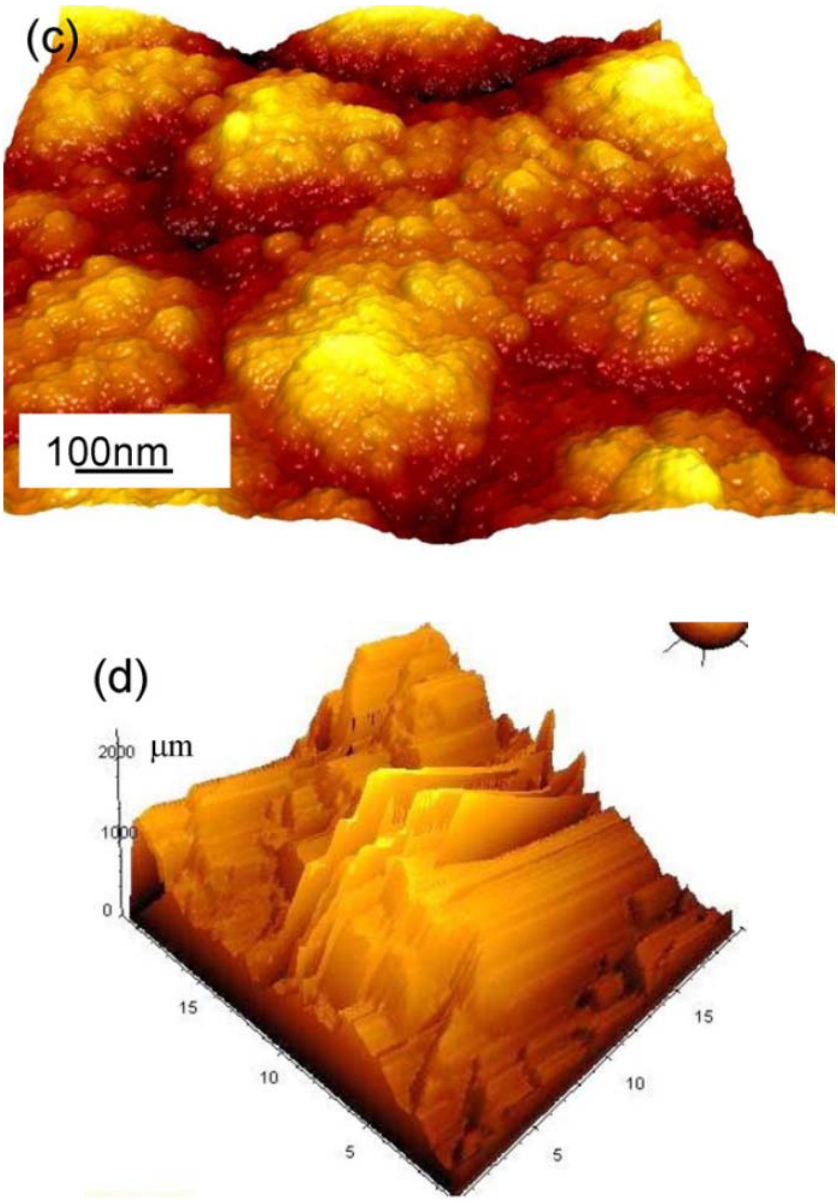

Figure 5-2. AFM images of diamond coatings synthesized on Ti alloy with 100% CH_4 (a–c) and 1% CH_4 (d).

Figure 5-3 (a) shows the Raman spectroscopy of nanocrystalline diamond coatings derived from pure methane. A small diamond characteristic peak at 1338 cm^{-1}, is broadened and shifted upward in comparison with its stand position at 1332 cm^{-1}. This can be primarily attributed to the reduced diamond grain size and accumulated residual stress in the film. In addition to this

diamond main peak, two additional peaks located at 1140 cm^{-1} and 1480 cm^{-1} are detected. These two peaks are usually attributed to nanocrystalline diamond. However, some other researchers demonstrated by analyzing the Raman spectra taken at different excitation energies that these peaks are actually a signature of transpolyacetylene and have nothing to do with C–C sp^3 vibrations [135]. Considering the ultrahigh CH_4 concentration we are using here, the atomic hydrogen coming from CH_4 dissociation has a much weaker etching effect on the graphitic carbon in comparison with that in H_2-rich environment. As a consequence, more sp^2 carbon may remain in the diamond films, especially enrich at grain boundaries for fine grain-sized diamond films. Nonetheless, because visible Raman is 70 times more sensitive to sp^2 sites than sp^3 sites, the absence or low intensity of any graphitic peaks indicates a high sp^3 fraction in the diamond films. Furthermore, the broad peak (G-band) centered at 1520 cm^{-1} is also an apparent signature of high fraction of sp^3 carbon, as a shift of the G-band frequency from stand (1580 cm^{-1}) to a smaller wavelength is normally accompanied by a higher sp^3 concentration [136]. Figure 5-3 (b) shows the C K-edge NEXAFS spectrum of diamond film synthesized with pure methane. A graphite spectrum is plotted as well for comparison. We can see that the diamond spectrum exhibits a sharp absorption edge at 289 eV and a large dip at 303 eV, characteristic features of pure diamond, confirming the films grown from pure methane are still dominated by sp^3 diamond in nature. A weak peak appears at 285.5 eV in the spectrum, typical signature of π bonding from the non-diamond carbon. This peak is very weak at 1% methane concentration and becomes a more intense at 100% methane, but it is insignificant comparing with that of graphite [137]. The combined evaluation by Raman and XAS determines that the nanocrystalline diamond films synthesized from pure methane consist of predominate diamond nanocrystallites with a small amount of sp^2 carbon.

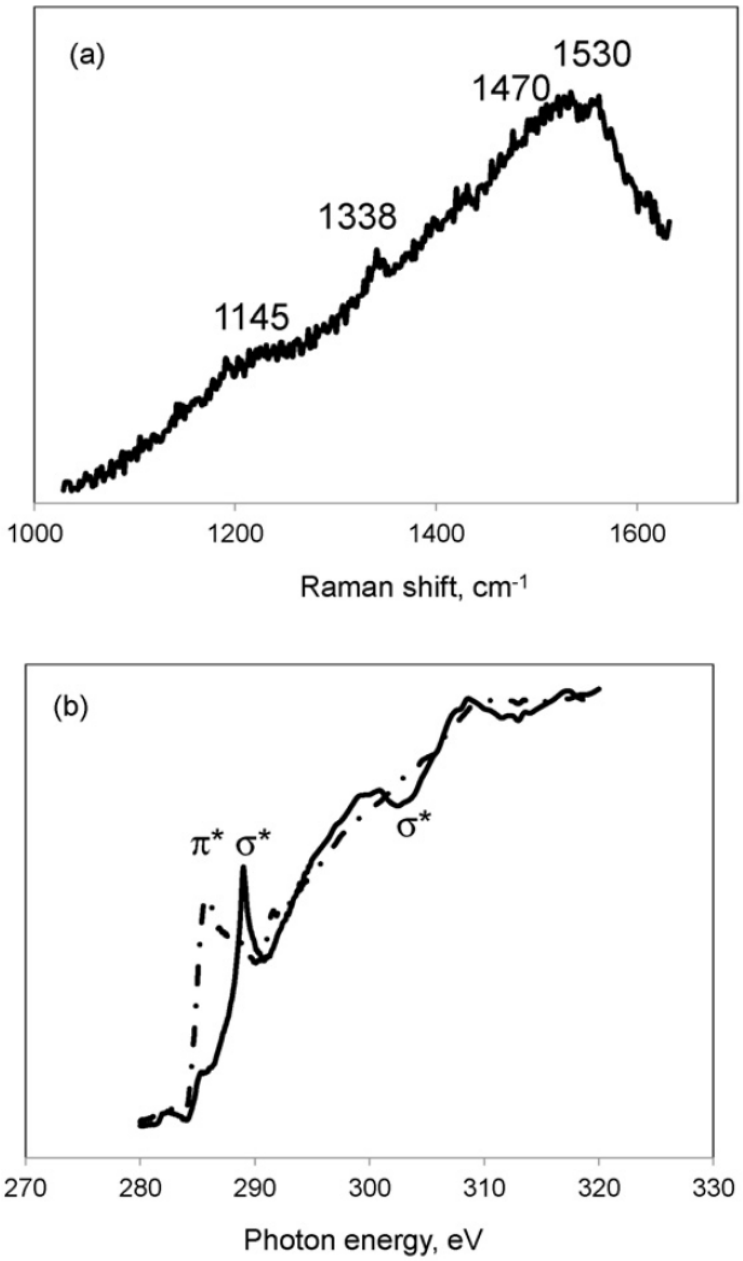

Figure 5-3. Raman (a) and synchrotron C–K edge XAS spectra (b) of nanodiamond coating synthesized with 100% CH_4.

Figure 5-4 shows typical XRD patterns of Ti alloy substrates subjected to different plasma treatments including diamond synthesis with 100% CH_4 and pure H_2 plasma etching. The XRD

patterns of pure diamond and as polished fresh Ti alloy are also plotted for comparison. After plasma treatment in pure methane, no clear diamond peaks are observed on as-polished Ti substrate. Instead, strong TiC phase patterns appear. This is because of significant carbon diffusion in the substrate during the plasma CVD process, which results in a lack of carbon supersaturation on the alloy surface and, consequently, a low diamond nucleation density. After a diamond paste pre-scratching treatment, continuous nanocrystalline diamond coating forms easily on the Ti alloy. When this top diamond coating is mechanically removed by repeating bending of the substrate till a fresh Ti alloy surface is exposed, the corresponding XRD patterns from such an interface reveal strong peak intensities of TiC phase, indicating a significant amount of residual TiC remained on the alloy surface. The function of this intermediate TiC layer will be discussed later. No clear patterns related to titanium hydride phase are detected. The reason may be due to the low percentage of atomic hydrogen presented in a pure methane environment, and hydrogen dissolved in the Ti ally substrate does not form hydride precipitate, or the fraction of titanium hydride formed is not high enough to be detected. For the Ti alloy subjected to a direct plasma etching in pure H_2, titanium hydride peaks appear but the intensity is highly temperature dependent, as shown in Figure 5-4 (b). At 500 ℃, the diffraction patterns are simple and only one TiH_2 peak is observed with a low intensity. At 800 ℃, a few more peaks corresponding to TiH_2 and/or β-Ti and TiH are measured. The complex microstructure changes and their effect on the mechanical behavior of the Ti alloys will be characterized in continued work. Anyway, this comparison indicates clearly that a high CVD temperature can dramatically affect the alloy microstructures [138]. A lower CVD temperature, as we employ in this study, has markedly reduced such a detrimental impact.

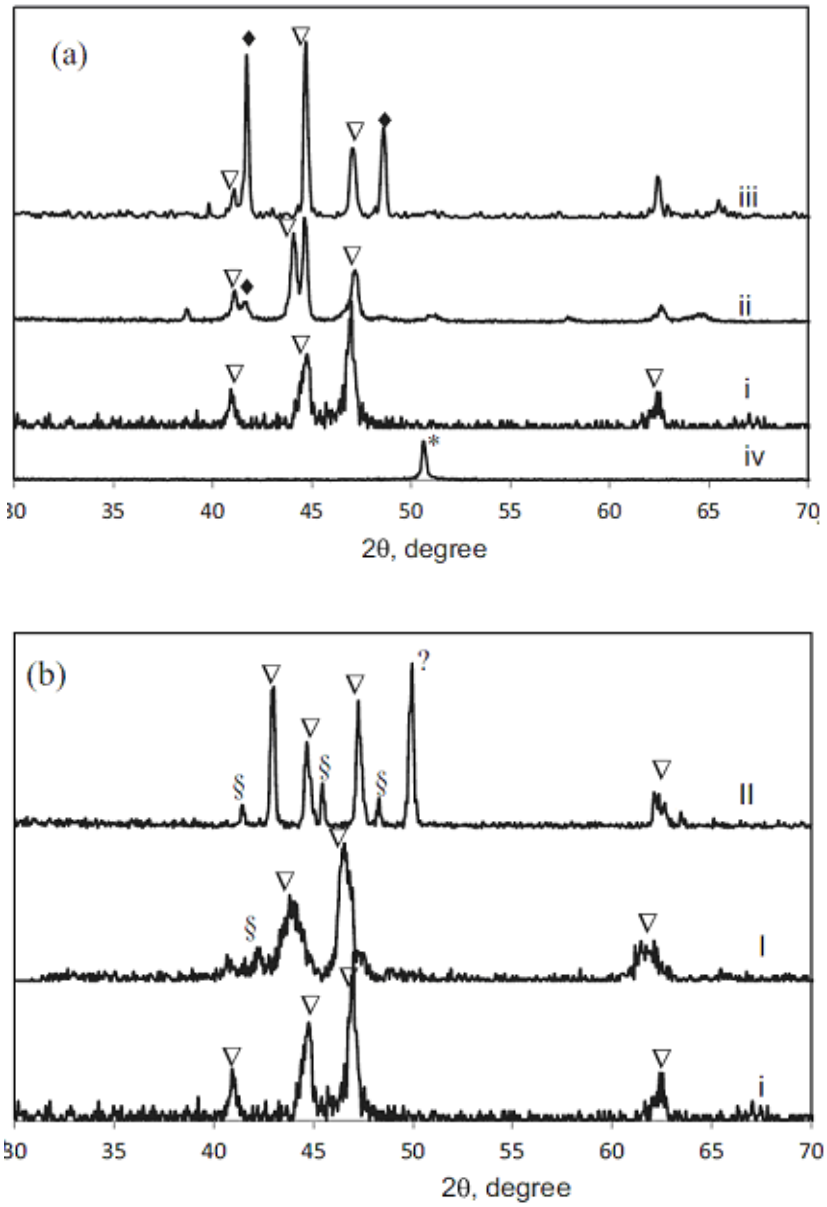

Figure 5-4. XRD patterns of Ti alloy substrate after treatment in pure methane (a) and pure H_2 (b) plasma atmospheres. (i): Freshly polished Ti alloy (ii) as polished Ti alloy and after CVD in 100% CH_4, (iii) diamond suspension pre-scratched Ti alloy surface, after CVD in 100% CH_4 and removal of top diamond film and (iv) pure diamond for reference. (I) Ti alloy after H_2 etching at 500 ℃, (II) Ti alloy after H_2 etching at 720 ℃. ▽, α-Ti; ◆, TiC; *, diamond; §, TiH_2 and β-Ti; ?, TiH.

To evaluate the interfacial bonding properties of diamond coatings grown on the Ti alloy substrate, a Rockwell C indentation test has been conducted using a load of 150 kg and the results are shown in Figure 5-5. For diamond coatings synthesized in a low methane concentration of 1%, severe spallation of the diamond coatings occurs after indentation test, as clearly shown in Figure 5-5 (a). However, less coating spallation is observed around the indentation imprint for diamond coatings produced with highly increased methane concentrations (Figure 5-5 (b) and (c)), except that some lateral cracks are initiated on the coating surface with crack radius varying from hundred to two hundred micrometers. The absence of a significant coating spallation under such a high indentation load confirms that the diamond coatings synthesized with pure CH_4 have high interfacial adhesion strength. When a Ti alloy plate covered with the nanocrystalline diamond coatings is cut off using a metal cutting machine, a bending deformation of alloy substrate happens along the cutting edges (Figure 5-6 (a)), and the diamond coating is subjected to a severe shear stress. Lateral cracking is observed in the shear zone of the diamond coatings, but spallation is observed only locally along the cutting edge (Figure 5-6 (b)), indicating the diamond coatings possess high interface fracture toughness and the related adhesion strength. For diamond coatings synthesized with a low methane concentration, as the conventional 1%, a severe coating delamination has been observed after indentation test (results not shown here). So the nanocrystalline diamond coatings synthesized with pure methane demonstrate enhanced adhesion properties on the Ti alloy substrates. The interfacial adhesion enhancement of diamond coatings synthesized from pure methane and at a moderate temperature may result from a few beneficial aspects. First is that a carbon supersaturation necessary for high nucleation density and rate of diamond can be easily

established on the Ti alloy surface, which effectively increases the contact sites of diamond coating with the underlying substrate and reduce the interfacial porosity [139, 140]. The second is that the deposition temperature adopted is relatively low, mitigating the coating delamination risk induced by thermal stress that arise due to mismatch in thermal expansion coefficients of coating substrate system [141]. The third is that an abundant carbon source supply facilitates fast formation of an intermediate titanium carbide layer, acting as a diffusion barrier to prohibit continued carbon diffusion and hydrogen penetration in the alloy substrate [142]. Figure 5-7 shows the TiC layer formed at the diamond-substrate interface. The debonding interface observation is realized by mechanical bending of the diamond-coated Ti substrate till the top diamond coating delamination occurs and a fresh substrate surface is exposed. It can be seen that a large fraction of TiC layer remains on the substrate surface, indicating a debonding of the nanocrystalline diamond coating has taken place both at the diamond–carbide layer interface and at the carbide layer–substrate interface (Fig. 5-7 (b)). Figure 5-8 shows a TEM image and the corresponding selected area electron diffraction (SAED) image from the alloy surface. A TiC intermediate layer has been clearly identified on the substrate surface. In fact, due to the very reactive nature of titanium to different gas species, the interface chemistry may be more complex and titanium oxide, carbide and hydride can co-exist on the surface or nears surface of the substrate materials, which markedly influence the subsequent diamond nucleation and adhesion. TiC has a thermal expansion coefficient between those of diamond and the Ti alloy. Theoretically, the formation of a titanium carbide intermediate layer helps reduce the thermal stress and enhance the adhesion of diamond coating. However, this effectiveness also depends on the properties of TiC layer in terms of its stoichiometry, structure and morphology. A porous and rough TiC layer will adversely results in cracking and spallation of top diamond coating, rather

than contributes to its adhesion strength. In this study, the diamond coating delamination occurs at different interfaces where a weaker interface strength dominates, indicating that optimized deposition conditions are required to further enhance the coating adhesion grown on such strong carbide-forming substrates.

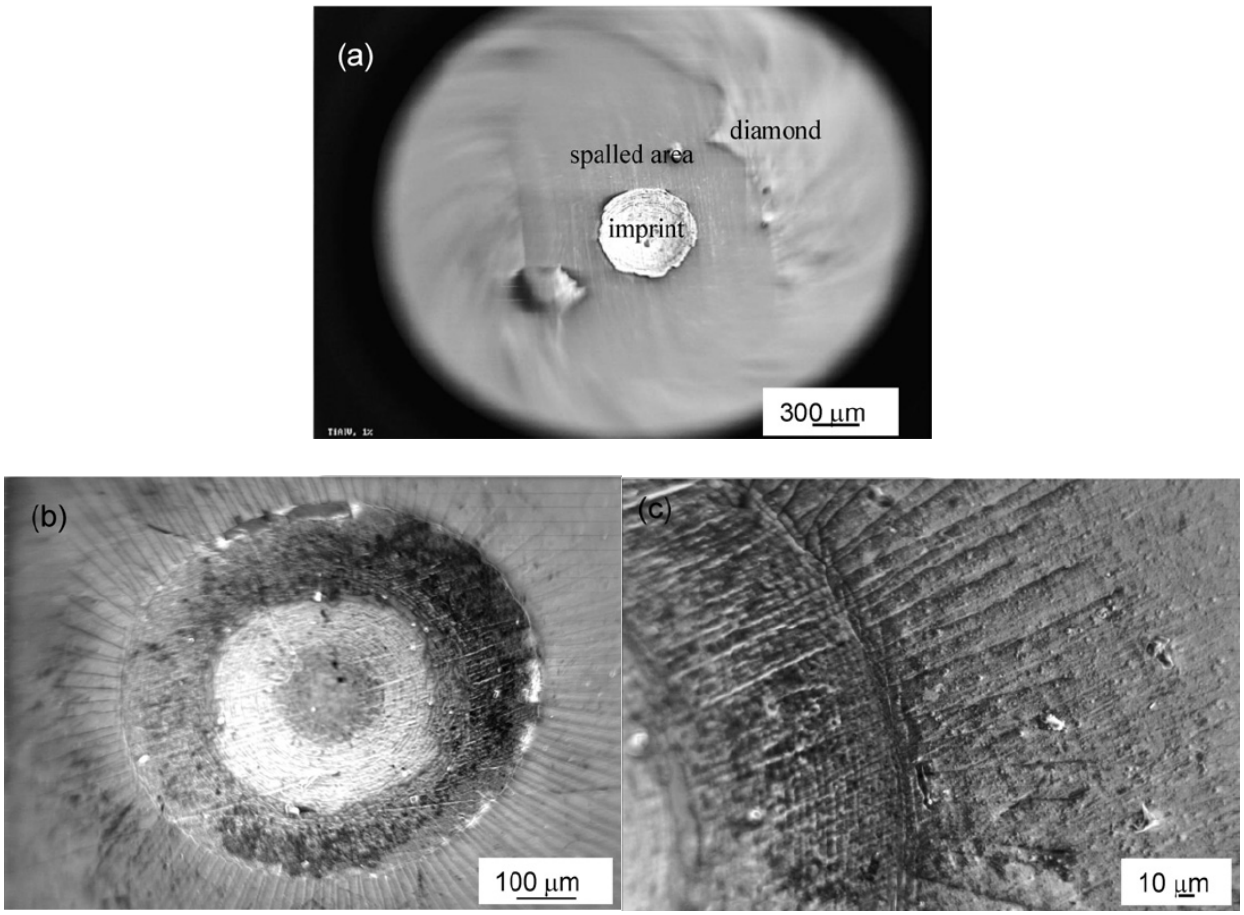

Figure 5-5. SEM images of diamond coatings after indentation test. (a) Synthesized with 1% CH4, (b) and (c) synthesized with 100% CH_4.

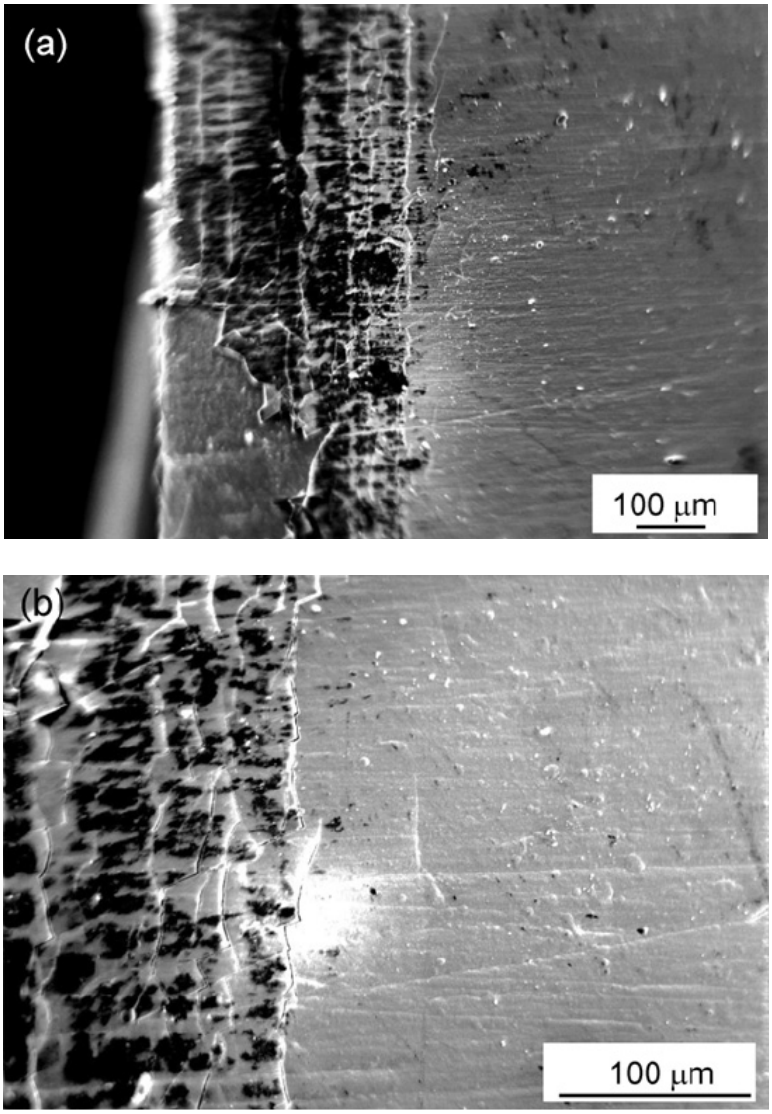

Figure 5-6. SEM surface images of diamond coated Ti alloy synthesized with 100% CH_4 and after cutting. (a) A general view and (b) a magnified view of shear deformation zone.

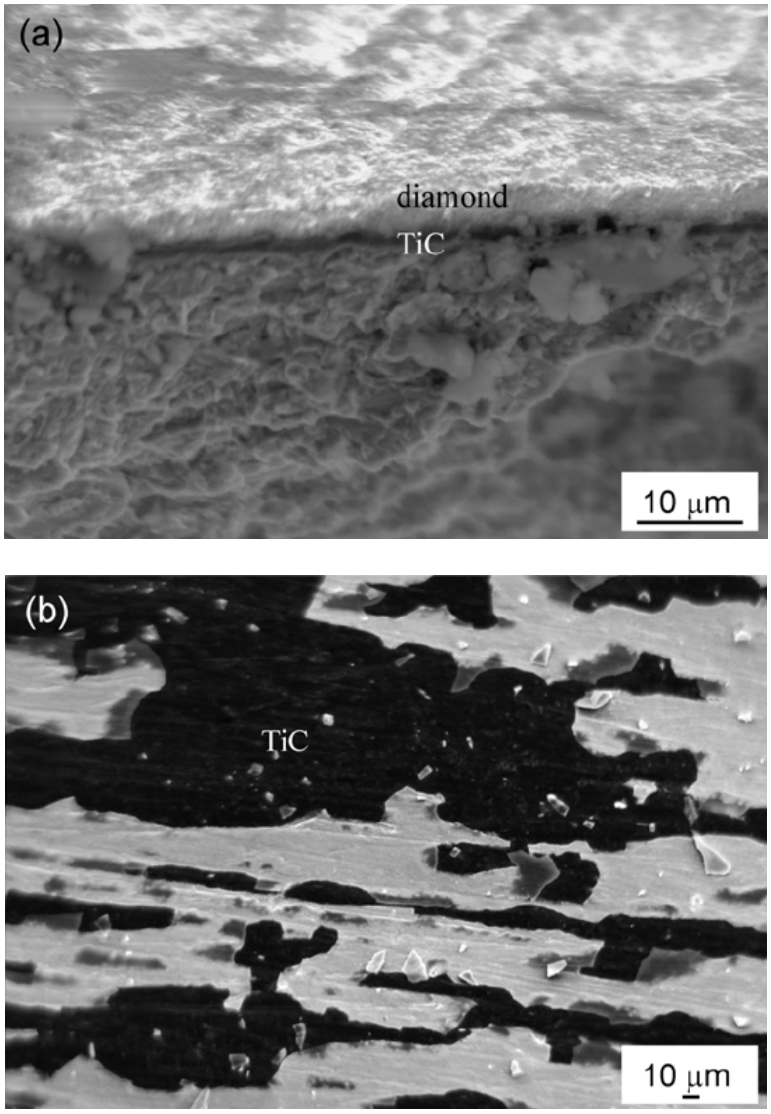

Figure 5-7. SEM images of (a): fractured cross section of diamond coated Ti alloy and (b) a top view of exposed alloy surface after removal of the top diamond coating.

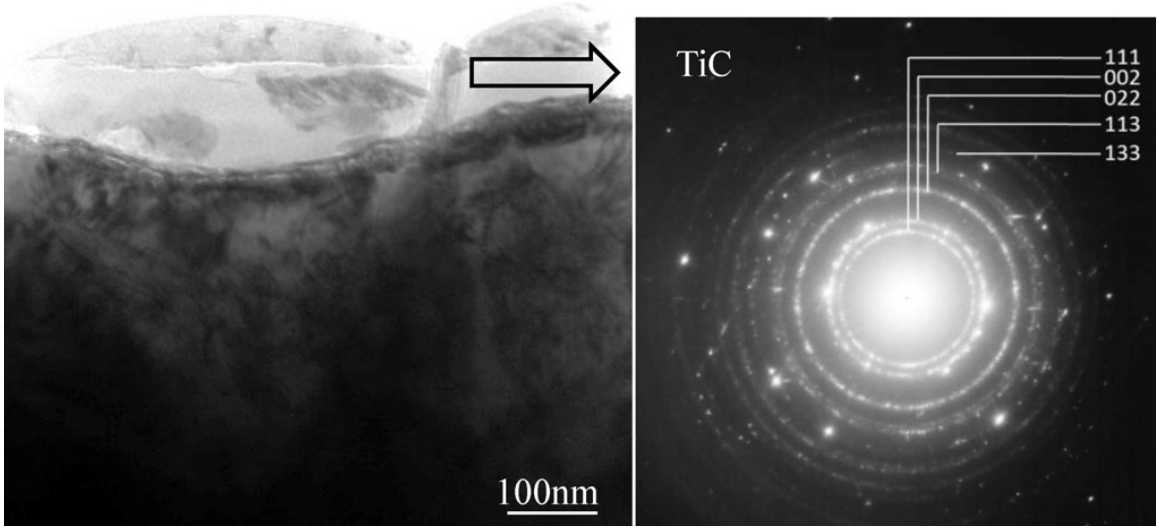

Figure 5-8. Cross sectional TEM image (a) and SAED (b) of diamond-coated Ti alloy.

Titanium and its alloys are well known very sensitive to hydrogen uptake. The hydrogen adsorption, penetration and formation of secondary phase titanium hydrides will alert the substrate microstructures, damage the mechanical properties such as hydrogen embrittlement and loss in tensile ductility, and possibly also influence the nucleation and adhesion of diamond coatings due to changed interface conditions. Some Ti alloy samples have been exclusively etched in pure hydrogen plasma and the etched substrate surfaces are shown in Figure 5-9. Many micro-cracks caused by the formation and rupture of brittle titanium hydride phases are observed. Figure 5-10 compares the Vickers microhardness values (under a 500 g load) of the alloy surfaces after different treatment. The lowest value of microhardness (320±17 HV) is measured on the as-polished Ti alloy. The value increases to 353±23 HV on the as-polished alloy following a treatment in pure methane plasma, and this is attributed to the formation of TiC by a carburization process on the near surface of the alloy. Similarly, the microhardness value measured on the alloy surface after removing the top diamond, approaches approximately 400 HV and it is attributed to a major contribution of residual TiC intermediate layer. Comparatively,

the pure hydrogen plasma etched Ti alloy demonstrates the highest value of surface microhardness up to 670, most probably because of a kind of hydrogen solution strengthening effect in combining with the formation of brittle titanium hydride phase and lattice defects [143].

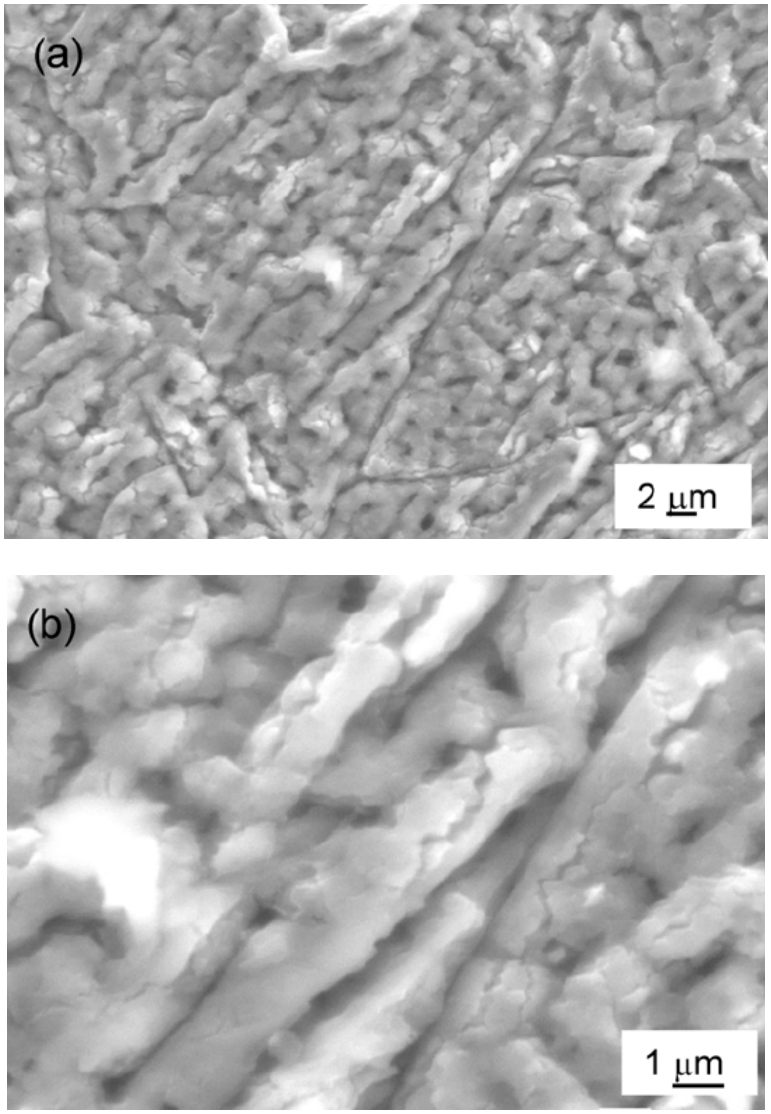

Figure 5-9. SEM micrographs of Ti alloy surface after plasma etching in pure hydrogen. (a) A general view and (b) a magnified view.

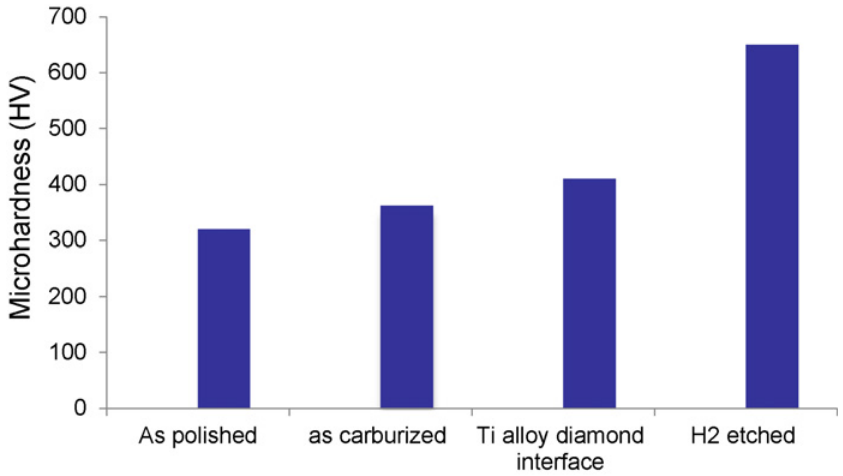

Figure 5-10. Microhardness changes (HV values) dependent upon the Ti alloy surface conditions.

5.4 Conclusions

Nanocrystalline diamond coatings are deposited on Ti6Al4V alloy substrate at a moderate deposition temperature with a pure CH_4 precursor. The nucleation density and adhesion strength of diamond coatings are markedly enhanced. A titanium carbide intermediate layer is formed between diamond coating and Ti substrate, and it strongly influences the subsequent diamond coating adhesion performance. Diamond coating delamination occurs at different interfaces including both diamond–TiC and TiC–substrate interfaces. Significant surface micro-hardness variations are observed due to the hydrogenation and/or carburization procedures. The low deposition temperature and H_2 concentration applied in this study are expected to mitigate such substrate damage and will be further investigated.

CHAPTER 6
NANOCRYSTALLINE DIAMOND THIN FILMS GROWN ON TI6AL4V ALLOY

Diamond nucleation and deposition on Ti6Al4V substrates were investigated using microwave plasma assisted chemical vapor deposition under different seeding and deposition conditions. The samples prepared were characterized by scanning electron microscopy and Raman spectroscopy. The results show that the nucleation density of diamond can be enhanced up to $10^{11}/cm^2$ by nanodiamond seeding and two-step deposition. By optimizing the seeding and deposition parameters, nanocrystalline diamond thin films were synthesized at relatively low microwave power (600 W) within a short time deposition; consequently, the microstructure change of Ti6Al4V as a result of hydrogen diffusion was significantly reduced due to the low deposition temperature and short deposition time.

6.1 Introduction

Diamond thin film coated Ti and titanium alloys possess great potential for a variety of applications such as jet propulsion systems, compressor blades, biomedical implants, and chemical engineering components [50, 144, 145]. Ti and Ti alloys exhibit high mechanical strength, good corrosion resistance and low density. These characteristics make them widely used in chemical, aerospace and biomedical engineering. However, there is a significant drawback of Ti and Ti alloys: low resistance against wear, fretting fatigue and erosion. Deposition of a well-adhered diamond coating is a promising way to solve this problem owing to the outstanding properties of diamond including its extreme hardness, low friction coefficient, chemical inertness and high thermal conductivity [23, 50, 144-147].

Generally, the methods to deposit diamond coating are chemical vapor deposition (CVD) with hot filament, microwave plasma and DC plasma [148]. However, because the deposition process is usually undertaken at high temperature (700–850 °C) in a hydrogen-rich environment, the

diffusion of hydrogen can lead to deterioration of the mechanical properties of the substrate, in particular, fatigue life and impact strength [143, 149-151]. Normally, this diffusion of hydrogen can be reduced by using low deposition temperature and short deposition time. However, the low growth rate of diamond on Ti alloy at low temperature make formation of continuous film in a short time even more difficult. In order to achieve a high nucleation density of diamonds on Ti, ultrasonic seeding [50, 152] and bias-enhanced nucleation [3] are frequently used. Enhanced nanodiamond seeding using a polymer matrix is also developed [153, 154]. In this paper, ultrasonic seeding with a two-step deposition technique was developed to solve this problem. Very thin smooth NCD thin films were grown on Ti6Al4V at low temperatures in a MPCVD within a short deposition time.

6.2 Experimental details

Ti6Al4V wafers with dimensions of 10 mm × 10 mm × 2 mm were ground and polished using silicon carbide paper (350 grit), 9 μm diamond slurry, and 3 μm diamond slurry sequentially and then cleaned in ethanol for 15 min. The final preparation step involved ultrasonic seeding for different durations (10 min, 20 min, 30 min, 45 min, 1 h, 2 h, 3 h, 5 h, 7 h) in a suspension (1 mg/ml, 0.1 wt.%) of ethanol and diamond powder (average crystal size of 4 – 5 nm for nanodiamond seeding, and 1 μm for microdiamond seeding), followed by ultrasonic cleaning, rinsing in ethanol and drying in air.

Diamond deposition on Ti6Al4V was conducted in a 2.45 GHz MPCVD reactor with CH_4/H_2 gas mixture. A two-step deposition method was used, 20 vol.% CH_4 for the nucleation step, and 0.5 vol.% CH_4 for the deposition step. The working pressure was maintained at 4 kPa. Microwave power was from 500 W to 1000 W. The detailed deposition parameters are listed in Table 6-1. After diamond deposition, the samples were characterized by SEM (JSM-6010LA,

manufactured by JEOL, operating voltage used was 15 kV) and Raman spectroscopy. The Raman spectra were obtained by a Renishaw micro-Raman system 2000 spectrometers operated at a laser wavelength of 514.5 nm generated by an argon laser. Nucleation density was calculated as the number of grains per area, averaging over 8 spots (1 μm × 1 μm) in SEM images for 4 samples prepared under same conditions.

Table 6-1. Deposition conditions of diamond thin films on Ti6Al4V substrate.

Parameters	First step (nucleation enhancement)	Second step (diamond growth)
H_2 flow rate (sccm)	40	199
CH_4 flow rate (sccm)	10	1
Total flow rate (sccm)	50	200
Gas pressure (kPa)	4	4
Microwave power (W)	500 600 700 800 900 1000	500 ~ 1000
Temperature (°C)	300 350 500 600 700 850	300 ~ 850
Deposition time (min)	10 ~ 60	10 ~ 120

6.3 Results and discussion

Figure 6-1 shows the SEM images of diamond on Ti6Al4V without seeding, seeding with micro- and nano- diamond particles for 3 h pretreatment followed by 10 min nucleation and 1 h growth. It can be seen that the nucleation density of diamond is in the order of $10^8/cm^2$ without seeding, $10^9/cm^2$ with micro-diamond seeding, and $10^{11}/cm^2$ with nanodiamond seeding. These results have demonstrated that nanodiamond seeding is a very effective method to enhance the nucleation of diamond on Ti6Al4V substrate.

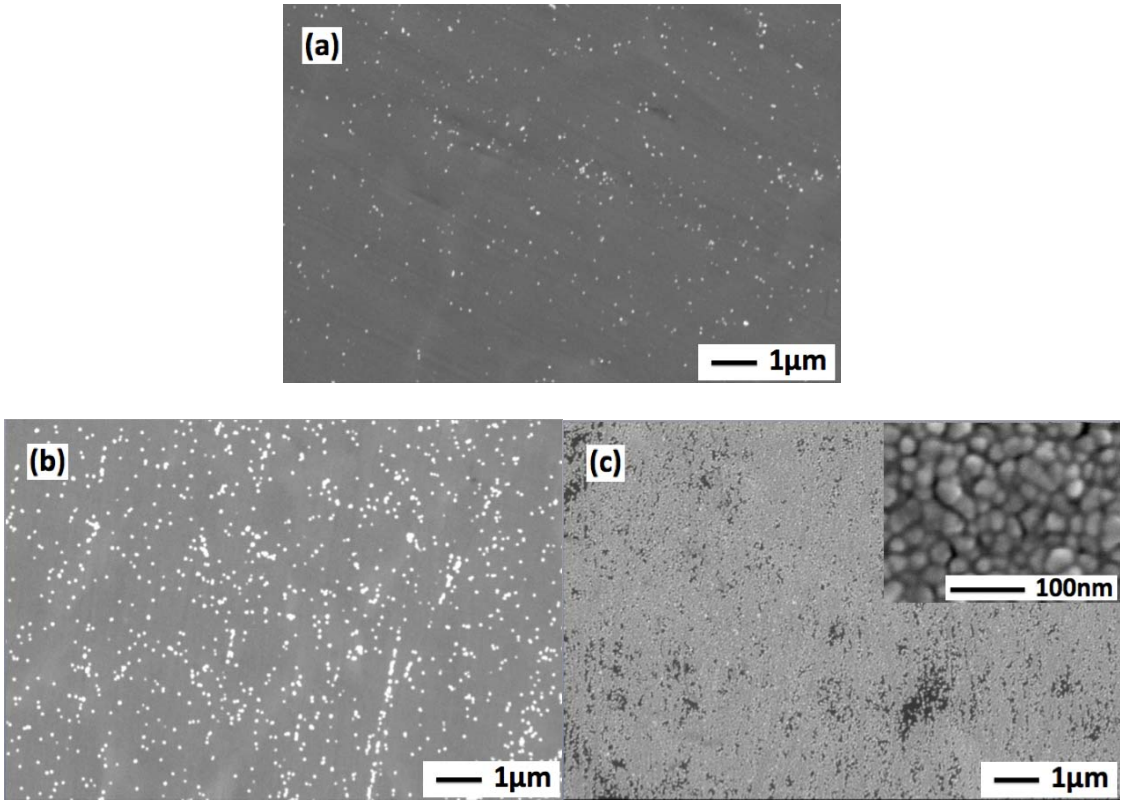

Figure 6-1. SEM images of diamond grown on Ti6Al4V (a) without seeding, (b) by micro-diamond seeding, (c) by nano-diamond seeding.

Figure 6-2 shows the SEM images of diamond on Ti6Al4V by nanodiamond seeding for 1 h, 3 h, 5 h and 7 h followed by 10 min nucleation and 1 h growth. It can be seen that under these conditions, 3 h is the optimal seeding time. This is because this seeding process can also cause nano-scale defects on Ti6Al4V surface due to bombardment of nanodiamond, including nano-scale pit, ditch and mound, which can be called the roughing effect. The defects increase with seeding time, reach a peak, and then fall due to the polishing effect (removal of the rough sites by nanodiamond bombardment). After 3 h, the nucleation density fails to increase further due to the balance between seeding, roughing, and polishing.

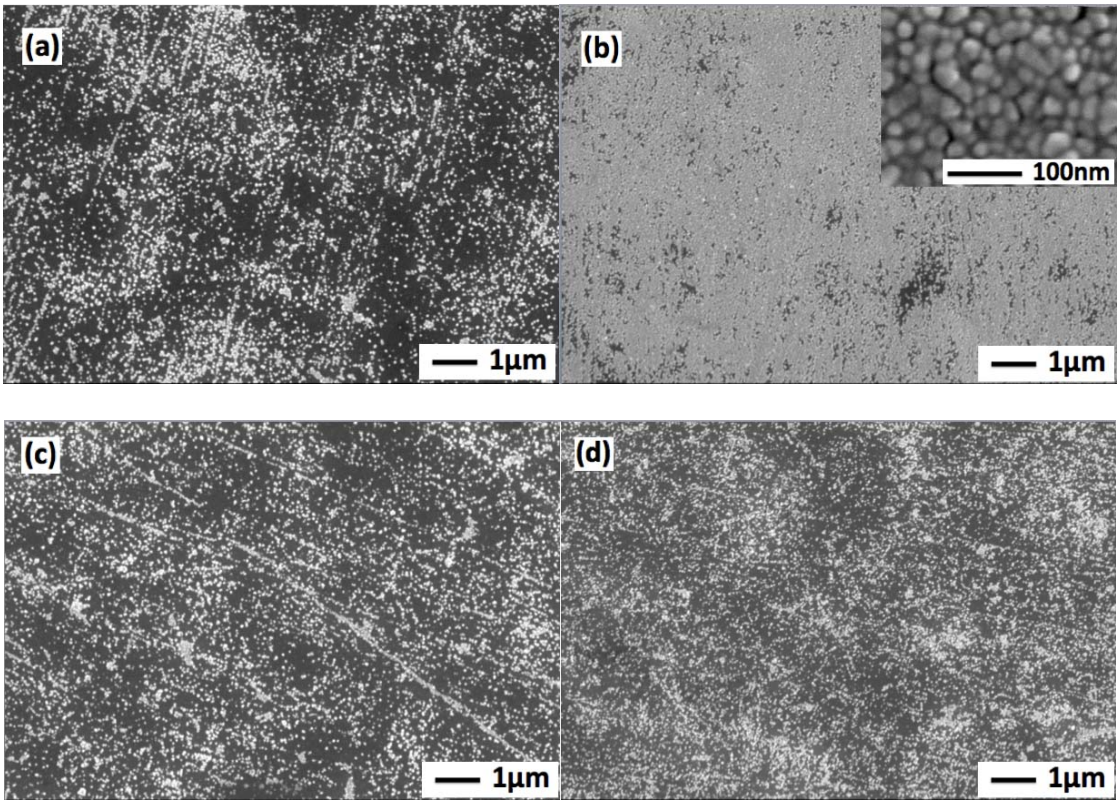

Figure 6-2. SEM images of diamond grown on Ti6Al4V by nano-diamond seeding for (a) 1 h, (b) 3 h, (c) 5 h, (d) 7 h.

Figure 6-3 shows the SEM images of diamond on Ti6Al4V by 1 h nanodiamond seeding without nucleation, and with 10 min, 30 min, and 45 min nucleation and 1 h growth. The results indicate that with 1 h nanodiamond seeding, nucleation density increases with the increase in nucleation time and a near-continuous NCD thin film can be formed after 45 min deposition, as shown in Figure 6-3 (d). However, due to the secondary nucleation, the diamond grain size shows no significant change with the change in nucleation time; grain size remains approximately 20 nm as shown in the inserts in Figure 6-2 (b) and Figure 6-3 (c).

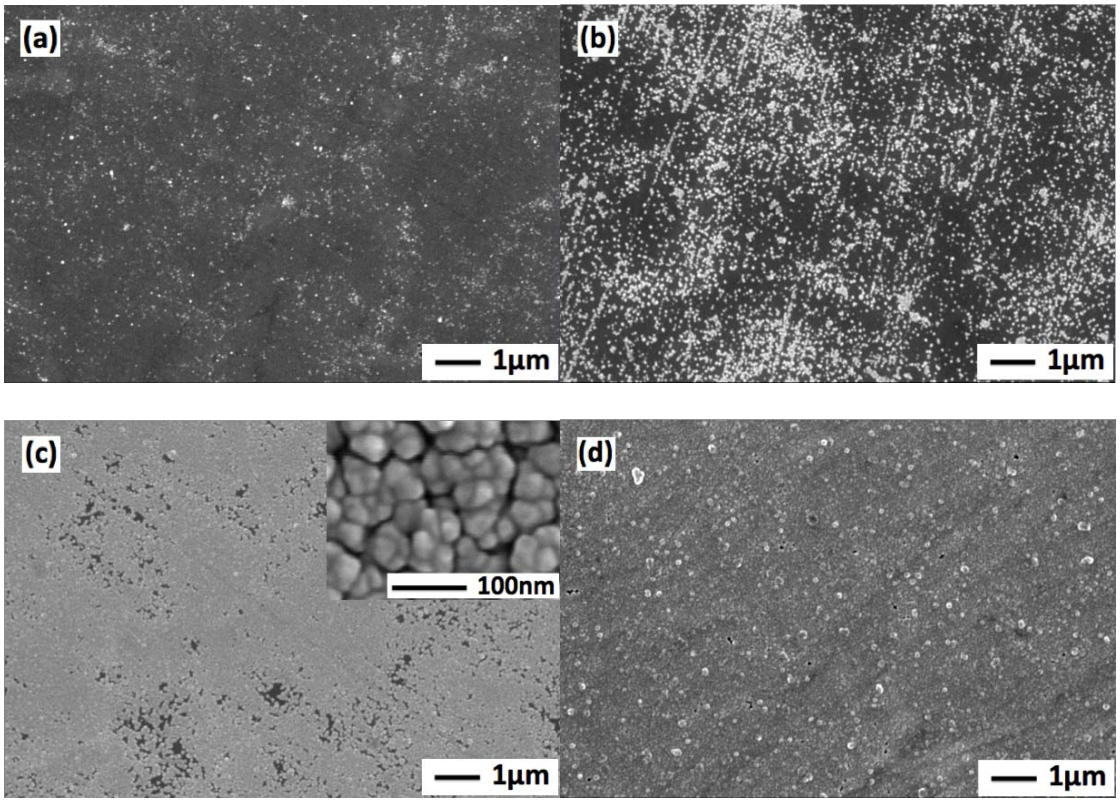

Figure 6-3. SEM images of diamond grown on Ti6Al4V by different nucleation time (a) without nucleation, (b) 10 min, (c) 30 min, (d) 45 min.

The nucleation density of diamond on Ti6Al4V under various seeding and nucleation time is summarized in Figure 6-4. It can be seen that 1 h & 3 h are the optimized seeding time and 45 min & 10 min are the optimized nucleation time for 1 h & 3 h seeding, respectively. For 3 h seeding, diamond nucleates quickly on Ti6Al4V within 10 min, whereas 1 h seeding samples need 45 min to reach their peak nucleation density. Compared with 1 h & 3 h seeding, 2 h, 5 h and 7 h seeding are less effective. This is probably due to the balance between seeding, roughing and polishing. During the diamond seeding process, the diamond seeding density and nano-scale defects induced on Ti6Al4V increase with seeding time before reaching a peak at approximately 1 h, and then decrease due to the polishing effect. After that, these defects and seeding density

increase again because of the bombardment of nanodiamond and peak at 3 h, and fall again after that due to over-polishing. Based on the results, 3 h seeding is most effective to enhance diamond nucleation, enabling NCD thin film formation within a short time (2-3 h) under low microwave power of 600 W as shown in Figure 6-4.

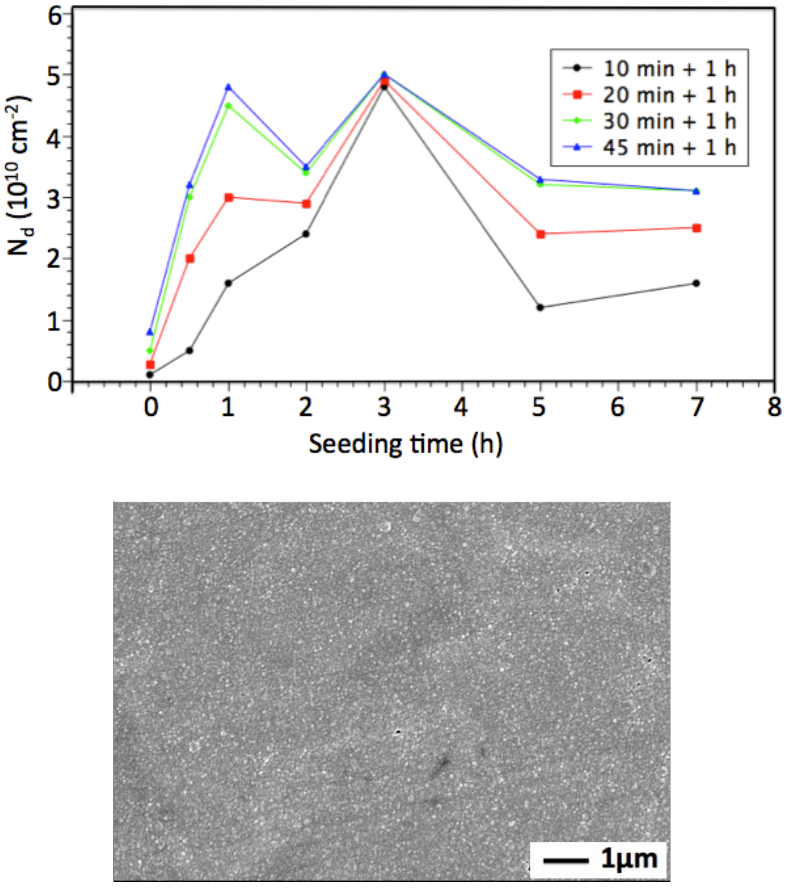

Figure 6-4. Nucleation density (Nd) of diamond on Ti6Al4V with different seeding and nucleation time and SEM image of NCD thin film on Ti6Al4V after total 3 h deposition.

Figure 6-5 shows the SEM images of diamond deposited on Ti6Al4V at different microwave powers. It can be seen that nucleation density is similar with different microwave power ranging from 500 W to 1000 W (by 1 h nano-diamond seeding, 45 min nucleation). In order to prevent

the deterioration of mechanical properties of Ti6Al4V and to decrease the interfacial thermal stress due to the thermal expansion coefficient, it is desirable to use low microwave power for the deposition. However, diamond growth rate is too low for microwave power of 500 W, thus 600 W was used for the investigation of nucleation and growth of diamond.

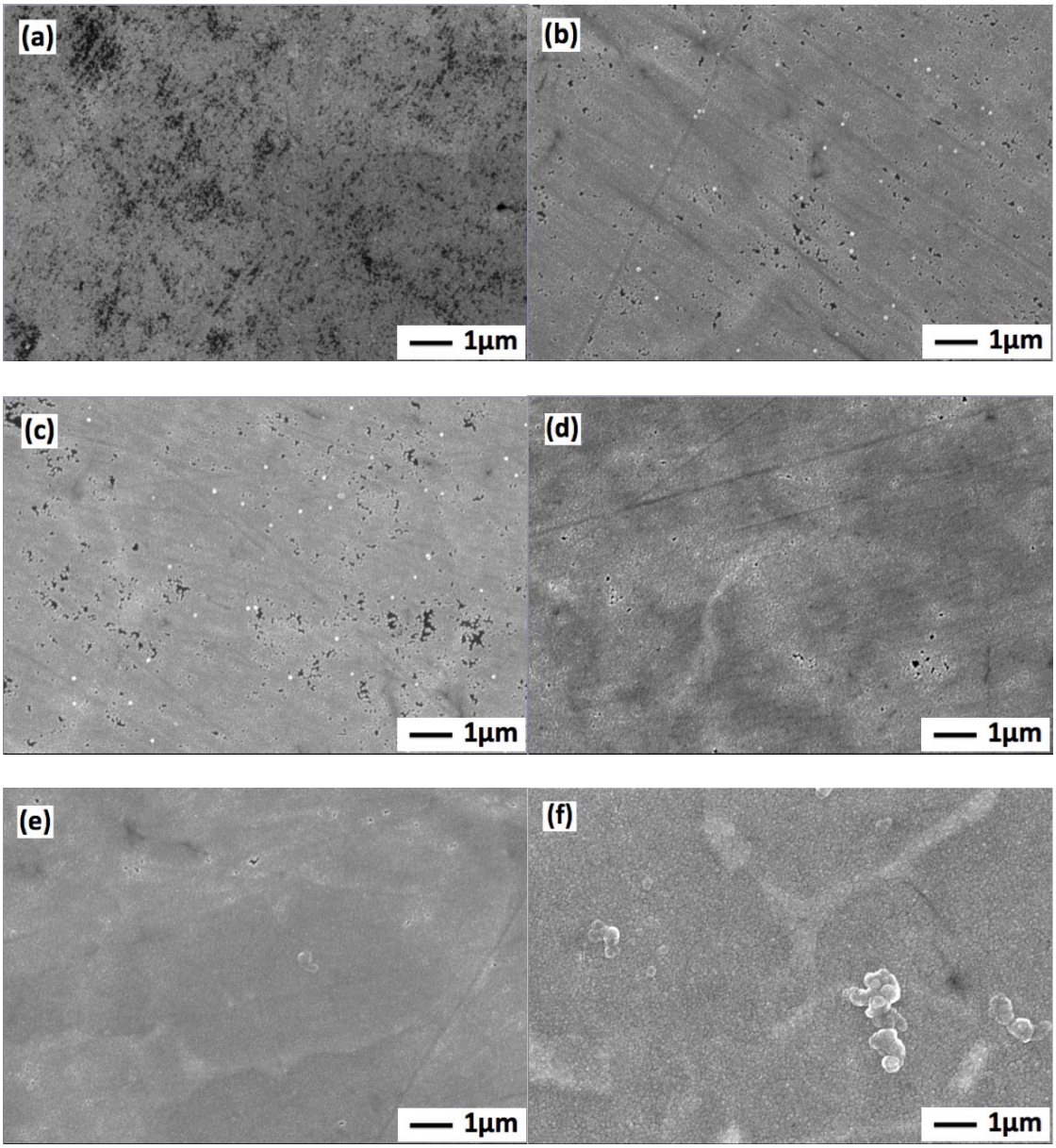

Figure 6-5. SEM images of diamond grown on Ti6Al4V at (a) 500 W, (b) 600 W, (c) 700 W, (d) 800 W, (e) 900 W, (f) 1000 W.

Figure 6-6 shows the Raman spectra of the diamond deposited on Ti6Al4V substrate for various nucleation times. All spectra show a diamond characteristic peak at 1332 cm^{-1}, confirming the diamond nature of the nuclei, and a broad peak at 1550 cm^{-1}, corresponding to sp^2-bonded non-diamond carbon [18, 155]. When the nucleation time is short (10 min), the peak is weak because of the low quantity of carbon (a mixture of diamond and sp^2-bonded non-diamond carbon) deposited. The peaks become stronger for nucleation time of 30 min and 45 min due to the increased quantity of carbon deposited, but the intensity ratio of diamond peak to non-diamond peak shows no significant change with nucleation time, indicating that the nucleation time has no significant effect on the quality of diamond nuclei.

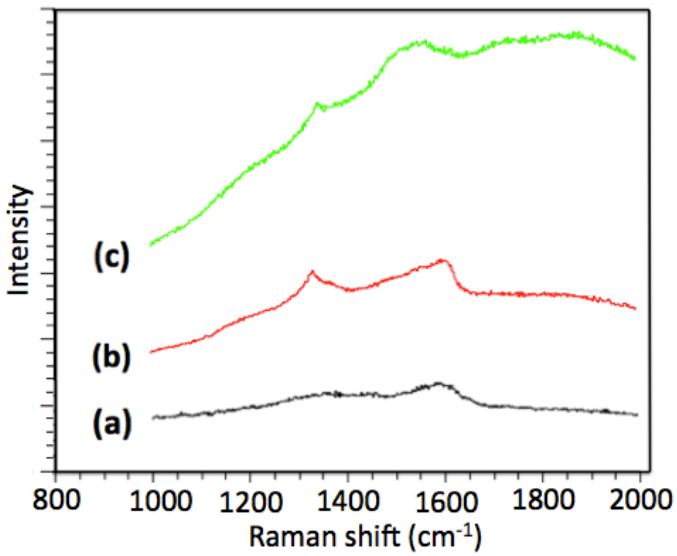

Figure 6-6. Raman spectra of diamond grown on Ti6Al4V with different nucleation time (by 1 h growth) (a) 10 min, (b) 30 min, (c) 45 min.

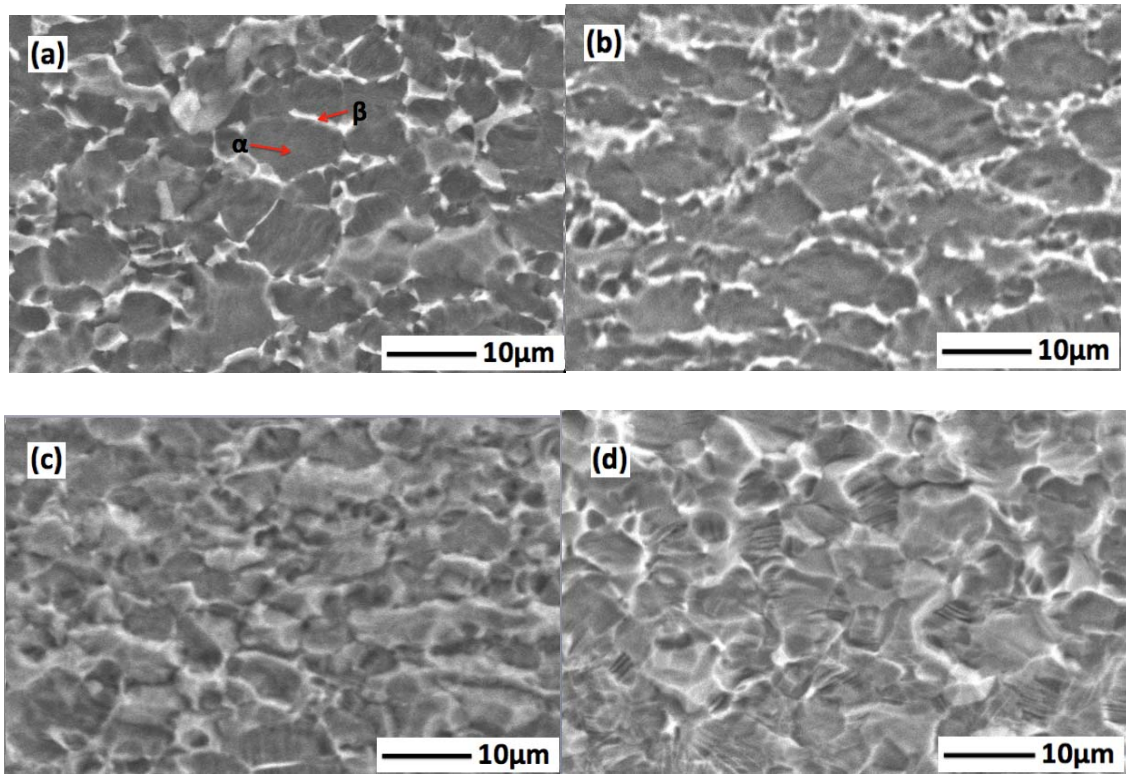

Figure 6-7. Microstructure of Ti6Al4V (a) as received and CVD-diamond coated at (b) 600 W – 3 h (c) 900W – 1 h (d) 500 W – 7 h by SEM.

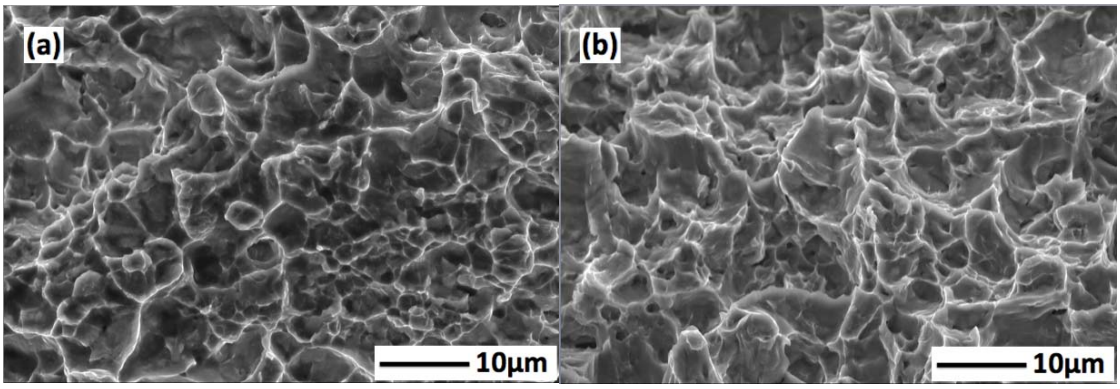

Figure 6-8. Fracture microstructure of Ti6Al4V (a) as received and CVD-diamond coated at (b) 600 W – 3 h.

Cross-sectional microstructures of Ti6Al4V were investigated before and after nanocrystalline diamond deposition by SEM. Figure 6-7 (a) shows the microstructure of as-received Ti6Al4V substrate before deposition. There are two phases: equiaxed α (black) and β (white) [156]. After 3 h deposition at 600 W, no structural changes of Ti6Al4V can be observed (see Figure 6-7 (b)), whereas phase transformation can be seen clearly at higher power or longer time as demonstrated in Fig. 6-7 (c) after 1 h deposition at 900 W and in Figure 6-7 (d) after 7 h deposition at 500 W. Both Figure 6-7 (c) and Figure 6-7 (d) show a decreased α grain size and increased β phase amount due to the α→β phase transformation via α/β interfacial migration. This is probably because of the combined effect of high temperature and diffusion of hydrogen. In the hydrogenation process, the hydrogen-rich phase (β) gradually increases with increasing hydrogen content due to the stabilization effect of hydrogen [157]. Figure 6-8 shows SEM fracture graphs of Ti6Al4V before and after diamond deposition. Both the as-received (Figure 6-8 (a)) and 600 W – 3 h deposited (Figure 6-8 (b)) samples show similar spherical dimples, characteristic of ductile fracture [158]. These results show that 600 W for 3 h is an appropriate deposition condition for diamond on Ti6Al4V as it does not induce significant changes in the microstructure of the substrate.

6.4 Conclusions

The research work done has demonstrated that NCD thin films can be deposited on Ti6Al4V substrates by MPCVD at relatively low microwave power of 600 W within 3 hours. Under these conditions, almost no structural change of Ti6Al4V can be observed, which indicates the deterioration of the mechanical properties of Ti6Al4V caused by diamond deposition can be significantly reduced. These results can widen the application of NCD on Ti6Al4V for aerospace

engineering, chemical engineering and biomedical implant applications, in which the mechanical properties of the substrate play a crucial role.

CHAPTER 7
ADHESION ENHANCEMENT OF DIAMOND-LIKE CARBON THIN FILMS ON TI ALLOYS BY INCORPORATION OF NANODIAMOND PARTICLES

Coating adherent DLC thin films directly on Ti alloys is technologically difficult. This research incorporates nanodiamond particles to form a diamond/DLC composite interlayer to enhance the adhesion of DLC thin films on Ti6Al4V substrates. Initially, nanodiamond particles were deposited on Ti6Al4V substrates by microwave plasma enhanced chemical vapor deposition from a methane-hydrogen gas mixture. A DLC thin film was then deposited, on top of the nanodiamond particles, by direct ion beam deposition. Scanning electron microscopy, Atomic force microscopy, X-ray Diffraction and Raman spectroscopy were used to characterize the microstructure and chemical bonding of the deposited particles and films, and Rockwell indentation testing was used to evaluate the adhesion of the deposited films. The results indicate that the pre-deposited nanodiamond particles significantly enhance the interfacial adhesion between the DLC thin film and the Ti6Al4V substrate, possibly by enhanced interfacial bonding, mechanical interlocking, and stress relief.

7.1 Introduction

Titanium and its alloys have been widely used in aerospace, bio-medical, chemical processing, marine facilities, and sports equipment because of their mechanical properties, including low density, very high tensile strength and toughness, and high corrosion resistance [121, 122]. The use of titanium and its alloys in other applications is restricted primarily by poor tribological properties. Coating of wear/corrosion resistant DLC thin films on titanium alloys can markedly enhance the durability and service performances of these materials [123, 124]. However, DLC thin films often suffer from poor adhesion on titanium alloy substrates due to high internal stress [74].

Various approaches have been used to relieve the internal stress of DLC films in order to enhance adhesion on Ti alloys: (1) optimization of deposition conditions [75]; (2) surface treatment of the substrate, including ion implantation [76], plasma immersion ion implantation [77], nitriding [78] and oxidizing [76, 79], (3) deposition of an interlayer, including a single (Si, Cr, W [81], TiN, TiC, TiCN and CrN [83]), or a graded layer (Ti/CN, Ti/TiC, Ti/TiN/TiC, and Ti/TiN/TiCN/TiC [84]), (4) incorporation of a metal or metal compound layer to form alternative multilayered films such as Ti/DLC and TiC/DLC [85], and (5) incorporation of non-metallic or metallic elements such as Si, Al, Cu, Ti, and W [86] into DLC films. Using these approaches, enhanced adhesion of DLC on Ti alloys has been achieved. However, the enhancement of adhesion is limited and at the expense of a reduction in hardness [18].

DLC has a high fraction of sp^3 carbon bonding, high hardness, and a low coefficient of thermal expansion similar to diamond. The structural and property similarities of DLC and diamond would ensure a strong interfacial bonding between them. Recent study has revealed that adherent nanodiamond particles or thin films can be synthesized on Ti6Al4V by MPCVD with insignificant substrate damage [119]. In this research, synthesis of nanodiamond incorporated DLC films onto Ti6Al4V substrates has been explored to obtain enhanced interfacial bonding of DLC to the substrate for potential wear and friction applications.

7.2 Experimental details

Ti6Al4V sheets with dimensions of 10 mm × 10 mm × 1 mm were ground and polished using silicon carbide paper (350 grit), 9 μm diamond slurry, and 3 μm diamond slurry sequentially and then cleaned in ethanol for 15 min. The sheets were then

ultrasonically seeded for 1 hr in a suspension of ethanol and nanodiamond powder (average crystal size of 4–5 nm) to enhance diamond nucleation, followed by ultrasonic cleaning, rinsing in ethanol and drying in air. The prepared sheets were used as substrates for diamond particle and DLC thin film deposition.

Nanodiamond particle deposition on Ti6Al4V was conducted in a 2.45GHz MPCVD reactor, described in a previous work [159], with a gas mixture of methane CH_4 and hydrogen H_2. The deposition parameters are listed Table 7-1. In order to investigate the effect of diamond content on the adhesion of DLC thin films, three groups of samples were prepared with varying deposition time.

Table 7-1. Deposition conditions of nanocrystalline diamond particles on Ti6Al4V.

Parameters	H_2 flow rate (sccm)	CH_4 flow rate (sccm)	Gas pressure (KPa)	Microwave power (W)	Deposition temperature (°C)	Deposition time (mins)
Sample#1	40	10	4	500	310	10
Sample#2	40	10	4	500	310	20
Sample#3	40	10	4	500	310	60

After diamond deposition, the samples were coated with a DLC film using an EH ion source (KRI EH-1000, manufactured by Kaufman & Robinson, Inc. USA) in an ion beam deposition system [115]. The sample stage was tilted 45° with respect to the ion beam, the ion source was supplied with 5 sccm of methane and the mean ion energy of the beam was 65 eV. The deposition was performed without any additional substrate heating with

a duration of three hours. The chamber base pressure was 2.67×10^{-5} Pa and the working pressure was 1.2×10^{-1} Pa. The thickness of the as-deposited DLC thin film was approximately 150 nm.

The morphology, microstructure and chemical bonding of the as prepared particle and film samples were characterized by SEM, AFM, X-ray diffraction and Raman spectroscopy. The Raman spectrometer was operated at a laser wavelength of 514.5 nm generated by an argon laser. The adhesion of DLC thin films on Ti6Al4V was examined by Rockwell C indentation tests at a load of 1470 N.

7.3 Results and discussion

A typical Raman spectrum of a DLC film directly deposited on Ti6Al4V without an initial deposition of nanodiamond is shown in Figure 7-1. The spectrum shows two broad peaks centered at around 1350 cm^{-1} and 1580 cm^{-1}, a typical DLC feature [116]. Figure 7-2 shows a typical SEM image of a DLC film without an initial deposition of nanodiamond. The dark area is covered with DLC film, and the light area is exposed substrate (Ti6Al4V) after local spallation of the DLC film caused by high internal stress. Figure 7-3 shows typical SEM images of the samples after diamond deposition for various times. It can be seen that with an increased deposition time from 10 mins to 60 mins, the diamond particle (light dots) density and particle size increase from 109 to 1010 $/cm^2$ and from 20 to 40 nm, respectively. The diamond particles grown on Ti6Al4V were characterized by Raman spectroscopy. The Raman spectrum of the nano particles exhibits a diamond characteristic peak centered around 1332 cm^{-1}, as shown in Figure 7-4 (a typical spectrum of sample #3). It should be noted that in order to minimize the property deterioration of the Ti6Al4V substrate, the microwave power used for diamond particle deposition is relative low (500 W), and without additional heating. In this case, diamond

nucleation rate is relatively low and nucleation density increases with deposition time from 10 mins to 60 mins, as shown in Figure 7-3.

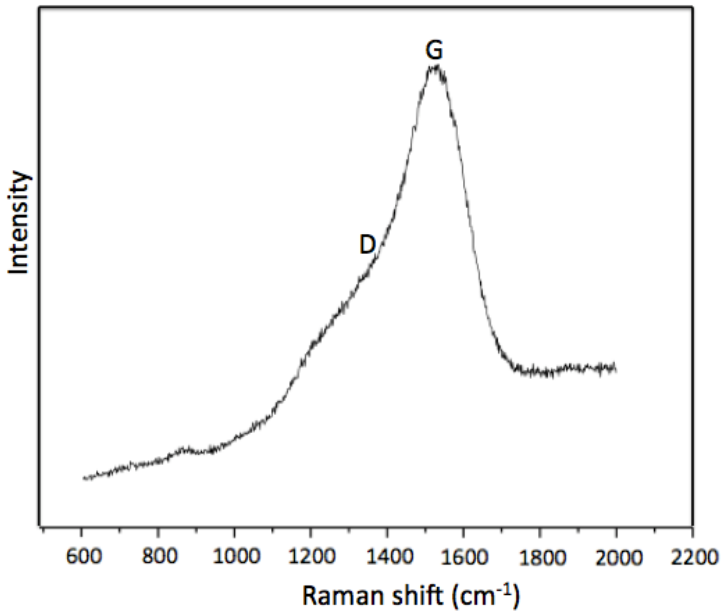

Figure 7-1. Typical Raman spectrum of DLC thin film grown on Ti6Al4V.

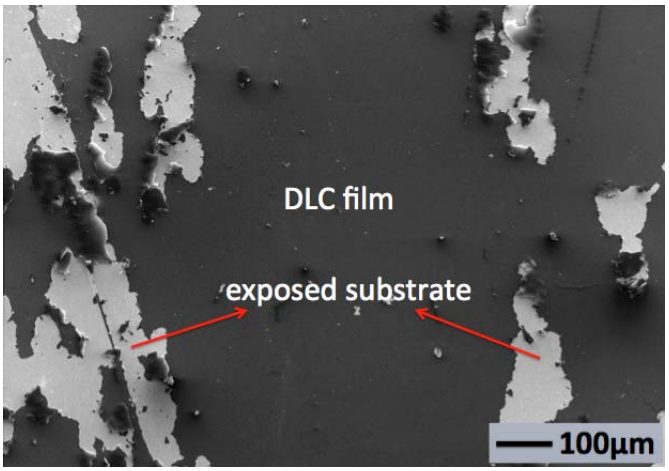

Figure 7-2. Typical SEM image of DLC thin film grown on Ti6Al4V.

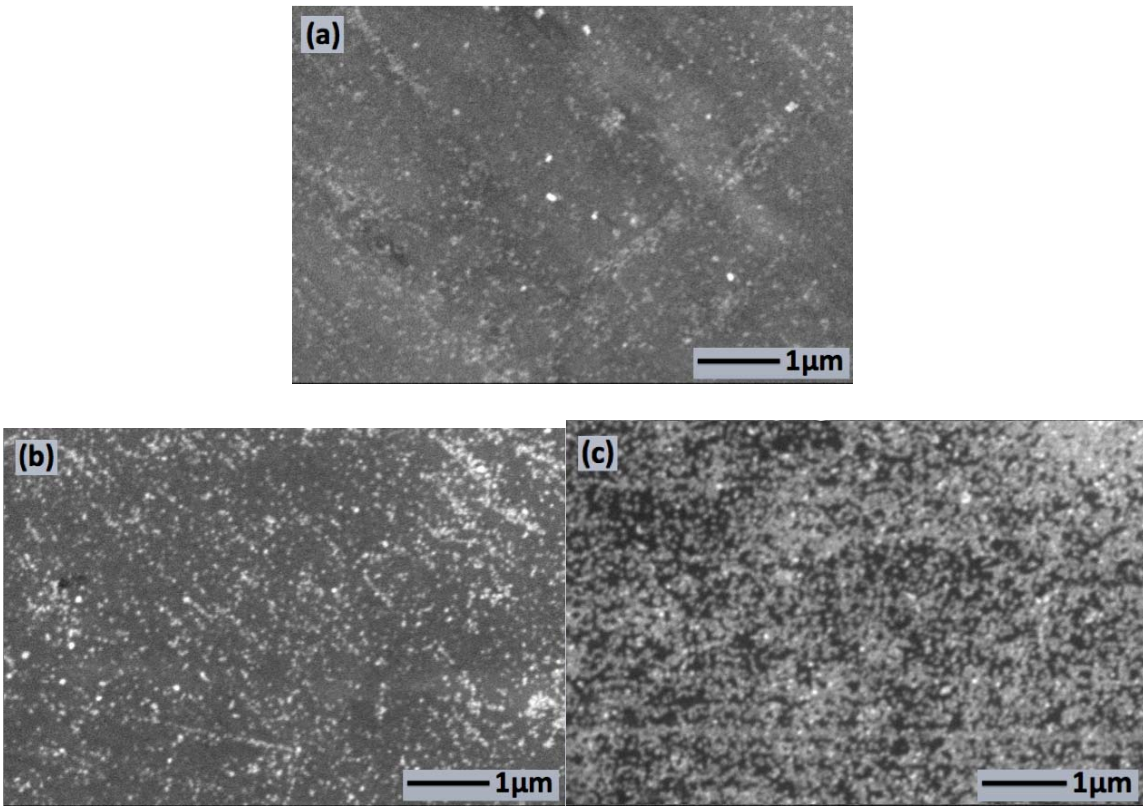

Figure 7-3. Typical SEM images of nanodiamond grown on Ti6Al4V with different deposition time (a) Dia_10mins, (b) Dia_20mins, (c) Dia_60mins.

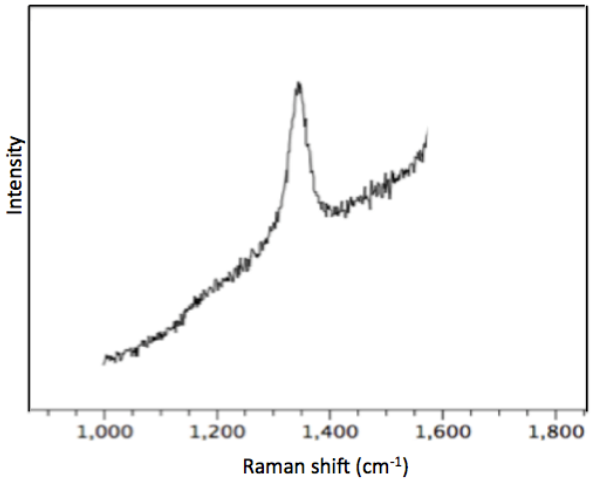

Figure 7-4. Typical Raman spectrum of diamond particles grown on Ti6Al4V (sample #3).

Typical SEM images of as-deposited DLC thin films with pre-deposited nanodiamond particles are illustrated in Figure 7-5. The protruding area indicates the DLC thin film with diamond particle incorporated underneath. The films are dense and there is no spallation occurring, indicating an enhanced adhesion after the incorporation of diamond nanoparticles. The roughness of the nanodiamond incorporated thin films has been measured by AFM over an area of 2 μm × 2 μm and the root-mean squared (RMS) roughness is listed in Table 7-2. The nanodiamond incorporated thin films are slightly rougher than pure DLC films, and the RMS roughness increases from sample #1 to sample #3, indicating that the roughness of nanodiamond incorporated thin films increases with increasing diamond deposition time. This may be associated with the size increase of pre-deposited nanodiamond particle with prolonged deposition time, as shown in Figure 7-3. The larger nanodiamond particle size on the substrate results in increased surface roughness, consequently increasing the roughness of the films deposited on it.

Figure 7-6 shows the typical XRD pattern of diamond/DLC composite thin films (sample #2) on Ti6Al4V, where diamond peaks are denoted as D. It can be seen that there are diamond peaks at 2θ=44°, 75°, and 92°, Ti peaks at 47°, 62°, and 84° (from the substrate), and TiC peaks at 41° and 91°, indicating the formation of a TiC intermediate layer on the substrate surface. The formation of a TiC interfacial layer is beneficial to the enhancement of adhesion of top films and the reduction of substrate damage caused by hydrogenation, as revealed by our recent investigations [119, 160].

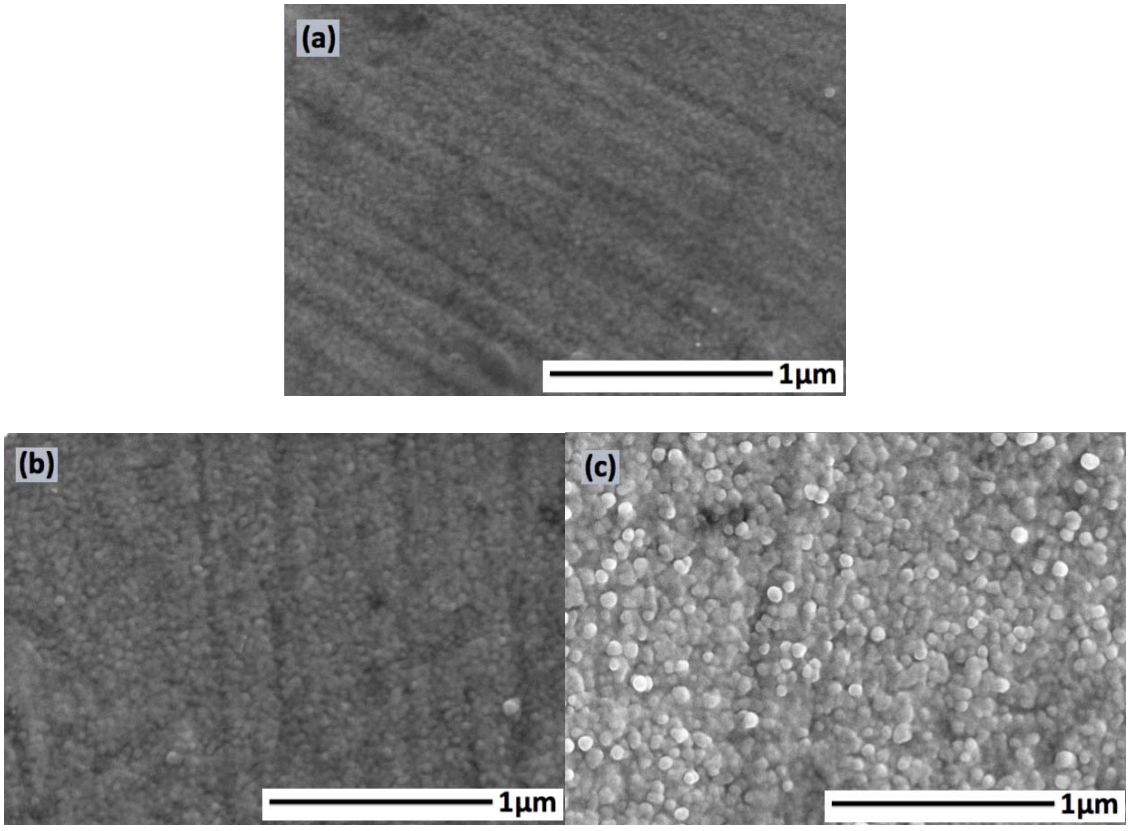

Figure 7-5. Typical SEM images of diamond/DLC composite thin films grown on Ti6Al4V (a) Dia_10mins/DLC, (b) Dia_20mins/DLC, (c) Dia_60mins/DLC.

Table 7-2. Surface roughness (Ra) of DLC and diamond/DLC composite thin films grown on Ti6Al4V. It was calculated base on three measurements at different locations of the films.

Samples	Root-mean squared Roughness (Å)
DLC	26.1 ± 0.3
Diamond/DLC#1	48.6 ± 1.2
Diamond/DLC#2	60.7 ± 0.7
Diamond/DLC#3	126.2 ± 4.5

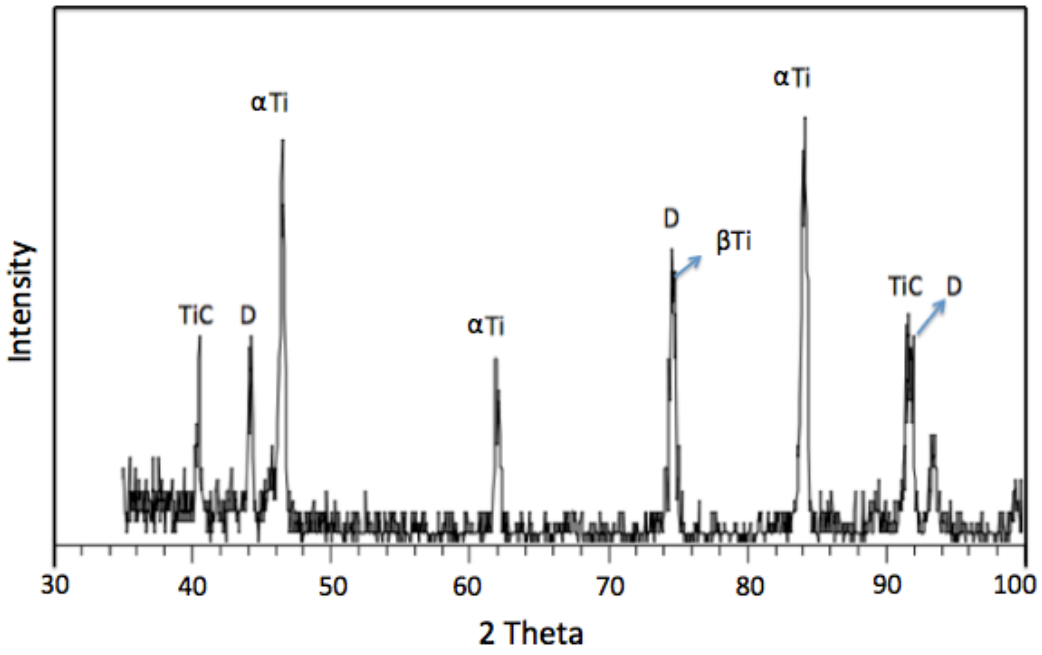

Figure 7-6. XRD patterns of diamond/DLC composite thin films grown on Ti6Al4V. D: diamond; Ti: Titanium.

Rockwell C indentation testing was conducted at a load of 1470 N to evaluate the adhesion of diamond/DLC composite thin films grown on Ti6Al4V. Figure 7-7 shows the SEM images of diamond/DLC films after Rockwell C indentation testing. For all of the samples, partial spallation or cracking of the films is observed in the areas around the imprint (see Figure 7-7-1). However, the spallation or cracking area decreases from sample #1 to sample #3, indicating that the adhesion of diamond/DLC thin films increases with increasing diamond deposition time. This is further confirmed by higher magnification images (Figure 7-7-2) of the spallation or cracking area surrounding the indenter imprint. The white area corresponds to exposed substrate after film spallation, and the dark area corresponds to the film remaining adhered to the substrate. On sample #1, the spallation area accounts for about one fifth of the entire area, as shown in Figure

7-7-2 (a), whereas much less spallation of the film is observed on sample #2 as shown in Figure 7-7-2 (b) and cracking instead of spallation is observed for sample #3 as shown in Figure 7-7-2 (c). These results show that adhesion of the composite films increases with an increase in the amount of nanodiamoand incorporated. The absence of significant film spallation under such a high indentation load for samples #2 and #3 indicates high adhesion of those films to substrate. For sample #1, micro-spallation of DLC induced by indentation occurs at the film/nanodiamond interface as shown in Figure 7-8. This is probably due to a stronger bonding between diamond and substrate/TiC.

The adhesion enhancement of DLC films on Ti alloys after incorporation of nanodiamond particles can be attributed to a few beneficial factors. At the first stage of nanodiamond particle deposition, a TiC buffer layer has initially formed on the Ti alloy, and its growth does not stop even with the nucleation and growth of diamond particles [160, 161], so the diamond actually grows on the top of a TiC layer, which continues to thicken with prolonged deposition period. The formation of such a carbide layer ensures good adhesion of diamond particles to the alloy surface by strong chemical bonding [134]. As the properties of TiC lies between those of diamond (also DLC) and the alloy substrate, a thick carbide buffer layer with long deposition time would enhance the adhesion of diamond particles and DLC films, as confirmed by the indentation test.

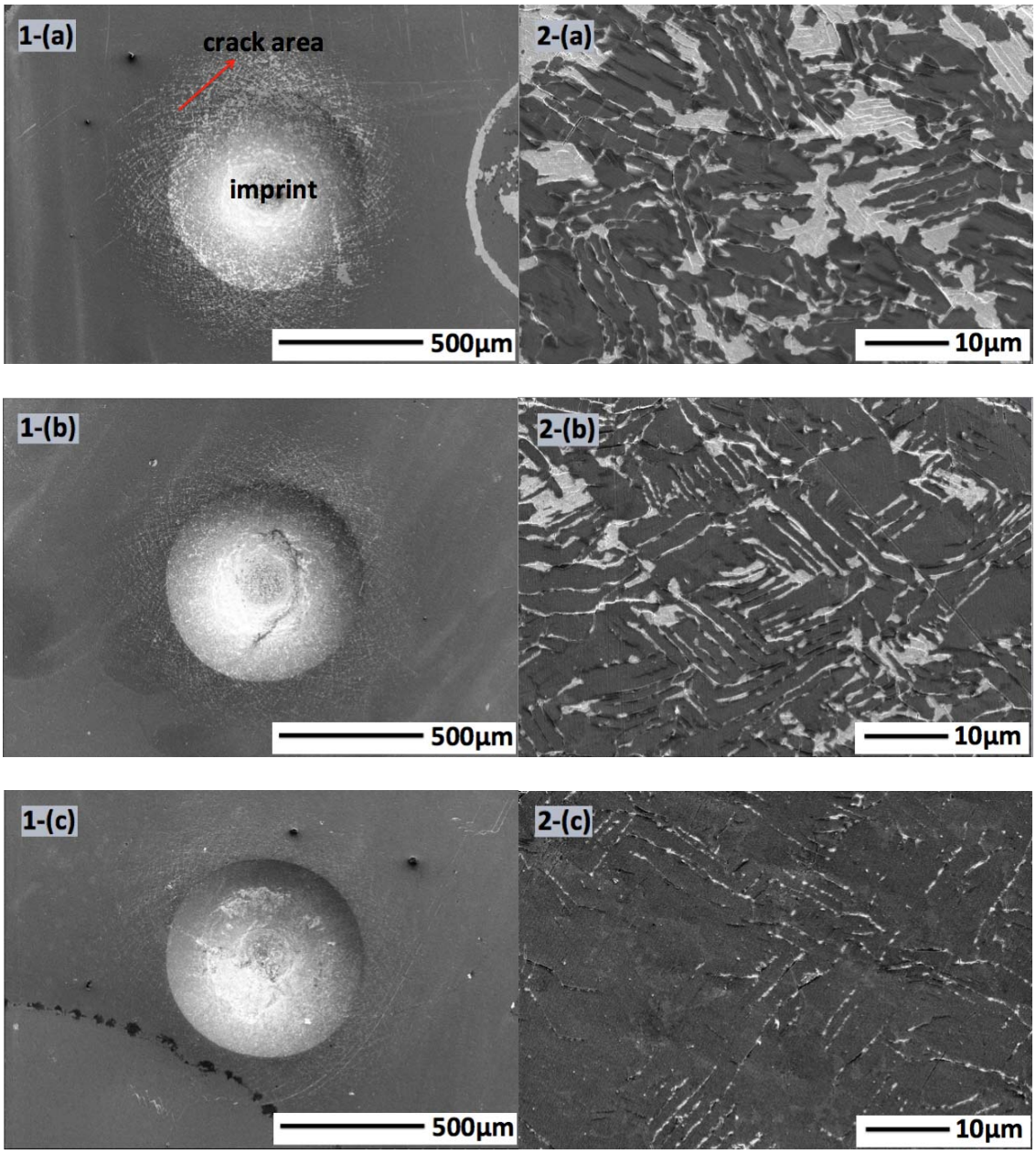

Figure 7-7. Typical SEM images of diamond/DLC-coated Ti alloys after Rockwell C indentation testing: (1) low magnification and (2) higher magnification of spallation or cracking area surround the indenter imprint. (a) Dia_10mins/DLC, (b) Dia_20mins/DLC, (c) Dia_60mins/DLC.

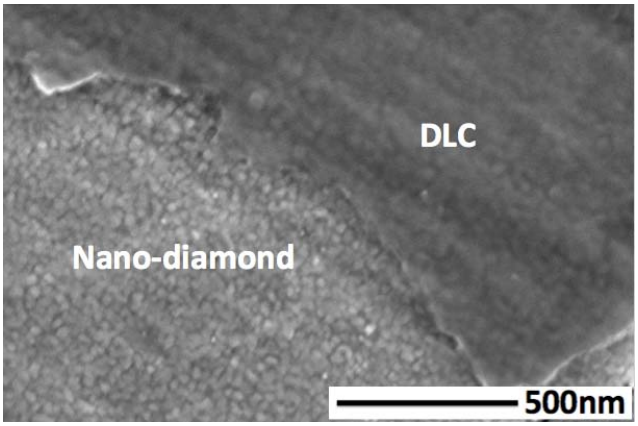

Figure 7-8. SEM image of DLC thin film peeled off on nanodiamond after Rockwell C indentation test.

Furthermore, the growth of the TiC intermediate layer and nanodiamond particles increases surface roughness of the alloy substrate. The roughing of the substrate surface enlarges the total surface area, so the entire effective contact area between DLC and substrate increases, which enhances the interface bonding strength and increases plastic deformation of the interfaces. Following the deposition of DLC film, these discontinuous nanodiamond particles are progressively embedded in the continuous DLC film and a diamond/DLC composite interlayer forms.

Due to its high chemical compatibility to DLC, the nanodiamond particles have strong interfacial bonding strength with DLC, which improves the toughness of the DLC film by providing strong mechanical interlocking and an anchoring effect [162]. It is also reported that a composite of DLC film with a very fine grained diamond film can reduce surface tension and improve adhesion [163].

Due to the reduced stress and increased interfacial strength and toughness, the nanodiamond particles have been demonstrated to be an effective adhesion promoter for DLC on the Ti alloy substrate.

7.4 Conclusions

This paper presents a new approach to enhance the adhesion of DLC thin films on Ti6Al4V substrates, in which high density nanodiamond particles were initially deposited on the substrate using the microwave plasma enhanced CVD method, at a moderate substrate temperature, with short deposition time, and subsequent deposition of a DLC thin film using ion beam deposition. The results have demonstrated that the incorporation of nanodiamond particles to form a diamond/DLC composite interlayer can significantly increase the adhesion of DLC on Ti alloys. The enhancement of adhesion is likely due to increased interfacial bonding, mechanical interlocking and stress relief from the nanodiamond particles.

CHAPTER 8
STUDY OF DIAMOND NUCLEATION AND GROWTH ON TI6AL4V WITH TUNGSTEN INTERLAYER

Diamond nucleation and growth on Ti6Al4V substrates with W interlayers were investigated using HFCVD. W interlayers were firstly deposited on Ti6Al4V substrates under different conditions by sputtering and diamond was then deposited on W coated Ti6Al4V using the same HFCVD reactor. X-ray Diffraction, Scanning electron microscopy, Energy disperse spectroscopy, Atomic force microscopy, Raman spectroscopy, synchrotron near-edge X-ray absorption fine structure spectroscopy and Rockwell C indentation tests were used for characterization. The effect of thickness and surface morphology of W interlayer on the nucleation, growth, and adhesion of diamond on the Ti alloy was investigated. The results show that the pre-deposited W interlayers act as a diffusion barrier for carbon, and thus significantly enhancing the nucleation of diamond. In addition, the W interlayer reacts with carbon to form WC and W_2C during the diamond deposition, and thus enhancing the adhesion of diamond on Ti6Al4V.

8.1 Introduction

Ti and its alloys have been preferentially used in aerospace ships, bio-medical devices, chemical processing, marine facilities, sports equipment, and many other challenging applications because of their high specific strength, superior properties, and high corrosion resistance [2, 113]. However, Ti alloys have significant drawbacks of poor abrasive wear resistance and high friction coefficient. Chemical vapor deposition of a well-adhered diamond coating on Ti alloys is a promising way to solve this drawback owing to the unique properties of diamond, including its extremely high hardness, low friction coefficient, chemical inertness, and high thermal conductivity [1, 121, 160].

Nevertheless, diamond thin films often suffer from poor adhesion on Ti alloy substrates due to the large thermal expansion coefficient mismatch between diamond and Ti alloys, which limit its practical applications [53]. In order to solve this problem, TiN and DLC interlayers were employed to enhance the adhesion of diamond on Ti alloys [9, 57]. Another problem involved in diamond deposition on Ti alloys is the high diffusion rate of carbon and hydrogen into the Ti alloy substrates during diamond deposition. This lowers diamond nucleation and growth rate on the alloys, consequently, a continuous diamond thin film is difficult to form and resulting in the property deterioration of Ti alloys [149, 143]. In our previous paper, a nanodiamond seeding with two-stage deposition was used to enhance diamond nucleation on Ti6Al4V and the property deterioration of Ti6Al4V was consequently reduced by a short deposition time [119]. Particularly, previous work of our group has demonstrated that a W/Al interlayer is promising for enhancing diamond nucleation and adhesion on WC-Co and stainless steel substrates [164, 165]. The results show that a W/Al double layer of nanoscale thickness is very effective to enhance diamond nucleation by suppressing interfacial graphitization induced by catalytic elements from the substrates, in which Al layer acts as a diffuse barrier for graphitization catalytic elements, e.g. Fe or Co, and W layer enhances the nucleation of diamond.

In order to reduce the diffusion of carbon and hydrogen into Ti6Al4V substrate and to understand the effect of W on the nucleation and adhesion of diamond on them, W interlayers with different thickness combined with nanodiamond seeding and two-stage deposition were employed in this work. The results show that diamond nucleation can be

significantly enhanced, consequently, smooth nanocrystalline diamond (NCD) thin films with high adhesion can be achieved on Ti6Al4V.

8.2 Experimental details

Ti6Al4V sheets with dimensions of 10 mm × 10 mm × 1 mm were ground and polished using silicon carbide paper (350 grit), 9 μm diamond slurry, and 3 μm diamond slurry sequentially, followed by ultrasonic cleaning in ethanol for 15 min, rinsing in ethanol, and drying in air.

W interlayers were deposited on Ti6Al4V by sputtering using a HFCVD reactor, described in a previous work [166], in an argon environment. The deposition parameters are listed in Table 8-1. In order to study the effect of thickness of W interlayers on the nucleation and adhesion of NCD thin films on Ti6Al4V, W interlayers were deposited with different during ranging from 20 min to 120 min.

Table 8-1. Deposition parameters for W interlayers.

Sample No.	Bias (V)	Current (A)	Ar flow rate (sccm)	Temperature (°C)	Deposition time (min)	Thickness (μm)
W-1	500	8	20	450	20	1.1
W-2	500	8	20	450	30	1.5
W-3	500	8	20	450	50	2.0
W-4	500	8	20	450	120	10.1

After W deposition, the W coated Ti6Al4V sheets were ultrasonically seeded for 20 min in a suspension of ethanol and nanodiamond powder (average crystal size of 4–5 nm) followed by ultrasonic cleaning and rinsing in ethanol and drying in air.

Diamond deposition on W coated Ti6Al4V after treatment was conducted in the same HFCVD reactor, with a gas mixture of CH_4 and H_2. The deposition parameters are listed in Table 8-2. In order to investigate the effect of W interlayers on the nucleation, growth, and adhesion of diamond thin films, two groups of samples with different deposition time of 30 min (10 min nucleation and 20 min growth) and 2 h (10 min nucleation and 110 min growth) were prepared. Direct diamond deposition on Ti6Al4V (10 min nucleation and 50 min growth) was used for comparison.

Table 8-2. Diamond nucleation and deposition parameters

Parameters	First step (nucleation enhancement)	Second step (diamond growth)
Gas pressure (kPa)	1.33	1.33
Temperature (°C)	450	450
H_2 flow rate (sccm)	49	49
CH_4 flow rate (sccm)	1	1
Deposition time (min)	10	20, 50, 110

The morphology, microstructure, and chemical bonding of the as prepared W and NCD film samples were characterized by scanning electron microscopy (SEM), energy disperse spectroscopy (EDS), atomic force microscopy (AFM), X-ray diffraction (XRD),

Raman spectroscopy, and synchrotron near-edge X-ray absorption fine structure (NEXAFS) spectroscopy. The Raman spectrometer was operated at a laser wavelength of 514.5 nm generated by an argon laser. The NEXAFS experiments were performed using the High Resolution Spherical Grating Monochromator (SGM) beamline at the Canadian Light Source Inc. (CLS), University of Saskatchewan. NEXAFS was recorded in total electron yield (TEY) mode by monitoring the sample current. The adhesion of diamond thin films on Ti6Al4V was evaluated using Rockwell C indentation tests at a load of 1470 N.

8.3 Results and discussion

Figure 8-1 shows typical SEM morphological images of as-deposited W layers. The deposition time is 20 min for sample #W-1, 30 min for sample #W-2, 50 min for sample #W-3, and 120 min for sample #W-4, the corresponding thickness of the W layers increases from 1.1 μm to 10.1 μm, as shown in Table 8-1. It can be seen that with increasing deposition time from 20 min (#W-1) to 120 min (#W-4), the W layers exhibit different surface morphologies. This is because the deposition was carried out at elevated temperature (450 °C), at which surface diffusion is activated to facilitate W to form crystalline structure [167]. At the early deposition stage, W nucleates on Ti6Al4V substrate with high density. Then the nuclei grow and emerge into each other, forming continuous W film as shown in Figure 8-1 (a). With increasing deposition time, W grains continue to grow bigger and bigger, and thus the roughness and thickness of as-deposited W films increase continuously, as shown in Figure 8-1 (b), (c), and (d), respectively. The increased roughness of the W interlayer with the increase of deposition time might be beneficial to the improvement of adhesion of diamond thin films. However, because of the thermal expansion coefficient difference between W and Ti6Al4V, the thermal stress

in the films increase with the increase of film thickness. As shown in Figure 8-1 (c), cracks were observed in sample #W-3 due to the high thermal stress, which would negatively affect the adhesion of diamond thin films on it. XRD patterns of as-deposited W interlayers are shown in Figure 8-2. The W peaks of (110), (200), (211), (220), and (310) can be found at 2θ=47°, 68°, 87°, 106°, and 127°, respectively, indicating that polycrystalline W thin films have been deposited onto the Ti alloy.

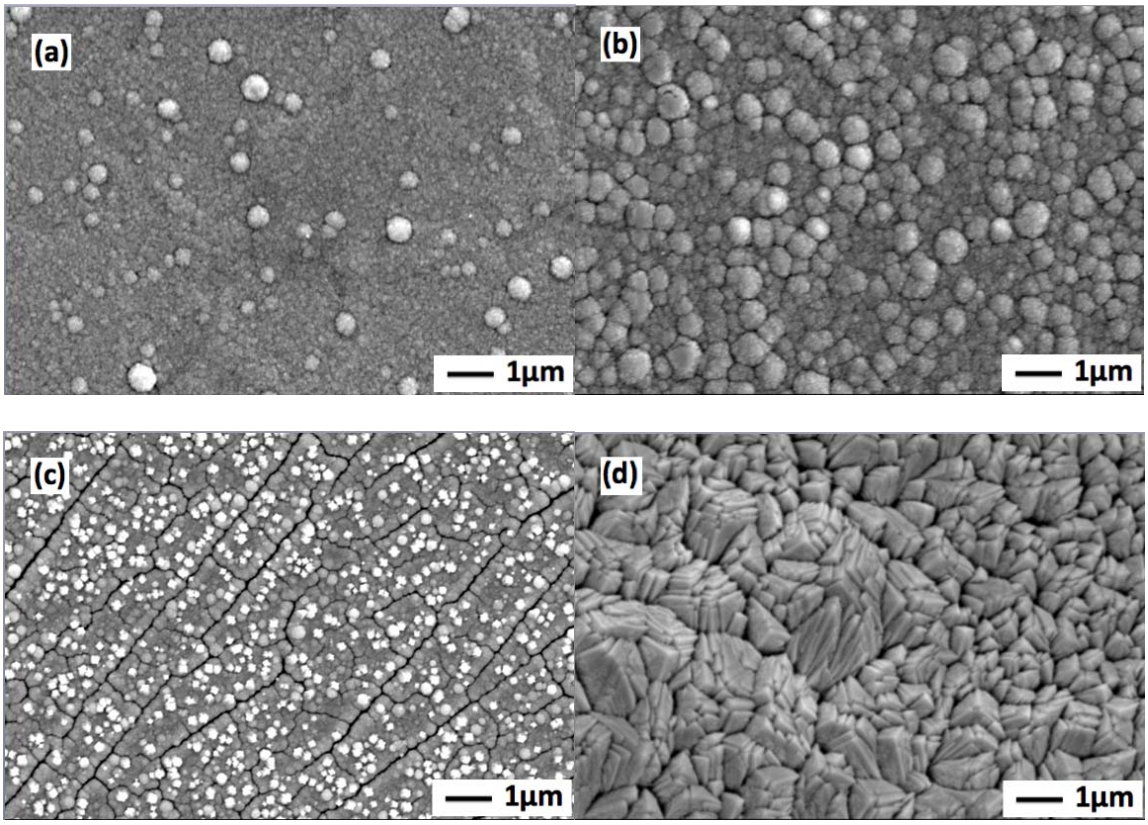

Figure 8-1. Typical SEM images of W interlayers deposited on Ti6Al4V: (a) W-1, (b) W-2, (c) W-3, (d) W-4.

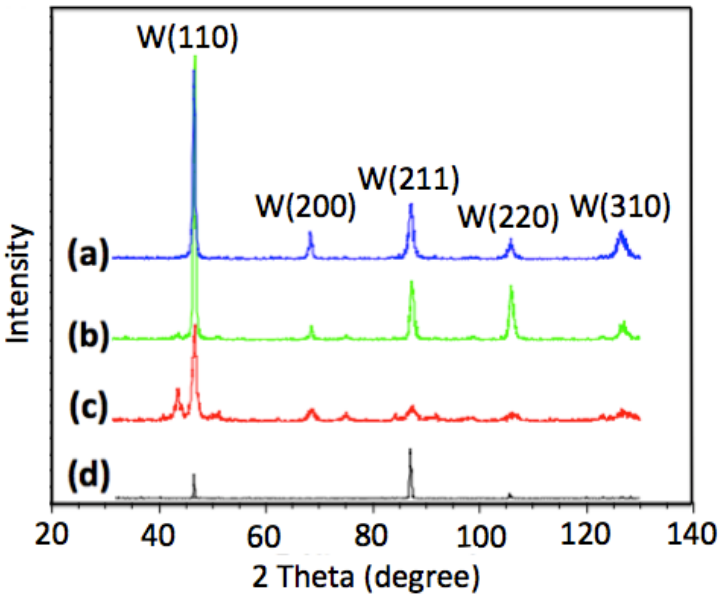

Figure 8-2. XRD patterns of W interlayers on Ti6Al4V (a) W-1, (b) W-2, (c) W-3, (d) W-4.

Figure 8-3 shows SEM (left) and EDS (C $K_{\alpha}1$, right) images of diamond particles grown on W coated Ti6Al4V substrates after 10 min nucleation and 20 min growth. As it is difficult to distinguish W and diamond crystallites under SEM, a carbon distribution by EDS has been used to reveal diamond distribution. For EDS images, the light area corresponds to the carbon (diamond particles) and the dark area corresponds to the W coated substrates. It can be seen that the nucleation density of diamond on all W coated Ti6Al4V samples is significantly higher than that of the diamond samples (with a loger deposition time of 1h) without W interlayer as shown in Figure 8-4. There are some very dark areas in sample #W-4/Dia-30min as depicted in Figure 8-3(d-2). This is probably because of the high roughness of the samples, as EDS has relatively low depth of focus. These results have clearly shown that W interlayer is very effective to enhance diamond nucleation on Ti6Al4V. The fact that diamond nucleation density is similar for all the W

coated samples indicates that the surface morphology and thickness of W interlayers do not have a significant effect on diamond nucleation.

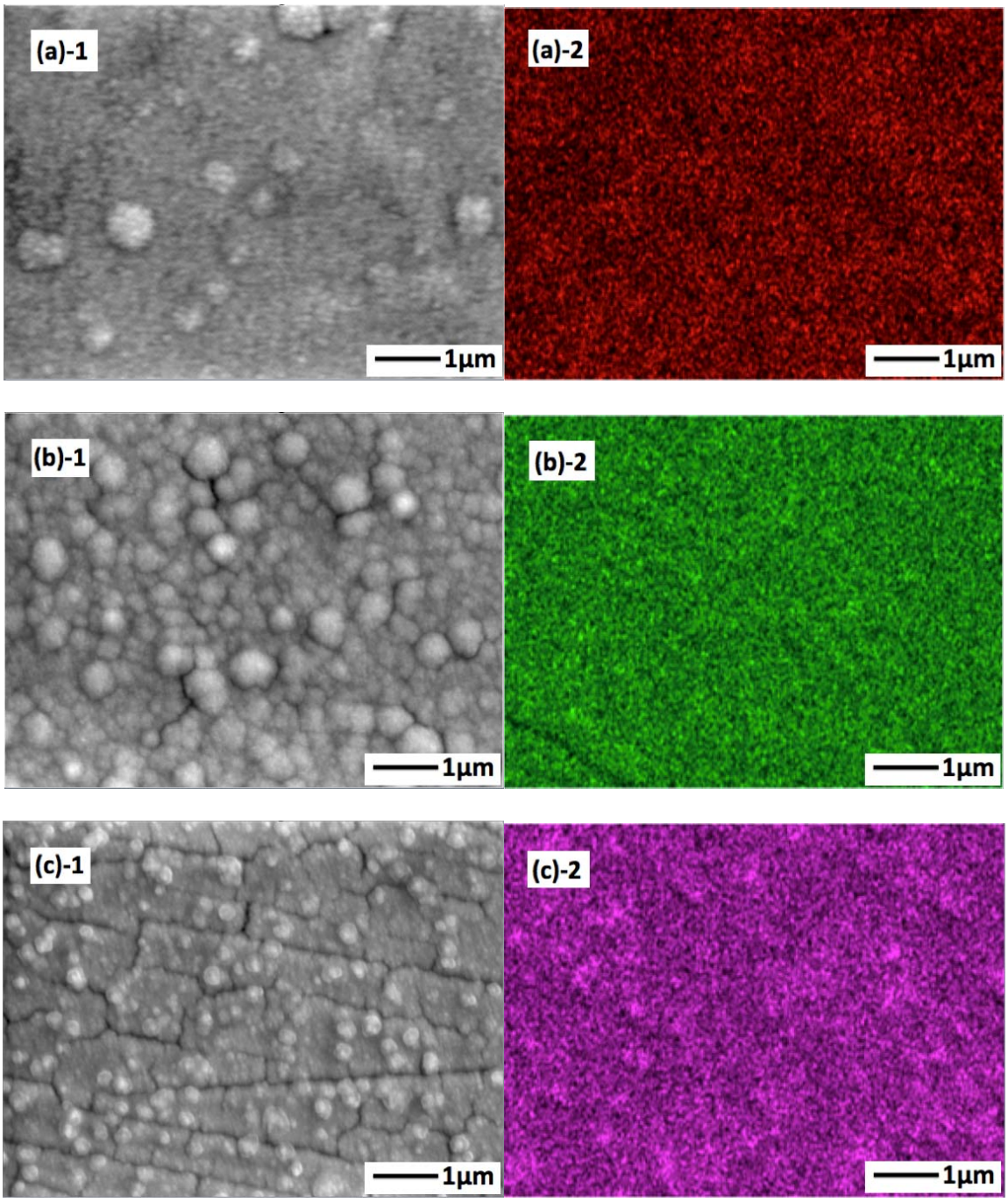

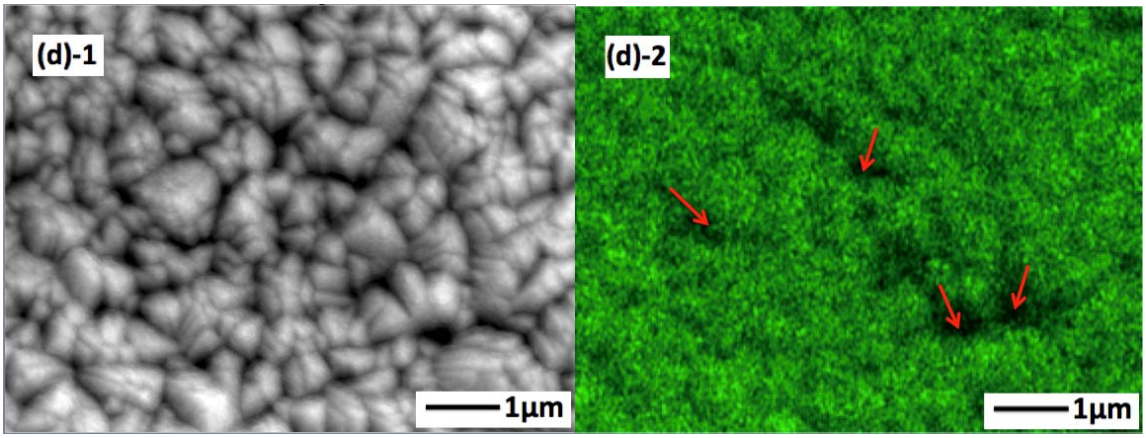

Figure 8-3. SEM (left) and EDS (C Kα1, right) images of diamond grown on Ti6Al4V with W interlayers: (a) W-1/Dia-30min, (b) W-2/Dia-30min, (c) W-3/Dia-30min, (d) W-4/Dia-30min.

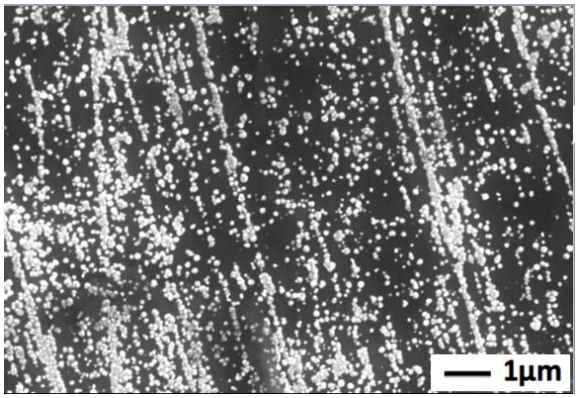

Figure 8-4. Typical SEM image of diamond grown on Ti6Al4V for 1 h (10 min nucleation + 50 min growth) without W interlayer.

Diamond nucleation enhancement by W interlayer can be attributed to the following two aspects. Firstly, the W interlayer with uniform nanocrystalline structure woud enhance nanodiamond seeding uniformity and efficiency by producing finer dispersion of nanodiamond seeds [168]. Secondly, W interlayer could act as a carbon diffusion barrier

to efficiently decrease the amount of carbon dissolved in the Ti alloy substrate during diamond nucleation and initial growth stage because the diffusivity of carbon in W ($(D_c)_W$= 1.0 × 10^{-13} cm^2/s)) is five orders of magnitude lower than that in Ti ($(D_c)_{Ti}$= 0.7 × 10^{-8} cm^2/s) [169]. Both the higher nanodiamond seeding efficiency and the higher carbon concentration on the substrate surface induced by W interlayer could result in higher diamond nucleation. As a result, diamond nucleation is greatly enhanced.

Figure 8-5 shows SEM images of diamond thin films grown on Ti6Al4V substrates with and without W interlayers by 10 min nucleation and 110 min growth. It can be seen that all the films except sample #W-4/Dia-2h have nanocrystalline structure and are dense and uniform with smooth surfaces. The roughness of the as-deposited diamond thin films has been measured by AFM over an area of 2.5 μm × 2.5 μm and the root-mean squared roughness (RMS) values are listed in Table 8-3. It shows that the root-mean squared roughness of W-1/Dia-2h, W-1/Dia-2h, and W-3/Dia-2h is low (below 21 nm) and very close to Dia-2h, the sample without W interlayer. However, W-4/Dia-2h has much higher surface roughness of 52.59 nm. This is probably because of the high roughness of the pre-deposited W interlayers W-4, as shown in Figure 8-1 (d). These results have demonstrated that smooth NCD thin film can be grown on Ti6Al4V with W interlayers of appropriate thickness and that the thickness of W interlayer has no significant effect on the smoothness of the resulted NCD films when the interlayer is relatively thin (<1.5 μm).

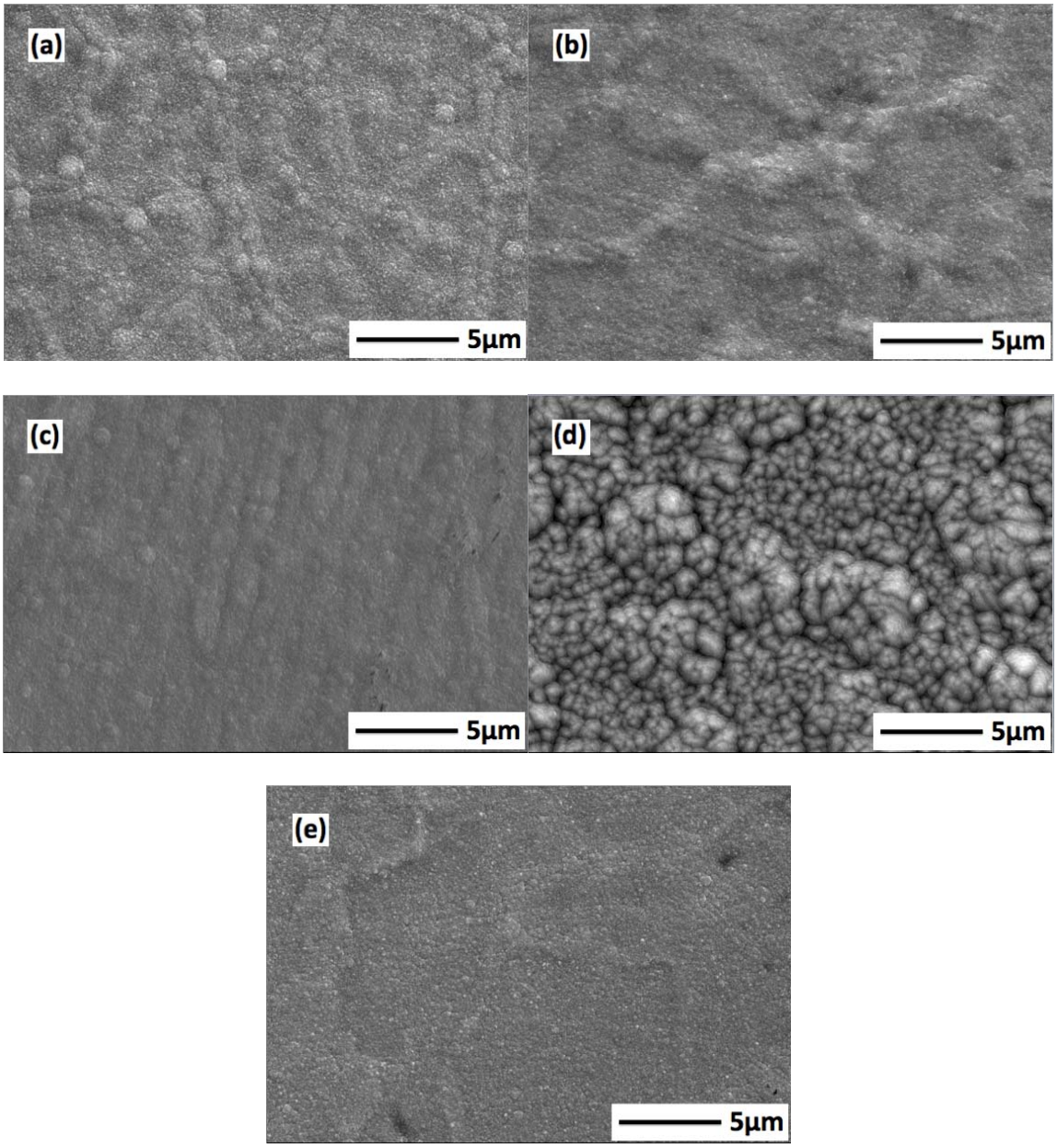

Figure 8-5. Typical SEM images of diamond thin films grown on Ti6Al4V with W interlayers: (a) W-1/Dia-2h, (b) W-2/Dia-2h, (c) W-3/Dia-2h, (d) W-4/Dia-2h, and (e) Dia-2h without W interlayer.

Table 8-3. Surface roughness (Ra) of diamond thin films on Ti6Al4V with and without W interlayers (based on three measurements at different locations of the films)

Samples	Root-mean squared roughness (nm)
W-1/Dia-2 h	17.44±0.05
W-2/Dia-2 h	17.04±0.03
W-3/Dia-2 h	20.68±0.13
W-4/Dia-2 h	52.59±0.32
Dia-2h	17.77±0.06

Figure 8-6 shows the Raman spectra of NCD thin films grown on Ti6Al4V substrates with and without W interlayers by 10 min nucleation and 110 min growth. All spectra show a diamond characteristic peak at 1332 cm^{-1}, confirming the diamond nature of the films. The spectra also show a broad peak at 1550 cm^{-1}, corresponding to the sp^2 bonded non-diamond carbon, and a peak at 1140 cm-1, corresponding to the hydrogen-carbon structure at the grain boundaries [168] or nanocrystalline diamond [170]. There is no significant difference in the intensity ratio of diamond peak to non-diamond peak. In order to further reveal the quality of the resulted NCD films, synchrotron NEXAFS spectroscopy was used to characterize the samples. Figure 8-7 shows the C K-edge NEXAFS spectra of NCD thin films grown on Ti6Al4V substrates with and without W interlayers by 10 min nucleation and 110 min growth recorded in TEY. One can see that all spectra exhibit a sharp spike at 289 eV as well as a large dip at 302 eV, chracteristic features of diamond, confirming the diamond nature of the films, in consistence with Raman results. The relatively small pre-edge peak at 285 eV is attributed to graphite-like

sp^2 bonded carbon of π^* states [102]. It can be found that the intensity of this peak varies with different W interlayers, indicating that the content of sp^2 bonded carbon changes with different W interlayers. All the samples show low peak intensity at 285 eV, indicating low content of sp^2 bonded carbon inside the films. Relatively, the 285 eV peak intensity of sample W-2/Dia-2h and W-4/Dia-2h is similar to that of sample Dia-2h, the sample without W interlayer, but lower than that of sample W-1/Dia-2h and W-3/Dia-2h, indicating relatively better diamond quality in sample W-2/Dia-2h, W-4/Dia-2h, and Dia-2h. These results show that a W interlayer of 1.5 μm thick is desirable for better diamond quality and higher surface smoothness although W interlayers has no significant effect on the quality of the resulted NCD films.

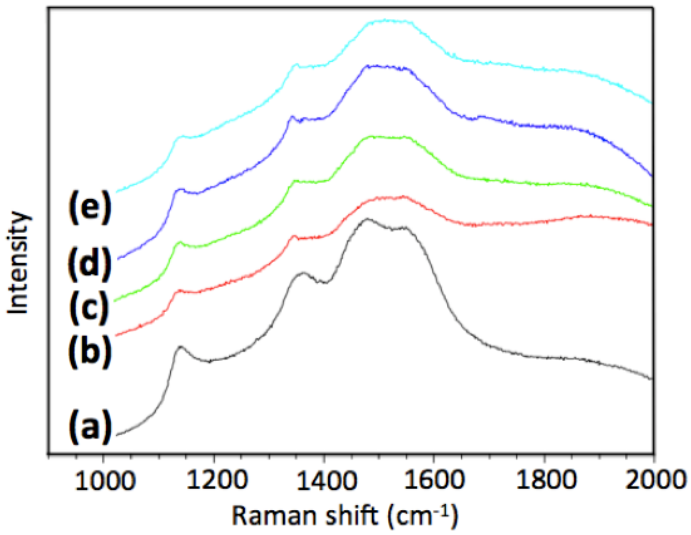

Figure 8-6. Typical Raman spectra of diamond thin films grown on Ti6Al4V with and without W interlayers: (a) W-1/Dia-2h, (b) W-2/Dia-2h, (c) W-3/Dia-2h, (d) W-4/Dia-2h, and (e) Dia-2h without W interlayer.

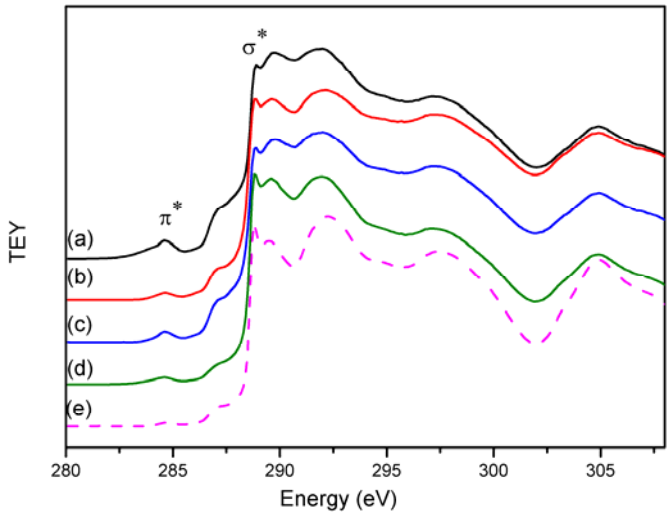

Figure 8-7. NEXAFS spectra of diamond thin films grown on Ti6Al4V with and without W interlayers: (a) W-1/Dia-2h, (b) W-2/Dia-2h, (c) W-3/Dia-2h, (d) W-4/Dia-2h, and (e) Dia-2h without W interlayer.

Figure 8-8 shows the XRD patterns of NCD thin films deposited on W coated Ti6Al4V, where diamond peaks are denoted as Dia. Broad diamond peaks (2θ = 44°, 75°, and 92°) are clearly seen in all the patterns, further confirming the deposition of NCD on the surface. In addition to the diamond peaks, W peaks (2θ = 47°, 87°, 106°, and 127°), WC peaks (2θ =37°, 42°, 56°, 90° and 123°), and W_2C peaks (2θ = 40°, 62°, 72°, and 83°) also appear, indicating that the top part of the W layer reacts with carbon to form WC and W_2C phases. The appearance of such a carbide interfacial layer between NCD and W layer could be beneficial to the adhesion of NCD thin films on W coated Ti6Al4V [167].

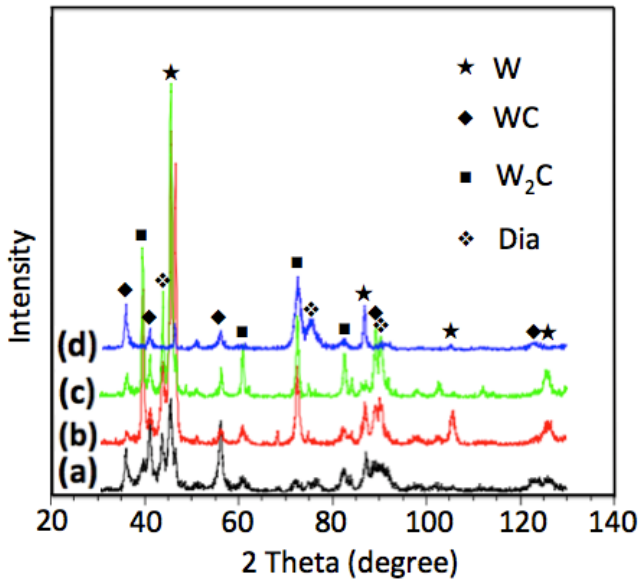

Figure 8-8. XRD patterns of diamond thin films grown on W coated Ti6Al4V: (a) W-1/Dia-2h, (b) W-2/Dia-2h, (c) W-3/Dia-2h, (d) W-4/Dia-2h.

Rockwell C indentation tests were conducted at a load of 1470 N to evaluate the adhesion of NCD thin films grown on Ti6Al4V with and without W interlayers. Figure 8-9 shows the SEM images of the NCD films after Rockwell C indentation testing. Significant cracking and partially spallation were found in NCD samples without a W interlayer as shown in Fig. 8-9 (e). With W interlayers, the degree of spallation or cracking decreases significantly, indicating that the adhesion of NCD thin films has been enhanced by W interlayers. As shown in Figure 8-9 (a), there are only a few small pieces of spallation occurring on sample W-1/Dia-2h and the sample has less cracking area comparing with sample Dia-2h without W interlayer, whereas no spallation of films can be observed for sample #W-2/Dia-2h, #W-3/Dia-2h and #W-4/Dia-2h, as shown in Figure 8-9 (b), (c), and (d), respectively. However, cracking is observed for sample W-3/Dia-2h and W-4/Dia-2h (see Figure 8-9 (c)). This is probably due to the high thermal

stress remained in the pre-deposited W layer. Among all of the samples prepared, W-2/Dia-2h shows the best diamond adhesion as no cracks and no film spallation were observed (see Figure 8-9 (b)). These results show that W interlayer is very effective in enhancing diamond adhesion on Ti6Al4V and that a W interlayer with intermediate thickness of 1.5 μm is more desirable.

The adhesion enhancement of NCD thin films on Ti6Al4V by W interlayer can be attributed to the following reasons. Firstly, at the early stage of NCD deposition, a tungsten carbide buffer layer was initially formed on the W coated Ti6Al4V as confirmed by the XRD results shown in Figure 8-8. The diamond thin films actually grow on the carbide layer. This layer has strong bonding with both the diamond and the W layer and a thermal expansion coefficient of 4.6×10^{-6}/K between diamond (1.1×10^{-6}/K) and W layer (5.7×10^{-6}/K), and thus enhancing the adhesion of diamond on W layer. Formation of a carbide layer on the top of pre-deposited W interlayer is known to be the reason of good adhesion of NCD films to W substrate [171]. Secondly, the enhanced nucleation density by W interlayer enlarges the total contact area between NCD and W coated substrate, and thus further improves adhesion between diamond and substrate. Finally, W interlayer has a thermal expansion coefficient between diamond and Ti6Al4V (8.6×10^{-6}/K) and has a strong bonding with the Ti alloy, thus has high adhesion with the Ti alloy substrate. In one word, due to the formation of a carbide layer and increased interfacial strength and toughness, the W interlayer has demonstrated to be very effective in enhancement of adhesion of NCD thin films on Ti6Al4V.

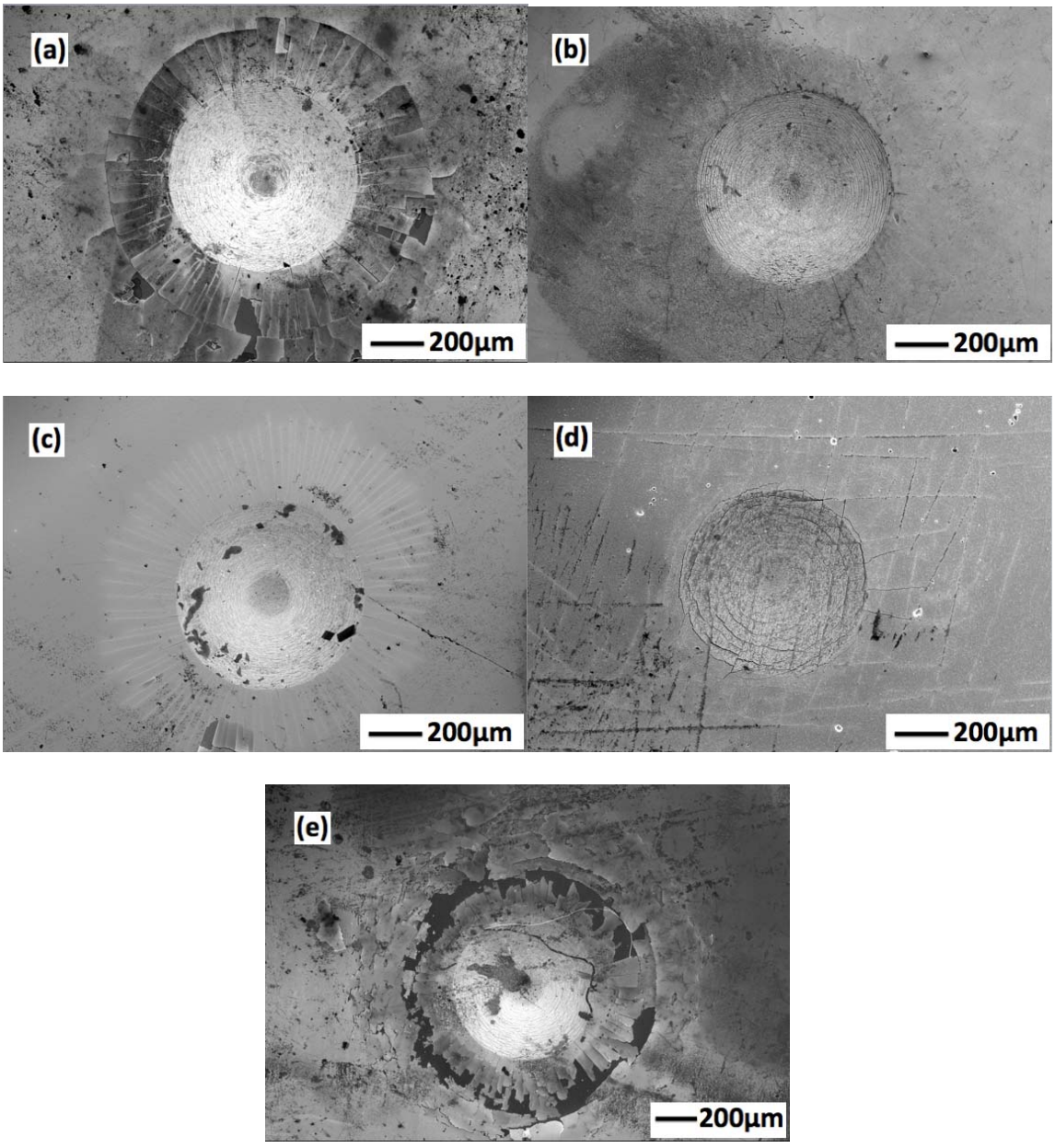

Figure 8-9. Typical SEM images of diamond coated Ti6Al4V with and without W interlayers after Rockwell C indentation testing: (a) W-1/Dia-2h, (b) W-2/Dia-2h, (c) W-3/Dia-2h, (d) W-4/Dia-2h, (e) Dia-2h without W interlayer.

8.4 Conclusions

By applying W interlayer, smooth NCD thin films with high nucleation density and better adhesion have achieved on Ti6Al4V. The thickness and surface morphology of W layers have no significant effect on diamond nucleation but plays important role on the adhesion and surface roughness of the resulted NCD thin films. Smooth W interlayer with a thickness of 1.5 μm works best for NCD adhesion enhancement on Ti6Al4V. The enhanced diamond nucleation probably ascribes to the enhanced nanodiamond seeding efficiency and the fast accumulation of carbon species on the deposition surface because W is a barrier for carbon inward diffusion. The adhesion improvement of NCD on Ti6Al4V is mainly attributed to the formation of a tungsten carbide layer, the high diamond nucleation density, and the thermal and mechanical buffer properties of W interlayer between diamond and the Ti alloy.

CHAPTER 9
CONCLUSIONS AND RECOMMENDATIONS FOR FUTURE WORK

9.1 Conclusions

In this research, a newly developed nanodiamond particles (NDP) incorporation method was used for adhesion enhancement of DLC coatings on Ti6Al4V. In addition, the interface and nucleation enhancement of diamond on Ti6Al4V were studied. The main findings in this thesis are as follows:

- Adhesion of DLC thin films directly deposited on Ti6Al4V substrates by direct ion beam deposition mainly depends on the ion energy used in deposition process. Higher ion energy resulted higher sp^3 concentration of DLC thin films, but lower adhesion of DLC on Ti6Al4V substrates when ion energy used is higher than 70 eV.
- The nucleation density of diamond on Ti6Al4V can be markedly enhanced by deposition at a moderate deposition temperature with a pure CH_4 precursor. Additionally, adhesion strength is improved due to formation of a titanium carbide intermediate layer between NCD film and Ti6Al4V substrate. In addition, the relatively low deposition temperature and high CH_4 concentration applied can mitigate the substrate damage due to hydrogen uptake during diamond deposition.
- Nucleation density of diamond can be enhanced up to 10^{11} cm^{-2} by nanodiamond seeding and two-step deposition. By optimizing the seeding and deposition parameters, NCD thin films can be synthesized at relatively low microwave power (600 W) within a short time (3 hours) deposition. Consequently, almost no structural change of Ti6Al4V can be observed under these conditions, which indicates the deterioration of the mechanical properties of Ti6Al4V caused by diamond deposition can be significantly reduced.

- A newly developed approach named NDP incorporation was used to enhance the adhesion of DLC thin films on Ti6Al4V substrates, in which high density nanodiamond particles were initially deposited on the substrate using the MPCVD method, at a moderate substrate temperature, within short deposition time, and subsequent deposition of a DLC thin film using ion beam deposition. Results have demonstrated that this NDP incorporation method can significantly increase the adhesion of DLC on Ti6Al4V. And the adhesion of DLC on Ti6Al4V increases with the NDP incorporation increasing. The enhancement of adhesion is likely due to increased interfacial bonding, mechanical interlocking and stress relief from the nanodiamond particles.
- By applying W interlayer, smooth NCD thin films with high nucleation density and better adhesion have achieved on Ti6Al4V. The thickness and surface morphology of W layers have no significant effect on diamond nucleation but plays important role on the adhesion and surface roughness of the resulted NCD thin films. Smooth W interlayer with a thickness of 1.5 μm works best for NCD adhesion enhancement on Ti6Al4V. The enhanced diamond nucleation probably ascribes to the enhanced nanodiamond seeding efficiency and the fast accumulation of carbon species on the deposition surface because W is a barrier for carbon inward diffusion. The adhesion improvement of NCD film on Ti6Al4V is mainly attributed to the formation of a tungsten carbide layer, the high diamond nucleation density, and the thermal and mechanical buffer properties of W interlayer between diamond and the Ti6Al4V alloy.
- The newly developed NDP incorporation method is very promising for adhesion enhancement of DLC on Ti6Al4V. It works better than application of W and TiN interlayers.

9.2 Recommendations for future work

Some recommendations for possible future work related to this research are listed below:

- NDP incorporation has been developed and successfully used for adhesion enhancement of DLC thin films on Ti6Al4V. Experimental results show that more NDP incorporation results in better adhesion of DLC. In order to further reveal the relation between adhesion and NDP incorporation, the adhesion of DLC on Ti6Al4V with further increased NDP incorporation needs to be investigated. Moreover, the effect of quality of NDP deposited with varying CH_4 concentration on adhesion and tribological properties of DLC composite films should be of great scientific and technical interests.
- As the newly developed NDP incorporation method is proved to be very promising for adhesion enhancement of DLC on Ti6Al4V, and it works better than application of W and TiN interlayers. More investigation needs to be performed for comparing NDP incorporation and other widely used adhesion enhancing interlayers for DLC.
- DLC coated Ti6Al4V is well known and widely used as biomaterial, especially in orthopedic applications. So it is necessary to evaluate the biomedical and biotribological properties of NDP/DLC composite film coated Ti6Al4V for future biomedical applications.
- Systematic investigation on the effects of experimental parameters on the deposition of diamond on Ti6Al4V is needed in order to better control the properties of deposited diamond. In addition, further studies on the interface between diamond and Ti6Al4V substrate should be of great scientific and technical interests.

LIST OF REFERENCES

[1] S.A. Catledge, Y.K. Vohra, J. Appl. Phys. 84 (1998) 6469-6471.

[2] A.V. Diniz, N.G. Ferreira, E.J. Corat, V.J. Trava-Airoldi, Diam. Relat. Mater. 12 (2003) 577-582.

[3] M.D. Fries, Y.K. Vohra, Diam. Relat. Mater. 13 (2004) 1740-1743.

[4] W. Kulisch, C. Popov, V. Vorlicek, P.N. Gibson, G. Favaro, Thin Solid Films 515 (2006) 1005-1010.

[5] U. Wiklund, I.M. Hutchings, Wear 251 (2001) 1034-1041.

[6] A. Dorner, C. Schürer, G. Reisel, G. irmer, O. Seidel, E. Müller, Wear 249 (2001) 489-497.

[7] C. Meunier, Y. Stauffer, A. Daglar, F. Chai, S. Mikhailov, H.F. Hildebrand, Surf. Coat. Technol. 200 (2006) 6346-6349.

[8] T.M. Manhabosco, L.L. Müller, Tribol. Lett. 33 (2009) 193-197.

[9] Z. Nibennanoune, D. George, F. Antoni, S. Ahzi, D. Ruch, J. Gracio, Y. Remond, Diam. Relat. Mater. 22 (2012) 105-112.

[10] K.L. Choy, E. Felix, Mater. Sci. Eng. A 278 (2000) 162-169.

[11] V.A. Joshi, Titanium Alloys, Taylor & Francis Group, Florida, 2006.

[12] C. Veiga, J.P. Davim, A.J.R. Loureiro, Rev. Adv. Mater. Sci. 32 (2012) 133-148.

[13] H.G. Nelson, D.P. Williams, J.E. Stein, Metall. Trans. 3 (1972) 469-475.

[14] B.G. Yuan, C.F. Li, H.P. Yu, D.L. Sun, Mater. Sci. Eng. A 527 (2010) 4185-4190.

[15] A. Krueger, Carbon Materials and Nanotechnology, Wiley-VCH, Würzburg, 2010.

[16] T.D. Burchell, Carbon Materials for Advanced Technologies, first ed., Elsevier Science, Oxford, 1999.

[17] J. Robertson, Adv. Phys. 35 (1986) 317-374.

[18] J. Robertson, Mater. Sci. Eng. R 37 (2002) 129-281.

[19] M. Scarselli, P. Castrucci, M.D. Crescenzi, J. Phys.: Condens. Matter 24 (2012) 313202.

[20] J.C. Sung, J. Lin, Diamond Nanotechnology, Pan Stanford Publishing, Singapore, 2010.

[21] K. Kobashi, Diamond Films, Elsevier, Oxford, 2005.

[22] J.C. Angus, and C.C. Hayman, Science, 241 (1988) 913-921.

[23] M. Amaral, P.S. Gomes, M.A. Lopes, J.D. Santos, R.F. Silva, and M.H. Fernandes, J. Nanomater. (2008) 894352.

[24] H.D. Wang, Q. Yang, C.H. Niu, I. Badea, Diam. Relat. Mater. 20 (2011) 1193-1198.

[25] F.G. Celli, J.E. Bultler, Ann. Rev. Phys. Chem. 42 (1991) 643-684.

[26] F.P. Bundy, J. Chem. Phys. 38 (1963) 631-643.

[27] S. Matsumoto, Y. Sato, M. Tsutsumi, and N. Setaka, J. Mater. Sci. 17 (1982) 3106-3112.

[28] P.E. Pehrsson, F.E. Celii, J.E. Butler, Diamond films and coatings, (1993) 68-146.

[29] B.V. Spitsyn, L.L. Bouilov, B.V. Deryagin, J. Cryst. Growth 52 (1981) 219-226.

[30] J.C. Angus, Y. Wang, M. Sunkara, Ann. Rev. Mater. Sci. 21 (1991) 221-248.

[31] W.G. Eversole, (1962) US Patent No. 3, 030, 187; 3, 030, 188.

[32] K. Mitsuda, Y. Kojima, T. Yoshida, K. Akashi, J. Mater. Sci. 22 (1987) 1557-1562.

[33] A. Sawabe, T. Inuzuka, Thin Solid Films 137 (1986) 89-99.

[34] K. Suzuki, A. Swabe, H. Yasuda, T. Inuzuka, Appl. Phys. Lett. 50 (1987) 728-729.

[35] C.P. Chang, D.L. Flamm, D.E. Ibbotson, J.A. Mucha, J. Appl. Phys. 63 (1988) 1744-1748.

[36] P.A. Denning, D.A. Stevenson, Proc. of the 2nd Int. Conf. on New Diamond Sci. and Techn, Pittsburg, PA, MRS (1991) 403-408.

[37] B. Singh, O. Mesker, A.W. Levine, Y. Arie, Report CN-5300, David Sarnoff Research Center, SRI International, Princeton, 1988.

[38] C.J. Chen, L. Chang, T.S. Lin, F.R. Chen, J. Mater. Res. 10 (1995) 3041-3049.

[39] S. Iijima, Y. Aikawa, K. Baba, J. Mater. Res. 6 (1991) 1491-1498.

[40] S.T. Lee, Z. Lin, X. Jiang, Mater. Sci. Eng. 25 (1999) 123-154.

[41] S. Yugo, T. Kanai, T. Kimura, T. Muto, Appl. Phys. Lett. 58 (1991) 1036-1038.

[42] X. Jiang, C.P. Klages, Diam. Relat. Mater. 2 (1993) 1112-1113.

[43] X. Jiang, C.P. Klages, R. Zachai, M. Hartweg, H.J. Fusser, Appl. Phys. Lett. 62 (1993) 3438-3440.

[44] B.R. Stoner, J.T. Glass, Appl. Phys. Lett. 60 (1992) 698-700.

[45] S. Yugo, T. Kimura, T. Kanai, Diam. Relat. Mater. 2 (1993) 328-332.

[46] B.R. Stoner, G.H. Ma, S.D. Wolter, W. Zhou, Y.C. Wang, R.F. Davis, J.T. Glass, Diam. Relat. Mater. 2 (1993) 142-146.

[47] X. Jiang, K. Schiffmann, C.P. Klages, Phys. Rev. B50 (1994) 8402-8410.

[48] L. Chandra, M. Chhowalla, G.A.J. Amaratunga, T.W. Clyne, Diam. Relat. Mater. 5 (1996) 299-304.

[49] A.F. Azevedo, E.J. Corata, N.F. Leitea, J. Vladimir, T. Airoldi, Diam. Relat. Mater. 11 (2002) 550-554.

[50] T. Grögler, E. Zeiler, A. Hörner, S.M. Rosiwal, R.F. Singer, Surf. Coat. Technol. 98 (1998) 1079-1091.

[51] D. Rats, L. Vandenbulcke, R. Herbin, R. Benoit, R. Erre, V.Serin, Thin Solid Films 270 (1995) 177-183.

[52] L. Vandenbulcke, D. Rats, R. Herbin, Mater. Lett. 27 (1996) 77-80.

[53] A.F. Azevedo, E.J. Corata, N.F. Leitea, J. Vladimir, T. Airoldi, Surf. Coat. Technol. 194 (2005) 271-275.

[54] M.D. Fries, Y.K. Vohra, J. Phys. D: Appl. Phys. 35 (2002) L105-L107.

[55] S.A. Catledge, Y. K. Vohra, Mater. Res. Soc. Symp. Proc. 505 (1997) 629-633.

[56] S.J. Askari, F. Akhtar, G.C. Chen, Q. He, F.Y. Wang, X.M. Meng, F.X. Lu, Mater. Lett. 61 (2007) 2127-2600.

[57] A. Sokolowska, J. Rudnicki, P. Niedzielski, A. Boczkowska, G. Boguslawski, Surf. Coat. Technol. 200 (2005) 87-89.

[58] Z.Nibennanoune, D.George, F.Antoni, S.Ahzi, D.Ruch, J.Gracio, Y.Remond, Diam. Relat. Mater. 22 (2012) 105-112.

[59] H. Tsai, D.B. Bogi, J. Vac. Sci. Technol. A5 (1987) 3287-3312.

[60] S. Aisenberg, R. Chabot, J. Appl. Phys. 42 (1971) 2953-2958.

[61] J. Robertson, Prog. Solid State Chem. 21 (1991) 199-333.

[62] J.C. Angus, P. Koidl, S. Domitz, Plasma Deposited Thin films, JRC Press, Florida, 1986.

[63] Y. Lifshitz, Diam. Relat. Mater. 8 (1999) 1659-1676.

[64] M. Weiler, K. Lang, E. Li, J. Robertson, Appl. Phys. Lett. 72 (1998) 1314-1316.

[65] N. Savvides, J. Appl. Phys. 59 (1989) 4133-4145.

[66] D.R. McKenzie, Rep. Prog. Phys. 59 (1996) 1611-1664.

[67] A.A. Voevodin, M.S. Donley, Surf. Coat. Technol. 82 (1996) 199-213.

[68] M.W. Geis, M.A. Tamor, Encycl. Appl. Phys. 5 (1993) 1-24.

[69] Y. Lifshitz, Diam. Relat. Mater. 5 (1996) 388-400.

[70] H.J. Steffen, C.D. Roux, D. Marton, J.W. Rabalais, Phys. Rev. B44 (1991) 3981-3990.

[71] J. Robertson, Surf. Coat. Technol. 50 (1992) 185-203.

[72] Y. Lifshitz, G.D. Lempert, E. Grossman, Phys. Rev. Lett. 72 (1994) 2753-2756.

[73] D. Schneider, H.J. Scheibe, Th. Schwarz, Diam. Relat. Mater. 2 (1993) 1396-1410.

[74] J. Lankford, C.R. Blanchard, C.M. Agrawal, D.M. Micallef, G. Dearnaley, A.R. McCabe, Nucl. Inst. Methods Phys. Res. B80 (1993) 1441-1445.

[75] Y.X. Leng, J.Y. Chen, P. Yang, H. Sun, G. J. Wan, N. Huang, Surf. Sci. 531 (2003) 177-184.

[76] H. Dong, W. Shi, T. Bell, Wear 225–229 (1999) 146-153.

[77] K.G. Kostov, M. Ueda, M. Lepiensky, P.C. Soares Jr., G.F. Gomes, M.M. Silva, H. Reuther, Surf. Coat. Technol. 186 (2004) 204-208.

[78] R. Wei, T. Booker, C. Rincon, J. Arps, Surf. Coat. Technol. 186 (2004) 305-313.

[79] P.A. Dearnley, K.L. Dahm, H. Çimenoğlu, Wear 256 (2004) 469-479.

[80] A. Antilla, R. Lappalainen, V.M. Tiainen, M. Hakovirta, Adv. Mater. 9 (1997) 1161-1164.

[81] N.J. Ianno, R.O. Dillon, A. Ali, and A. Ahmad, Thin Solid Films, 270 (1995) 275-278.

[82] K.H. Dittrich, D. Oelsner, Int. J. Refract. Met. Hard Mater. 20 (2002) 121-127.

[83] H.Y. Ueng, C.T. Guo, K.H. Dittrich, Surf. Coat. Technol. 200 (2006) 2900-2908.

[84] H. Dong, T. Bell, Ind. Lubr. Tribol. 50 (1998) 282-289.

[85] S. Anders, D.L. Callahan, G.M. Pharr, C.S. Bhatia, Surf. Coat. Technol. 94 (1997) 189-194.

[86] M. Chhowalla, Diam. Relat. Mater. 10 (2001) 1011-1016.

[87] R.F. Bonshah, Handbook of Hard Coatings, Noyes, New York, 2001.

[88] M. Kamo, S. Matsumoto, Y. Sato, N. Setaka, (1984) US patent No. 4,434,188.

[89] F.-W. Bach, A. Laarmann, T. Wenz, Modern Surface Technology, WILEY-VCH, WeinHeim, 2006.

[90] R.F. Egerton, Physical Principles of Electron Microscopy, Springer, Edmonton, 2005.

[91] http://www2.warwick.ac.uk/fac/sci/physics/current/postgraduate/regs/mpags/ex5/techniques/elec

tronic/sem-copy/, accessed on July 5th, 2013.

[92] G. Binning, C.F. Quate, C. Gerber, Phys. Rev. Lett. 56 (1986) 930-933.

[93] http://nano.mtu.edu/afm.htm, accessed on July 5th, 2013.

[94] http://archive.nrc-cnrc.gc.ca/eng/projects/ibd/raman-spectroscopy.html, accessed on August 4th, 2013.

[95] F. Tuinstra, J.L. Koening, J. Chem. Phys. 53 (1970) 1126-1130.

[96] http://serc.carleton.edu/research_education/geochemsheets/techniques/XRD.html, accessed on August 4th, 2013.

[97] http://chemwiki.ucdavis.edu/Analytical_Chemistry/Instrumental_Analysis/Diffraction/Powder_X-ray_Diffraction, accessed on August 5th, 2013.

[98] C. Suryanarayana, M. G. Norton, X-ray Diffraction A Practical Approach, Plenum Press, New York, 1998.

[99] J. Stöhr, NEXAFS Spectroscopy, Springer, Heidelberg, 1992.

[100] B. Watts, L. Thomsen, P.C. Dastoor, J. Electron. Spectrosc. Relat. Phenom. 151 (2006) 105-120.

[101] T. Hemrai-Benny, S. Banerjee, S. Sambasivan, M. Balasubramanian, D.A. Fischer, G. Eres, A.A. Puretzky, D.B. Geohegan, D.H. Lowndes, W. Han, J.A. Misewish, S.S. Wong, Small 2 (2006) 26-35.

[102] B.W. Yates, Y.F. Hu, K.H. Tan, G. Retzlaff, R.G. Cavell, T.K. Sham, G.M. Bancroft, 326 J. Synchrotron Rad. 7 (2000) 296-300.

[103] X. Li, B. Bhushan, Mater. Charact. 48 (2002) 11-36.

[104] C.A. Schuh, Mater. Today 9 (2006) 32-40.

[105] http://www.nanoindentation.cornell.edu/Machine/commercial_machine.htm, , accessed on August 5th, 2013.

[106] K.L. Mittal, Adhesion Measurement of Thin Films, Thick Films, and Bulk coatings, American Society for Testing and Materials, 1978.

[107] P.A. Engel, G.C. Pedroza, Adhesion Aspects of Polymeric Coatings, Plenum, New York, 1983.

[108] R. Lacombe, Adhesion Measurement Methods: Theory and Practice, CRC Press, Florida, 2006.

[109] D.C. Jiles, Introduction to The Principles of Materials Evaluation, CRC Press, Florida, 2008.

[110] M. Allen, B. Myer, N. Rushton, J. Biome. Mater. Res. 58 (2001) 319-328.

[111] S.W. Jiang, B. Jiang, Y. Li, Y.R. Li, G.F. Yin, C.Q. Zheng, Appl. Surf. Sci. 236 (2004) 285-291.

[112] Z.X. Zhang, H. Dong, T. Bell, B.S. Xu, J. Alloys Compd. 464 (2008) 519-525.

[113] C.Z. Zhang, Y. Tang, Y.S. Li, Q. Yang, Thin Solid Films 528 (2013) 111-115.

[114] C.Z. Zhang, H. Niakan, L. Yang, Y.S. Li, Y.F. Hu, Q. Yang, Surf. Coat. Technol. (2013) in press.

[115] Y. Tang, Y.S. Li, C.Z. Zhang, J. Wang, Q. Yang, A. Hirose, Diam. Relat. Mater. 20 (2011) 538-541.

[116] A.C. Ferrari, J. Robertson, Phys. Rev. B 61 (2000) 95-107.

[117] Y. Pauleau, Tribology of Diamond-like Carbon Films (2008) 102-136.

[118] J.E.E. Baglin, Materials and Processes for Surface and Interface Engineering NATO ASI Series 290 (1995) 111-149.

[119] C.Z. Zhang, Y.S. Li, Y. Tang, L. Yang, L. Zhang, Y. Sun, Q. Yang, A. Hirose, Thin Solid Films 527 (2013) 59-64.

[120] http://en.wikipedia.org/wiki/Tungsten, accessed on June 25th, 2014.

[121] http://en.wikipedia.org/wiki/Titanium_nitride, accessed on June 25th, 2014.

[122] http://en.wikipedia.org/wiki/Nanoindentation, accessed on June 25th, 2014.

[120] O.R. Monteiro, Invited article for the 33rd IUVSTA Workshop and IV Brazilian Meeting on Diamond, Diamond-Like, Nanotubes, Nitrides and Silicon Carbide, November 28th-30th, Sao Paulo, Brazil, 2001.

[121] G. Heinrich, T. Grogler, S.M. Rosiwal, R.F. Singer, Surf. Coat. Technol. 94–95 (1997) 1-3.

[122] W. Osterle, D. Klaffke, M. Griepentrog, U. Gross, I. Kranz, C. Knabe, Wear 264 (2008) 505-517.

[123] M.I. De Barros, L. Vandenbulcke, J. Fontaine, G. Farges, M. Vayer, R. Erre, Surf. Coat. Technol. 127 (2000) 193-202.

[124] S.J. Askari, Surf. Eng. 25 (2009) 482-486.

[125] L. Chandra, M. Chhowalla, G.A.J. Amaratunga, T.W. Clyne, Diamond Relat. Mater. 5 (1996) 674-681.

[126] T. Grogler, E. Zeiler, M. Dannenfeldt, S.M. Rosiwal, R.F. Singer, Diamond Relat. Mater. 6 (1997) 1658-1667.

[127] X.L. Peng, T.W. Clyne, Thin Solid Films 293 (1997) 261-269.

[128] S.S. Perry, J.W. Ager II., G.A. Somorjai, R.J. McClell, M.D. Drory, J. Appl. Phys. 74 (1993) 7542-7550.

[129] S.J. Askari, F. Akhtar, G.C. Chen, Q. He, F.Y. Wang, X.M. Meng, F.X. Lu, Mater. Lett. 61 (2007) 2139-2142.

[130] M.A. Lowe, A.E. Fischer, G.M. Swain, J. Electrochem. Soc. 153 (2006) B506-B511.

[131] E. Tal-Gutelmacher, D. Eliezer, J. Alloys Compd. 404-406 (2005) 621-625.

[132] D.S. Shin, I.M. Robertson, H.K. Birnbaum, Acta Metall. 36 (1988) 111-124.

[133] E. Buccioni, E. Braca, J.M. Kenny, M.L. Terranova, Diamond Relat. Mater. 8 (1999) 17-24.

[134] Y.S. Li, Y. Tang, Q. Yang, C. Xiao, A. Hirose, Appl. Surf. Sci. 256 (2010) 7653-7657.

[135] A.C. Ferrari, J. Robertson, Philos. Trans. R. Soc. Lond. A 362 (2004) 2477-2512.

[136] A.C. Ferrari, J. Robertson, Mater. Res. Soc. Symp. Proc. 593 (2000) 299-304.

[137] Q. Yang, S. Yang, Y.S. Li, X. Lu, A. Hirose, Diamond Relat. Mater. 16 (2007) 730-734.

[138] Y.Q. Fu, B. Yan, N.L. Loh, Surf. Coat. Technol. 130 (2000) 173-185.

[139] Y.S. Li, A. Hirose, Chem. Phys. Lett. 433 (2006) 150-153.

[140] C.R. Lin, C.T. Kuo, R.M. Chang, Diamond Relat. Mater. 7 (1998) 1628-1632.

[141] Y.S. Li, Y. Tang, Q. Yang, C. Xiao, A. Hirose, Mater. Chem. Phys. 116 (2009) 649-653.

[142] L. Vandenbulcke, D. Rats, M.I. De Barros, R. Benoît, R. Erre, P. Andreazza, Appl. Phys. Lett. 72 (1998) 501-503.

[143] J.W. Zhao, H. Ding, W.J. Zhao, X.F. Tian, H.L. Hou, Y.Q. Wang, Trans. Nonferrous Met. Soc. China 18 (2008) 506-511.

[144] G. Heinrich, T. GrÖgler, S.M. Rosiwal, R.F. Singer, Surf. Coat. Technol. 514 (1997) 94-95.

[145] X. Liu, P.K. Chu, C. Ding, Mater. Sci. Eng. R 47 (2004) 49-121.

[146] Q. Wei, Z. Yu, L. Ma, D. Yin, Int. J. Mod. Phys. B 23 (2009) 1676-1682.

[147] M.D. Drory, J.W. Hutchinson, Sci. 263 (1994) 1753-1755.

[148] O.A.Williams, Diam. Relat. Mater. 20 (2011) 621-640.

[149] G. Heinrich, T. GrÖgler, S.M. Rosiwal, R.F. Singer, R. StÖckel, L. Ley, Diam. Relat. Mater. 5 (1996) 304-307.

[150] D.B. Shan, Y.Y. Zong, T.F. Lu, Y. Lv, J. Alloy. Compd. 427 (2007) 229-234.

[151] D. Hardie, S. Ouyang, Corros. Sci. 41 (1999) 155-177.

[152] R. Sharma, N. Woehrl, P.K. Barhai, V. Buck, J. Optoelectron. Adv. M. 12 (2010) 1915-1920.

[153] E. Scorsone, S. Saada, J.C. Arnault, P. Bergonzo, J. Appl. Phys. 106 (2009) 014908.

[154] H.A. Girard, S. Perruchas, C. Gesset, M. Chaigneau, L. Vieille, J.C. Arnault, P. Bergonzo, J.P. Boilot, T. Gacoin, ACS Appl. Mater. Interf. 1 (2009) 2738-46.

[155] Y. Tang, Y.S. Li, Q, Yang, A. Hirose, Diam. Relat. Mater. 19 (2010) 496-499.

[156] M.B. Ivanov, S.S. Manokhin, Y.R. Kolobov, D.A. Nechayenko, Mater. Phys. Mech. 10 (2010) 62-71.

[157] H. Liu, J. Cao, P. He, J.G. Feng, Int. J. Hydrogen Energ. 34 (2009) 1108-1113.

[158] W.D. Callister, Fundamentals of Materials Science and Engineering, fifth ed., John Wiley & Sons, Inc., New York, 2001.

[159] Q. Yang, W. Chen, C. Xiao, A. Hirose, M. Bradley, Carbon, 43 (2005) 748-754.

[160] Y.S. Li, C.Z. Zhang, H.T. Ma, L.Z. Yang, Y. Tang, L.L. Zhang, X.J. Li, L.L. He, R. Feng, Q. Yang, A. Hirose, Materials Chemistry and Physics 134 (2012) 145-152.

[161] P. Scardi, M. Leoni, G. Cappuccio, V. Sessa and M.L. Terranova, Diamond Relat. Mater. 6 (1997) 807-811.

[162] M.P. Larsson, M.M. Ahmad, J. Micromech. Microeng. 16 (2006) S161-S168.

[163] F. Deuerler, H. van den Berg, R. Tabersky, A. Freundlieb, M. Pies, V. Buck. Diamond

Relat. Mater. 5 (1996) 1478-1489.

[164] Y. Tang, Y.S. Li, Q. Yang, A. Hirose, Diam. Relat. Mater. 19 (2010) 496-499.

[161] Y.S. Li, Y. Tang, Q. Yang, J. Maley, R. Sammynailken, T. Regier, C. Xiao, A. Hirose, ACS Appl. Mat. Interfaces 2 (2010) 335-338.

[166] S.L. Yang, Q. Yang, Can. Metall. Quart. 48 (2009) 27-32.

[167] V.G. Ralchenko, A.A. Smolin, V.G. Pereverzev, E.D. Obraztsova, K.G. Korotoushenko, V.I. Konov, Yu.V. Lakhotkin, E.N. Loubnin, Diam. Relat. Mater. 4 (1995) 754-758.

[168] Y.C. Chu, C.H. Tu, G. Jiang, C. Chang, C.P. Liu, J.M. Ting, H.L. Lee, Y. Tzeng, O. Auciello, J. Appl. Phys. 111 (2012) 124328.

[169] L.J. Chen, C.C. Liu, N.H. Tai, C.Y. Lee, W. Fang, I.N. Lin, J. Phys. Chem. C 112 (2008) 3759-3765.

[170] D.M. Gruen, Annu. Rev. Mater. Sci. 29 (1999) 211-259.

[171] W. Zhu, R.C. McCune, J.E. deVries, M.A. Tamor, K.Y. Simon Ng, Diam. Relat. Mater. 4 (1995) 220-233.

APPENDIX
COPYRIGHT PERMISSION

The Following papers have been published and permission to include these published papers has been sought and responses from the publishers are appended. Where copyright issues have been raised, permission to include theses papers in the thesis has been given.

The permissions by each publisher are included as follows:

1. The permission for including the paper “CVD nanocrystalline diamond coatings on Ti alloy: A synchrotron-assisted interfacial investigation” in the Chapter 5

12/11/13 Rightslink Printable License

ELSEVIER LICENSE
TERMS AND CONDITIONS

Dec 11, 2013

This is a License Agreement between Chunzi Zhang ("You") and Elsevier ("Elsevier") provided by Copyright Clearance Center ("CCC"). The license consists of your order details, the terms and conditions provided by Elsevier, and the payment terms and conditions.

All payments must be made in full to CCC. For payment instructions, please see information listed at the bottom of this form.

Supplier	Elsevier Limited The Boulevard,Langford Lane Kidlington,Oxford,OX5 1GB,UK
Registered Company Number	1982084
Customer name	Chunzi Zhang
Customer address	410–107Cumberland Ave.S. Saskatoon, SK S7N2R6
License number	3286140655214
License date	Dec 11, 2013
Licensed content publisher	Elsevier

Licensed content publication	Materials Chemistry and Physics
Licensed content title	CVD nanocrystalline diamond coatings on Ti alloy: A synchrotron–assisted interfacial investigation
Licensed content author	Y.S. Li,C.Z. Zhang,H.T. Ma,L.Z. Yang,L.L. Zhang,Y. Tang,X.J. Li,L.L. He,R. Feng,Q. Yang,A. Hirose
Licensed content date	15 May 2012
Licensed content volume number	134
Licensed content issue number	1
Number of pages	8
Start Page	145
End Page	152
Type of Use	reuse in a thesis/dissertation
Intended publisher of new work	other
Portion	full article
Format	both print and electronic
Are you the author of this Elsevier article?	Yes

Will you be translating?	No
Title of your thesis/dissertation	ADHESION ENHANCEMENT OF DIAMOND AND DIAMOND-LIKE CARBON THIN FILMS ON TITANIUM ALLOY
Expected completion date	Jan 2014
Estimated size (number of pages)	150
Elsevier VAT number	GB 494 6272 12
Permissions price	0.00 USD
VAT/Local Sales Tax	0.00 USD / 0.00 GBP
Total	0.00 USD
Terms and Conditions	

INTRODUCTION

1. The publisher for this copyrighted material is Elsevier. By clicking "accept" in connection with completing this licensing transaction, you agree that the following terms and conditions apply to this transaction (along with the Billing and Payment terms and conditions established by Copyright Clearance Center, Inc. ("CCC"), at the time that you opened your Rightslink account and that are available at any time at http://myaccount.copyright.com).

GENERAL TERMS

2. Elsevier hereby grants you permission to reproduce the aforementioned material subject to the terms and conditions indicated.

3. Acknowledgement: If any part of the material to be used (for example, figures) has appeared in our publication with credit or acknowledgement to another source, permission must also be sought from that source. If such permission is not obtained then that material may not be included in your publication/copies. Suitable acknowledgement to the source must be made, either as a footnote or in a reference list at the end of your publication, as follows:

"Reprinted from Publication title, Vol /edition number, Author(s), Title of article / title of chapter, Pages No., Copyright (Year), with permission from Elsevier [OR APPLICABLE SOCIETY COPYRIGHT OWNER]." Also Lancet special credit - "Reprinted from The Lancet, Vol. number, Author(s), Title of article, Pages No., Copyright (Year), with permission from Elsevier."

4. Reproduction of this material is confined to the purpose and/or media for which permission is hereby given.

5. Altering/Modifying Material: Not Permitted. However figures and illustrations may be altered/adapted minimally to serve your work. Any other abbreviations, additions, deletions and/or any other alterations shall be made only with prior written authorization of Elsevier Ltd. (Please contact Elsevier at permissions@elsevier.com)

6. If the permission fee for the requested use of our material is waived in this instance, please be advised that your future requests for Elsevier materials may attract a fee.

7. Reservation of Rights: Publisher reserves all rights not specifically granted in the combination of (i) the license details provided by you and accepted in the course of this

licensing transaction, (ii) these terms and conditions and (iii) CCC's Billing and Payment terms and conditions.

8. License Contingent Upon Payment: While you may exercise the rights licensed immediately upon issuance of the license at the end of the licensing process for the transaction, provided that you have disclosed complete and accurate details of your proposed use, no license is finally effective unless and until full payment is received from you (either by publisher or by CCC) as provided in CCC's Billing and Payment terms and conditions. If full payment is not received on a timely basis, then any license preliminarily granted shall be deemed automatically revoked and shall be void as if never granted. Further, in the event that you breach any of these terms and conditions or any of CCC's Billing and Payment terms and conditions, the license is automatically revoked and shall be void as if never granted. Use of materials as described in a revoked license, as well as any use of the materials beyond the scope of an unrevoked license, may constitute copyright infringement and publisher reserves the right to take any and all action to protect its copyright in the materials.

9. Warranties: Publisher makes no representations or warranties with respect to the licensed material.

10. Indemnity: You hereby indemnify and agree to hold harmless publisher and CCC, and their respective officers, directors, employees and agents, from and against any and all claims arising out of your use of the licensed material other than as specifically authorized pursuant to this license.

11. No Transfer of License: This license is personal to you and may not be sublicensed, assigned, or transferred by you to any other person without publisher's written permission.

12. No Amendment Except in Writing: This license may not be amended except in a writing signed by both parties (or, in the case of publisher, by CCC on publisher's behalf).

13. Objection to Contrary Terms: Publisher hereby objects to any terms contained in any purchase order, acknowledgment, check endorsement or other writing prepared by you, which terms are inconsistent with these terms and conditions or CCC's Billing and Payment terms and conditions. These terms and conditions, together with CCC's Billing and Payment terms and conditions (which are incorporated herein), comprise the entire agreement between you and publisher (and CCC) concerning this licensing transaction. In the event of any conflict between your obligations established by these terms and conditions and those established by CCC's Billing and Payment terms and conditions, these terms and conditions shall control.

14. Revocation: Elsevier or Copyright Clearance Center may deny the permissions described in this License at their sole discretion, for any reason or no reason, with a full refund payable to you. Notice of such denial will be made using the contact information provided by you. Failure to receive such notice will not alter or invalidate the denial. In no event will Elsevier or Copyright Clearance Center be responsible or liable for any costs, expenses or damage incurred by you as a result of a denial of your permission request, other than a refund of the amount(s) paid by you to Elsevier and/or Copyright Clearance Center for denied permissions.

LIMITED LICENSE

The following terms and conditions apply only to specific license types:

15. **Translation**: This permission is granted for non-exclusive world **English** rights only

unless your license was granted for translation rights. If you licensed translation rights you may only translate this content into the languages you requested. A professional translator must perform all translations and reproduce the content word for word preserving the integrity of the article. If this license is to re-use 1 or 2 figures then permission is granted for non-exclusive world rights in all languages.

16. **Website**: The following terms and conditions apply to electronic reserve and author websites:
Electronic reserve: If licensed material is to be posted to website, the web site is to be password-protected and made available only to bona fide students registered on a relevant course if:
This license was made in connection with a course,
This permission is granted for 1 year only. You may obtain a license for future website posting,
All content posted to the web site must maintain the copyright information line on the bottom of each image,
A hyper-text must be included to the Homepage of the journal from which you are licensing at http://www.sciencedirect.com/science/journal/xxxxx or the Elsevier homepage for books at http://www.elsevier.com , and
Central Storage: This license does not include permission for a scanned version of the material to be stored in a central repository such as that provided by Heron/XanEdu.

17. **Author website** for journals with the following additional clauses:

All content posted to the web site must maintain the copyright information line on the bottom of each image, and the permission granted is limited to the personal version of your paper.
You are not allowed to download and post the published electronic version of your article

(whether PDF or HTML, proof or final version), nor may you scan the printed edition to create an electronic version. A hyper-text must be included to the Homepage of the journal from which you are licensing at http://www.sciencedirect.com/science/journal/xxxxx . As part of our normal production process, you will receive an e-mail notice when your article appears on Elsevier's online service ScienceDirect (www.sciencedirect.com). That e-mail will include the article's Digital Object Identifier (DOI). This number provides the electronic link to the published article and should be included in the posting of your personal version. We ask that you wait until you receive this e-mail and have the DOI to do any posting.

Central Storage: This license does not include permission for a scanned version of the material to be stored in a central repository such as that provided by Heron/XanEdu.

18. **Author website** for books with the following additional clauses:
Authors are permitted to place a brief summary of their work online only.
A hyper-text must be included to the Elsevier homepage at http://www.elsevier.com . All content posted to the web site must maintain the copyright information line on the bottom of each image. You are not allowed to download and post the published electronic version of your chapter, nor may you scan the printed edition to create an electronic version.

Central Storage: This license does not include permission for a scanned version of the material to be stored in a central repository such as that provided by Heron/XanEdu.

19. **Website** (regular and for author): A hyper-text must be included to the Homepage of the journal from which you are licensing at http://www.sciencedirect.com/science/journal/xxxxx.

or for books to the Elsevier homepage at http://www.elsevier.com

20. **Thesis/Dissertation**: If your license is for use in a thesis/dissertation your thesis may be submitted to your institution in either print or electronic form. Should your thesis be published commercially, please reapply for permission. These requirements include permission for the Library and Archives of Canada to supply single copies, on demand, of the complete thesis and include permission for UMI to supply single copies, on demand, of the complete thesis. Should your thesis be published commercially, please reapply for permission.

21. **Other Conditions**:

v1.6

If you would like to pay for this license now, please remit this license along with your payment made payable to "COPYRIGHT CLEARANCE CENTER" otherwise you will be invoiced within 48 hours of the license date. Payment should be in the form of a check or money order referencing your account number and this invoice number RLNK501180230.
Once you receive your invoice for this order, you may pay your invoice by credit card. Please follow instructions provided at that time.

Make Payment To:
Copyright Clearance Center
Dept 001
P.O. Box 843006
Boston, MA 02284–3006

For suggestions or comments regarding this order, contact RightsLink Customer Support: customercare@copyright.com or +1-877-622-5543 (toll free in the US) or +1-978-646-2777.

Gratis licenses (referencing $0 in the Total field) are free. Please retain this printable license for your reference. No payment is required.

2. The permission for including the paper “Nanocrystalline diamond thin films grown on Ti6Al4V alloy” in the Chapter 6

ELSEVIER LICENSE
TERMS AND CONDITIONS

Dec 11, 2013

This is a License Agreement between Chunzi Zhang ("You") and Elsevier ("Elsevier") provided by Copyright Clearance Center ("CCC"). The license consists of your order details, the terms and conditions provided by Elsevier, and the payment terms and conditions.

All payments must be made in full to CCC. For payment instructions, please see information listed at the bottom of this form.

Supplier	Elsevier Limited The Boulevard,Langford Lane Kidlington,Oxford,OX5 1GB,UK
Registered Company Number	1982084
Customer name	Chunzi Zhang
Customer address	410-107Cumberland Ave.S. Saskatoon, SK S7N2R6

License number	3286140329059
License date	Dec 11, 2013
Licensed content publisher	Elsevier
Licensed content publication	Thin Solid Films
Licensed content title	Nanocrystalline diamond thin films grown on Ti6Al4V alloy
Licensed content author	C.Z. Zhang,Y.S. Li,Y. Tang,L. Yang,L. Zhang,Y. Sun,Q. Yang,A. Hirose
Licensed content date	1 January 2013
Licensed content volume number	527
Licensed content issue number	
Number of pages	6
Start Page	59
End Page	64
Type of Use	reuse in a thesis/dissertation
Intended publisher of new work	other
Portion	full article
Format	both print and electronic
Are you the author of this Elsevier article?	Yes
Will you be translating?	No

Title of your thesis/dissertation	ADHESION ENHANCEMENT OF DIAMOND AND DIAMOND-LIKE CARBON THIN FILMS ON TITANIUM ALLOY
Expected completion date	Jan 2014
Estimated size (number of pages)	150
Elsevier VAT number	GB 494 6272 12
Permissions price	0.00 USD
VAT/Local Sales Tax	0.00 USD / 0.00 GBP
Total	0.00 USD
Terms and Conditions	

INTRODUCTION

1. The publisher for this copyrighted material is Elsevier. By clicking "accept" in connection with completing this licensing transaction, you agree that the following terms and conditions apply to this transaction (along with the Billing and Payment terms and conditions established by Copyright Clearance Center, Inc. ("CCC"), at the time that you opened your Rightslink account and that are available at any time at http://myaccount.copyright.com).

GENERAL TERMS

2. Elsevier hereby grants you permission to reproduce the aforementioned material subject to the terms and conditions indicated.

3. Acknowledgement: If any part of the material to be used (for example, figures) has appeared in our publication with credit or acknowledgement to another source, permission must also be sought from that source. If such permission is not obtained then that material may not be included in your publication/copies. Suitable acknowledgement to the source must be made, either as a footnote or in a reference list at the end of your publication, as follows:

"Reprinted from Publication title, Vol /edition number, Author(s), Title of article / title of chapter, Pages No., Copyright (Year), with permission from Elsevier [OR APPLICABLE SOCIETY COPYRIGHT OWNER]." Also Lancet special credit - "Reprinted from The Lancet, Vol. number, Author(s), Title of article, Pages No., Copyright (Year), with permission from Elsevier."

4. Reproduction of this material is confined to the purpose and/or media for which permission is hereby given.

5. Altering/Modifying Material: Not Permitted. However figures and illustrations may be altered/adapted minimally to serve your work. Any other abbreviations, additions, deletions and/or any other alterations shall be made only with prior written authorization of Elsevier Ltd. (Please contact Elsevier at permissions@elsevier.com)

6. If the permission fee for the requested use of our material is waived in this instance, please be advised that your future requests for Elsevier materials may attract a fee.

7. Reservation of Rights: Publisher reserves all rights not specifically granted in the combination of (i) the license details provided by you and accepted in the course of this licensing transaction, (ii) these terms and conditions and (iii) CCC's Billing and Payment terms

and conditions.

8. License Contingent Upon Payment: While you may exercise the rights licensed immediately upon issuance of the license at the end of the licensing process for the transaction, provided that you have disclosed complete and accurate details of your proposed use, no license is finally effective unless and until full payment is received from you (either by publisher or by CCC) as provided in CCC's Billing and Payment terms and conditions. If full payment is not received on a timely basis, then any license preliminarily granted shall be deemed automatically revoked and shall be void as if never granted. Further, in the event that you breach any of these terms and conditions or any of CCC's Billing and Payment terms and conditions, the license is automatically revoked and shall be void as if never granted. Use of materials as described in a revoked license, as well as any use of the materials beyond the scope of an unrevoked license, may constitute copyright infringement and publisher reserves the right to take any and all action to protect its copyright in the materials.

9. Warranties: Publisher makes no representations or warranties with respect to the licensed material.

10. Indemnity: You hereby indemnify and agree to hold harmless publisher and CCC, and their respective officers, directors, employees and agents, from and against any and all claims arising out of your use of the licensed material other than as specifically authorized pursuant to this license.

11. No Transfer of License: This license is personal to you and may not be sublicensed, assigned, or transferred by you to any other person without publisher's written permission.

12. No Amendment Except in Writing: This license may not be amended except in a writing signed by both parties (or, in the case of publisher, by CCC on publisher's behalf).

13. Objection to Contrary Terms: Publisher hereby objects to any terms contained in any purchase order, acknowledgment, check endorsement or other writing prepared by you, which terms are inconsistent with these terms and conditions or CCC's Billing and Payment terms and conditions. These terms and conditions, together with CCC's Billing and Payment terms and conditions (which are incorporated herein), comprise the entire agreement between you and publisher (and CCC) concerning this licensing transaction. In the event of any conflict between your obligations established by these terms and conditions and those established by CCC's Billing and Payment terms and conditions, these terms and conditions shall control.

14. Revocation: Elsevier or Copyright Clearance Center may deny the permissions described in this License at their sole discretion, for any reason or no reason, with a full refund payable to you. Notice of such denial will be made using the contact information provided by you. Failure to receive such notice will not alter or invalidate the denial. In no event will Elsevier or Copyright Clearance Center be responsible or liable for any costs, expenses or damage incurred by you as a result of a denial of your permission request, other than a refund of the amount(s) paid by you to Elsevier and/or Copyright Clearance Center for denied permissions.

LIMITED LICENSE

The following terms and conditions apply only to specific license types:

15. **Translation**: This permission is granted for non-exclusive world **English** rights only unless your license was granted for translation rights. If you licensed translation rights you

may only translate this content into the languages you requested. A professional translator must perform all translations and reproduce the content word for word preserving the integrity of the article. If this license is to re-use 1 or 2 figures then permission is granted for non-exclusive world rights in all languages.

16. **Website**: The following terms and conditions apply to electronic reserve and author websites:
Electronic reserve: If licensed material is to be posted to website, the web site is to be password-protected and made available only to bona fide students registered on a relevant course if:
This license was made in connection with a course,
This permission is granted for 1 year only. You may obtain a license for future website posting,
All content posted to the web site must maintain the copyright information line on the bottom of each image,
A hyper-text must be included to the Homepage of the journal from which you are licensing at http://www.sciencedirect.com/science/journal/xxxxx or the Elsevier homepage for books at http://www.elsevier.com , and
Central Storage: This license does not include permission for a scanned version of the material to be stored in a central repository such as that provided by Heron/XanEdu.

17. **Author website** for journals with the following additional clauses:

All content posted to the web site must maintain the copyright information line on the bottom of each image, and the permission granted is limited to the personal version of your paper. You are not allowed to download and post the published electronic version of your article

(whether PDF or HTML, proof or final version), nor may you scan the printed edition to create an electronic version. A hyper-text must be included to the Homepage of the journal from which you are licensing at http://www.sciencedirect.com/science/journal/xxxxx . As part of our normal production process, you will receive an e-mail notice when your article appears on Elsevier's online service ScienceDirect (www.sciencedirect.com). That e-mail will include the article's Digital Object Identifier (DOI). This number provides the electronic link to the published article and should be included in the posting of your personal version. We ask that you wait until you receive this e-mail and have the DOI to do any posting.

Central Storage: This license does not include permission for a scanned version of the material to be stored in a central repository such as that provided by Heron/XanEdu.

18. **Author website** for books with the following additional clauses:
Authors are permitted to place a brief summary of their work online only.
A hyper-text must be included to the Elsevier homepage at http://www.elsevier.com . All content posted to the web site must maintain the copyright information line on the bottom of each image. You are not allowed to download and post the published electronic version of your chapter, nor may you scan the printed edition to create an electronic version.

Central Storage: This license does not include permission for a scanned version of the material to be stored in a central repository such as that provided by Heron/XanEdu.

19. **Website** (regular and for author): A hyper-text must be included to the Homepage of the journal from which you are licensing at http://www.sciencedirect.com/science/journal/xxxxx. or for books to the Elsevier homepage at http://www.elsevier.com

20. **Thesis/Dissertation**: If your license is for use in a thesis/dissertation your thesis may be submitted to your institution in either print or electronic form. Should your thesis be published commercially, please reapply for permission. These requirements include permission for the Library and Archives of Canada to supply single copies, on demand, of the complete thesis and include permission for UMI to supply single copies, on demand, of the complete thesis. Should your thesis be published commercially, please reapply for permission.

21. **Other Conditions**:

v1.6

If you would like to pay for this license now, please remit this license along with your payment made payable to "COPYRIGHT CLEARANCE CENTER" otherwise you will be invoiced within 48 hours of the license date. Payment should be in the form of a check or money order referencing your account number and this invoice number RLNK501180229.
Once you receive your invoice for this order, you may pay your invoice by credit card. Please follow instructions provided at that time.

Make Payment To:
Copyright Clearance Center
Dept 001
P.O. Box 843006
Boston, MA 02284-3006

For suggestions or comments regarding this order, contact RightsLink Customer Support: customercare@copyright.com or +1-877-622-5543 (toll free in the US) or +1-978-646-2777.

Gratis licenses (referencing $0 in the Total field) are free. Please retain this printable license for your reference. No payment is required.

3. The permission for including the paper “Adhesion enhancement of diamond-like carbon thin films on Ti alloys by incorporation of nanodiamond particles” in the Chapter 7

ELSEVIER LICENSE
TERMS AND CONDITIONS

Dec 11, 2013

This is a License Agreement between Chunzi Zhang ("You") and Elsevier ("Elsevier") provided by Copyright Clearance Center ("CCC"). The license consists of your order details, the terms and conditions provided by Elsevier, and the payment terms and conditions.

All payments must be made in full to CCC. For payment instructions, please see information listed at the bottom of this form.

Supplier	Elsevier Limited The Boulevard,Langford Lane Kidlington,Oxford,OX5 1GB,UK
Registered Company Number	1982084
Customer name	Chunzi Zhang
Customer address	410–107Cumberland Ave.S. Saskatoon, SK S7N2R6

License number	3286140038251
License date	Dec 11, 2013
Licensed content publisher	Elsevier
Licensed content publication	Thin Solid Films
Licensed content title	Adhesion enhancement of diamond-like carbon thin films on Ti alloys by incorporation of nanodiamond particles
Licensed content author	C.Z. Zhang,Y. Tang,Y.S. Li,Q. Yang
Licensed content date	15 January 2013
Licensed content volume number	528
Licensed content issue number	
Number of pages	5
Start Page	111
End Page	115
Type of Use	reuse in a thesis/dissertation
Portion	full article
Format	both print and electronic
Are you the author of this Elsevier article?	Yes
Will you be translating?	No
Title of your	ADHESION ENHANCEMENT OF DIAMOND AND DIAMOND-LIKE

thesis/dissertation	CARBON THIN FILMS ON TITANIUM ALLOY
Expected completion date	Jan 2014
Estimated size (number of pages)	150
Elsevier VAT number	GB 494 6272 12
Permissions price	0.00 USD
VAT/Local Sales Tax	0.00 USD / 0.00 GBP
Total	0.00 USD
Terms and Conditions	

INTRODUCTION

1. The publisher for this copyrighted material is Elsevier. By clicking "accept" in connection with completing this licensing transaction, you agree that the following terms and conditions apply to this transaction (along with the Billing and Payment terms and conditions established by Copyright Clearance Center, Inc. ("CCC"), at the time that you opened your Rightslink account and that are available at any time at http://myaccount.copyright.com).

GENERAL TERMS

2. Elsevier hereby grants you permission to reproduce the aforementioned material subject to the terms and conditions indicated.

3. Acknowledgement: If any part of the material to be used (for example, figures) has appeared in our publication with credit or acknowledgement to another source, permission must also be sought from that source. If such permission is not obtained then that material may not be included in your publication/copies. Suitable acknowledgement to the source must be made, either as a footnote or in a reference list at the end of your publication, as follows:

"Reprinted from Publication title, Vol /edition number, Author(s), Title of article / title of chapter, Pages No., Copyright (Year), with permission from Elsevier [OR APPLICABLE SOCIETY COPYRIGHT OWNER]." Also Lancet special credit - "Reprinted from The Lancet, Vol. number, Author(s), Title of article, Pages No., Copyright (Year), with permission from Elsevier."

4. Reproduction of this material is confined to the purpose and/or media for which permission is hereby given.

5. Altering/Modifying Material: Not Permitted. However figures and illustrations may be altered/adapted minimally to serve your work. Any other abbreviations, additions, deletions and/or any other alterations shall be made only with prior written authorization of Elsevier Ltd. (Please contact Elsevier at permissions@elsevier.com)

6. If the permission fee for the requested use of our material is waived in this instance, please be advised that your future requests for Elsevier materials may attract a fee.

7. Reservation of Rights: Publisher reserves all rights not specifically granted in the combination of (i) the license details provided by you and accepted in the course of this licensing transaction, (ii) these terms and conditions and (iii) CCC's Billing and Payment terms

and conditions.

8. License Contingent Upon Payment: While you may exercise the rights licensed immediately upon issuance of the license at the end of the licensing process for the transaction, provided that you have disclosed complete and accurate details of your proposed use, no license is finally effective unless and until full payment is received from you (either by publisher or by CCC) as provided in CCC's Billing and Payment terms and conditions. If full payment is not received on a timely basis, then any license preliminarily granted shall be deemed automatically revoked and shall be void as if never granted. Further, in the event that you breach any of these terms and conditions or any of CCC's Billing and Payment terms and conditions, the license is automatically revoked and shall be void as if never granted. Use of materials as described in a revoked license, as well as any use of the materials beyond the scope of an unrevoked license, may constitute copyright infringement and publisher reserves the right to take any and all action to protect its copyright in the materials.

9. Warranties: Publisher makes no representations or warranties with respect to the licensed material.

10. Indemnity: You hereby indemnify and agree to hold harmless publisher and CCC, and their respective officers, directors, employees and agents, from and against any and all claims arising out of your use of the licensed material other than as specifically authorized pursuant to this license.

11. No Transfer of License: This license is personal to you and may not be sublicensed, assigned, or transferred by you to any other person without publisher's written permission.

12. No Amendment Except in Writing: This license may not be amended except in a writing signed by both parties (or, in the case of publisher, by CCC on publisher's behalf).

13. Objection to Contrary Terms: Publisher hereby objects to any terms contained in any purchase order, acknowledgment, check endorsement or other writing prepared by you, which terms are inconsistent with these terms and conditions or CCC's Billing and Payment terms and conditions. These terms and conditions, together with CCC's Billing and Payment terms and conditions (which are incorporated herein), comprise the entire agreement between you and publisher (and CCC) concerning this licensing transaction. In the event of any conflict between your obligations established by these terms and conditions and those established by CCC's Billing and Payment terms and conditions, these terms and conditions shall control.

14. Revocation: Elsevier or Copyright Clearance Center may deny the permissions described in this License at their sole discretion, for any reason or no reason, with a full refund payable to you. Notice of such denial will be made using the contact information provided by you. Failure to receive such notice will not alter or invalidate the denial. In no event will Elsevier or Copyright Clearance Center be responsible or liable for any costs, expenses or damage incurred by you as a result of a denial of your permission request, other than a refund of the amount(s) paid by you to Elsevier and/or Copyright Clearance Center for denied permissions.

LIMITED LICENSE

The following terms and conditions apply only to specific license types:

15. **Translation**: This permission is granted for non-exclusive world **English** rights only unless your license was granted for translation rights. If you licensed translation rights you

may only translate this content into the languages you requested. A professional translator must perform all translations and reproduce the content word for word preserving the integrity of the article. If this license is to re-use 1 or 2 figures then permission is granted for non-exclusive world rights in all languages.

16. **Website**: The following terms and conditions apply to electronic reserve and author websites:
Electronic reserve: If licensed material is to be posted to website, the web site is to be password-protected and made available only to bona fide students registered on a relevant course if:
This license was made in connection with a course,
This permission is granted for 1 year only. You may obtain a license for future website posting,
All content posted to the web site must maintain the copyright information line on the bottom of each image,
A hyper-text must be included to the Homepage of the journal from which you are licensing at http://www.sciencedirect.com/science/journal/xxxxx or the Elsevier homepage for books at http://www.elsevier.com , and
Central Storage: This license does not include permission for a scanned version of the material to be stored in a central repository such as that provided by Heron/XanEdu.

17. **Author website** for journals with the following additional clauses:

All content posted to the web site must maintain the copyright information line on the bottom of each image, and the permission granted is limited to the personal version of your paper. You are not allowed to download and post the published electronic version of your article

(whether PDF or HTML, proof or final version), nor may you scan the printed edition to create an electronic version. A hyper-text must be included to the Homepage of the journal from which you are licensing at http://www.sciencedirect.com/science/journal/xxxxx . As part of our normal production process, you will receive an e-mail notice when your article appears on Elsevier's online service ScienceDirect (www.sciencedirect.com). That e-mail will include the article's Digital Object Identifier (DOI). This number provides the electronic link to the published article and should be included in the posting of your personal version. We ask that you wait until you receive this e-mail and have the DOI to do any posting.

Central Storage: This license does not include permission for a scanned version of the material to be stored in a central repository such as that provided by Heron/XanEdu.

18. **Author website** for books with the following additional clauses:
Authors are permitted to place a brief summary of their work online only.
A hyper-text must be included to the Elsevier homepage at http://www.elsevier.com . All content posted to the web site must maintain the copyright information line on the bottom of each image. You are not allowed to download and post the published electronic version of your chapter, nor may you scan the printed edition to create an electronic version.

Central Storage: This license does not include permission for a scanned version of the material to be stored in a central repository such as that provided by Heron/XanEdu.

19. **Website** (regular and for author): A hyper-text must be included to the Homepage of the journal from which you are licensing at http://www.sciencedirect.com/science/journal/xxxxx. or for books to the Elsevier homepage at http://www.elsevier.com

20. **Thesis/Dissertation**: If your license is for use in a thesis/dissertation your thesis may be submitted to your institution in either print or electronic form. Should your thesis be published commercially, please reapply for permission. These requirements include permission for the Library and Archives of Canada to supply single copies, on demand, of the complete thesis and include permission for UMI to supply single copies, on demand, of the complete thesis. Should your thesis be published commercially, please reapply for permission.

21. **Other Conditions**:

v1.6

If you would like to pay for this license now, please remit this license along with your payment made payable to "COPYRIGHT CLEARANCE CENTER" otherwise you will be invoiced within 48 hours of the license date. Payment should be in the form of a check or money order referencing your account number and this invoice number RLNK501180225.
Once you receive your invoice for this order, you may pay your invoice by credit card. Please follow instructions provided at that time.

Make Payment To:
Copyright Clearance Center
Dept 001
P.O. Box 843006
Boston, MA 02284-3006

For suggestions or comments regarding this order, contact RightsLink Customer Support: customercare@copyright.com or +1-877-622-5543 (toll free in the US) or +1-978-646-2777.

Gratis licenses (referencing $0 in the Total field) are free. Please retain this printable license for your reference. No payment is required.

4. The permission for including the paper “Study of diamond nucleation and growth on Ti6Al4V with tungsten interlayer” in the Chapter 8

ELSEVIER LICENSE
TERMS AND CONDITIONS

Dec 11, 2013

This is a License Agreement between Chunzi Zhang ("You") and Elsevier ("Elsevier") provided by Copyright Clearance Center ("CCC"). The license consists of your order details, the terms and conditions provided by Elsevier, and the payment terms and conditions.

All payments must be made in full to CCC. For payment instructions, please see information listed at the bottom of this form.

Supplier	Elsevier Limited The Boulevard,Langford Lane Kidlington,Oxford,OX5 1GB,UK
Registered Company Number	1982084
Customer name	Chunzi Zhang
Customer address	410–107Cumberland Ave.S. Saskatoon, SK S7N2R6

License number	3286140946535
License date	Dec 11, 2013
Licensed content publisher	Elsevier
Licensed content publication	Surface and Coatings Technology
Licensed content title	Study of diamond nucleation and growth on Ti6Al4V with tungsten interlayer
Licensed content author	C.Z. Zhang,H. Niakan,L. Yang,Y.S. Li,Y.F. Hu,Q. Yang
Licensed content date	25 December 2013
Licensed content volume number	237
Licensed content issue number	
Number of pages	7
Start Page	248
End Page	254
Type of Use	reuse in a thesis/dissertation
Intended publisher of new work	other
Portion	full article
Format	both print and electronic
Are you the author of this Elsevier article?	Yes

Will you be translating?	No
Title of your thesis/dissertation	ADHESION ENHANCEMENT OF DIAMOND AND DIAMOND-LIKE CARBON THIN FILMS ON TITANIUM ALLOY
Expected completion date	Jan 2014
Estimated size (number of pages)	150
Elsevier VAT number	GB 494 6272 12
Permissions price	0.00 USD
VAT/Local Sales Tax	0.00 USD / 0.00 GBP
Total	0.00 USD
Terms and Conditions	

INTRODUCTION

1. The publisher for this copyrighted material is Elsevier. By clicking "accept" in connection with completing this licensing transaction, you agree that the following terms and conditions apply to this transaction (along with the Billing and Payment terms and conditions established by Copyright Clearance Center, Inc. ("CCC"), at the time that you opened your Rightslink account and that are available at any time at http://myaccount.copyright.com).

GENERAL TERMS

2. Elsevier hereby grants you permission to reproduce the aforementioned material subject to the terms and conditions indicated.

3. Acknowledgement: If any part of the material to be used (for example, figures) has appeared in our publication with credit or acknowledgement to another source, permission must also be sought from that source. If such permission is not obtained then that material may not be included in your publication/copies. Suitable acknowledgement to the source must be made, either as a footnote or in a reference list at the end of your publication, as follows:

"Reprinted from Publication title, Vol /edition number, Author(s), Title of article / title of chapter, Pages No., Copyright (Year), with permission from Elsevier [OR APPLICABLE SOCIETY COPYRIGHT OWNER]." Also Lancet special credit - "Reprinted from The Lancet, Vol. number, Author(s), Title of article, Pages No., Copyright (Year), with permission from Elsevier."

4. Reproduction of this material is confined to the purpose and/or media for which permission is hereby given.

5. Altering/Modifying Material: Not Permitted. However figures and illustrations may be altered/adapted minimally to serve your work. Any other abbreviations, additions, deletions and/or any other alterations shall be made only with prior written authorization of Elsevier Ltd. (Please contact Elsevier at permissions@elsevier.com)

6. If the permission fee for the requested use of our material is waived in this instance, please be advised that your future requests for Elsevier materials may attract a fee.

7. Reservation of Rights: Publisher reserves all rights not specifically granted in the

combination of (i) the license details provided by you and accepted in the course of this licensing transaction, (ii) these terms and conditions and (iii) CCC's Billing and Payment terms and conditions.

8. License Contingent Upon Payment: While you may exercise the rights licensed immediately upon issuance of the license at the end of the licensing process for the transaction, provided that you have disclosed complete and accurate details of your proposed use, no license is finally effective unless and until full payment is received from you (either by publisher or by CCC) as provided in CCC's Billing and Payment terms and conditions. If full payment is not received on a timely basis, then any license preliminarily granted shall be deemed automatically revoked and shall be void as if never granted. Further, in the event that you breach any of these terms and conditions or any of CCC's Billing and Payment terms and conditions, the license is automatically revoked and shall be void as if never granted. Use of materials as described in a revoked license, as well as any use of the materials beyond the scope of an unrevoked license, may constitute copyright infringement and publisher reserves the right to take any and all action to protect its copyright in the materials.

9. Warranties: Publisher makes no representations or warranties with respect to the licensed material.

10. Indemnity: You hereby indemnify and agree to hold harmless publisher and CCC, and their respective officers, directors, employees and agents, from and against any and all claims arising out of your use of the licensed material other than as specifically authorized pursuant to this license.

11. No Transfer of License: This license is personal to you and may not be sublicensed, assigned, or transferred by you to any other person without publisher's written permission.

12. No Amendment Except in Writing: This license may not be amended except in a writing signed by both parties (or, in the case of publisher, by CCC on publisher's behalf).

13. Objection to Contrary Terms: Publisher hereby objects to any terms contained in any purchase order, acknowledgment, check endorsement or other writing prepared by you, which terms are inconsistent with these terms and conditions or CCC's Billing and Payment terms and conditions. These terms and conditions, together with CCC's Billing and Payment terms and conditions (which are incorporated herein), comprise the entire agreement between you and publisher (and CCC) concerning this licensing transaction. In the event of any conflict between your obligations established by these terms and conditions and those established by CCC's Billing and Payment terms and conditions, these terms and conditions shall control.

14. Revocation: Elsevier or Copyright Clearance Center may deny the permissions described in this License at their sole discretion, for any reason or no reason, with a full refund payable to you. Notice of such denial will be made using the contact information provided by you. Failure to receive such notice will not alter or invalidate the denial. In no event will Elsevier or Copyright Clearance Center be responsible or liable for any costs, expenses or damage incurred by you as a result of a denial of your permission request, other than a refund of the amount(s) paid by you to Elsevier and/or Copyright Clearance Center for denied permissions.

LIMITED LICENSE

The following terms and conditions apply only to specific license types:

15. **Translation**: This permission is granted for non-exclusive world **English** rights only unless your license was granted for translation rights. If you licensed translation rights you may only translate this content into the languages you requested. A professional translator must perform all translations and reproduce the content word for word preserving the integrity of the article. If this license is to re-use 1 or 2 figures then permission is granted for non-exclusive world rights in all languages.

16. **Website**: The following terms and conditions apply to electronic reserve and author websites:
Electronic reserve: If licensed material is to be posted to website, the web site is to be password-protected and made available only to bona fide students registered on a relevant course if:
This license was made in connection with a course,
This permission is granted for 1 year only. You may obtain a license for future website posting,
All content posted to the web site must maintain the copyright information line on the bottom of each image,
A hyper-text must be included to the Homepage of the journal from which you are licensing at http://www.sciencedirect.com/science/journal/xxxxx or the Elsevier homepage for books at http://www.elsevier.com , and
Central Storage: This license does not include permission for a scanned version of the material to be stored in a central repository such as that provided by Heron/XanEdu.

17. **Author website** for journals with the following additional clauses:

All content posted to the web site must maintain the copyright information line on the bottom of each image, and the permission granted is limited to the personal version of your paper. You are not allowed to download and post the published electronic version of your article (whether PDF or HTML, proof or final version), nor may you scan the printed edition to create an electronic version. A hyper-text must be included to the Homepage of the journal from which you are licensing at http://www.sciencedirect.com/science/journal/xxxxx . As part of our normal production process, you will receive an e-mail notice when your article appears on Elsevier's online service ScienceDirect (www.sciencedirect.com). That e-mail will include the article's Digital Object Identifier (DOI). This number provides the electronic link to the published article and should be included in the posting of your personal version. We ask that you wait until you receive this e-mail and have the DOI to do any posting.

Central Storage: This license does not include permission for a scanned version of the material to be stored in a central repository such as that provided by Heron/XanEdu.

18. **Author website** for books with the following additional clauses:
Authors are permitted to place a brief summary of their work online only.
A hyper-text must be included to the Elsevier homepage at http://www.elsevier.com . All content posted to the web site must maintain the copyright information line on the bottom of each image. You are not allowed to download and post the published electronic version of your chapter, nor may you scan the printed edition to create an electronic version.

Central Storage: This license does not include permission for a scanned version of the material to be stored in a central repository such as that provided by Heron/XanEdu.

19. **Website** (regular and for author): A hyper-text must be included to the Homepage of the

journal from which you are licensing at http://www.sciencedirect.com/science/journal/xxxxx. or for books to the Elsevier homepage at http://www.elsevier.com

20. **Thesis/Dissertation**: If your license is for use in a thesis/dissertation your thesis may be submitted to your institution in either print or electronic form. Should your thesis be published commercially, please reapply for permission. These requirements include permission for the Library and Archives of Canada to supply single copies, on demand, of the complete thesis and include permission for UMI to supply single copies, on demand, of the complete thesis. Should your thesis be published commercially, please reapply for permission.

21. **Other Conditions**:

v1.6

If you would like to pay for this license now, please remit this license along with your payment made payable to "COPYRIGHT CLEARANCE CENTER" otherwise you will be invoiced within 48 hours of the license date. Payment should be in the form of a check or money order referencing your account number and this invoice number RLNK501180234.
Once you receive your invoice for this order, you may pay your invoice by credit card. Please follow instructions provided at that time.

Make Payment To:
Copyright Clearance Center
Dept 001
P.O. Box 843006
Boston, MA 02284–3006

For suggestions or comments regarding this order, contact RightsLink Customer Support: customercare@copyright.com or +1–877–622–5543 (toll free in the US) or +1–978–646–2777.

Gratis licenses (referencing $0 in the Total field) are free. Please retain this printable license for your reference. No payment is required.
